

Aus der Neurochirurgischen Klinik und Poliklinik
Klinikum der Ludwig-Maximilians-Universität München

Vorstand: Prof. Dr. Jörg Christian Tonn

A study on the control of vascular permeability in GBM.

The role of pericytes, myeloid-like cells (TAMEP) and the angiogenic factors

APLN and ANGPT2.

Dissertation

zum Erwerb des Doktorgrades der Medizin

an der Medizinischen Fakultät der

Ludwig-Maximilians-Universität zu München



vorgelegt von

Huabin Zhang

aus

Fujian, P.R. China

2021

Mit Genehmigung der Medizinischen Fakultät

der Universität München

Berichterstatter: Prof. Dr. rer. nat. Rainer Glaß

Mitberichterstatter: Prof. Dr. Jochen Herms

Prof. Dr. Florian Ringel

Mitbetreuung durch den

promovierten Mitarbeiter: Dr. Roland Kälin

Dekan: Prof. Dr. med. Thomas Gudermann

Tag der mündlichen Prüfung: 25. 11. 2021

Content

<i>Content</i>	3
<i>List of figures</i>	8
<i>List of tables</i>	10
1. Introduction	13
1.1 Glioma	13
1.2 GBM	13
1.2.1 Angiogenesis of GBM	13
1.2.2 Pericytes in GBM	14
1.2.3 GBM microenvironment	16
1.2.4 TAMEP in the GBM microenvironment	17
1.2.5 Diagnosis of GBM	18
1.2.6 Radiogenomic analysis in GBM	19
1.2.7 Role of APLN in the angiogenesis of GBM	20
1.2.8 Role of ANGPT2 in the angiogenesis of GBM	21
1.3 Objectives	22
2. Materials	23
2.1 Devices	23

Content

2.2	Consumables	24
2.3	Cell culture materials	26
2.4	Reagents and Chemicals	26
2.5	Primary antibodies	28
2.6	Secondary antibodies	29
2.7	Streptavidin conjugates	29
2.8	Mouse strains	30
3.	Methods	31
3.1	Cell culture	31
3.2	Animal experiments	31
3.2.1	Animal care	31
3.2.2	Tamoxifen sensitivity of Nestin-creERT2 mouse-strains	31
3.2.3	Tumor implantation	32
3.2.4	Intracerebral application of substances	33
3.2.5	Mice cerebral ischemic stroke model	33
3.2.6	Analysis of vascular permeability by Evans Blue assay	33
3.2.7	Dextran leakage assay	34
3.3	Histology	35
3.3.1	Perfusion and tissue processing	35
3.3.2	H&E staining	36

Content

3.3.3 Cresyl-violet (Nissl) staining	36
3.3.4 Quantification of tumor volume	37
3.4 Immunofluorescence staining	37
3.4.1 Immunofluorescence staining of mouse brain sections	37
3.4.2 Quantification of tumor microvascular pattern	38
3.5 Bioinformatics analysis on clinical data from public database	39
3.5.1 Data collection and preprocessing	39
3.5.2 Pan-cancer gene expression analysis in TIMER2.0	40
3.5.3 Gene correlation analysis in LinkedOmics	40
3.5.4 Kaplan–Meier plots	40
3.5.5 Gene set enrichment analysis	41
3.6 Statistics	41
4. Results	42
4.1 Different roles of pericytes in early and advanced GBM	42
4.1.1 Pericyte lineage-tracing and -depleting models	42
4.1.2 Pericyte reduction in pericyte-depletion advanced GBM model	45
4.1.3 Replenishment of pericytes in tumor-free areas	47
4.1.4 Pericyte ablation inhibits the expansion of GBM	49
4.1.5 Pericyte ablation inhibits the angiogenesis of GBM	51
4.1.6 Pericyte ablation in early, but not advanced GBM, boosts Evans Blue extravasation	54
4.1.7 Pericyte ablation in early, but not advanced GBM, boosts 70 KDa dextran leakiness	57

Content

4.1.8 Pericyte ablation in early, but not advanced GBM, inhibits collagen IV synthesis	59
4.1.9 Pericyte ablation in early GBM promotes transcytosis in tumoral endothelial cells	61
4.2 Functions of TAMEP in GBM	64
4.2.1 Nes-RFP model traces two different cell types in GBM	64
4.2.2 Nes-RFP model exhibits higher sensitivity to tamoxifen than NesERT2 R26-RFP model-2	66
4.2.3 TAMEP promote GBM growth	68
4.2.4 TAMEP promote and shapes GBM angiogenesis	69
4.2.5 TAMEP maintain the tumoral vascular permeability of GBM	71
4.2.6 Effects of TAMEP on collagen IV production in GBM	74
4.2.7 Angiogenesis of GBM does not affect the number of TAMEP	76
4.2.8 TAMEP do not accumulate in cerebral ischemia	78
1.3 Role of APLN and ANGPT2 mRNA in GBM	79
4.3.1 Loss of APLN increases the tumoral vascular permeability in GL261 experimental glioma	79
4.3.2 Expression levels of APLN mRNA in the TCGA pan-cancer datasets	81
4.3.3 APLN-associated genes in the TCGA-GBM database	82
4.3.4 Gene ontology (GO) annotations of APLN-associated genes in GBM	85
4.3.5 Strong positive correlation between APLN and ANGPT2 expression levels in GBM	86
4.3.6 High APLN/low ANGPT2 expression levels are associated with milder peritumoral edema	89

Content

4.3.7 Potential roles of ANGPT2-associated genes in TCGA-GBM dataset.....	91
4.3.8 Different roles of APLN- and ANGPT2-associated genes in angiogenesis of GBM.....	92
4.3.9 High APLN/low ANGPT2 expression levels in GBM are associated with prolonged survival.....	93
5. Discussion.....	96
5.1 The role of pericytes in early and advanced GBM	96
5.2 Depleting TAMEP disrupt angiogenesis of GBM	99
5.3 High APLN/low ANGPT2 mRNA expression levels are associated with vascular tightness and prolonged survival	101
6. Summary.....	106
7. References	112
8. Acknowledgement	125
9. Affidavit	126

List of figures

Figure 1 Pericyte lineage-tracing and -depletion models.....	44
Figure 2 Pericyte reduction in pericyte-depletion models.	46
Figure 3 Pericytes are replenished in tumor-free areas.	48
Figure 4 Pericyte ablation inhibits the expansion of GBM.....	50
Figure 5 Pericyte ablation inhibits GBM angiogenesis.	53
Figure 6 Pericyte ablation in early, but not advanced GBM, boosts Evans- Blue extravasation.	56
Figure 7 Pericyte ablation in early, but not advanced GBM, boosts 70 KDa dextran leakiness.	59
Figure 8 Effect of pericytes on collagen IV production.....	60
Figure 9 Pericyte ablation in early GBM promotes transcytosis in tumoral endothelial cells.....	63
Figure 100 Vascular RFP+ and avascular RFP+ cells in the Nes-RFP GBM model.....	66
Figure 111 Differences in tamoxifen sensitivity in two Nes-RFP mouse strains.	67
Figure 12 TAMEP promote the expansion of GBM.	68
Figure 13 TAMEP control the angiogenesis of GBM.	70
Figure 14 TAMEP maintain the vascular tightness of GBM.....	73
Figure 15 TAMEP promote the production of collagen IV in GBM.....	75
Figure 16 Inhibition of angiogenesis does not affect the number of TAMEP..	77
Figure 17 TAMEP do not accumulate in cerebral ischemia.	78
Figure 18 Loss of APLN expression increases the tumoral vascular permeability in the GL261 mouse model.	81
Figure 19 Expression of APLN in TCGA pan-cancer database.	82

Content

Figure 20 APLN-associated genes in TCGA-GBM database.	84
Figure 21 Potential functions of APLN-associated genes in GBM.....	86
Figure 22 Strong positive correlation between APLN and ANGPT2 expression levels in GBM.....	88
Figure 23 High APLN/low ANGPT2 expression levels are associated with milder peritumoral edema.	90
Figure 24 Potential roles of ANGPT2-associated genes in GBM.	92
Figure 25 Different roles of APLN- and ANGPT2-associated genes in angiogenesis of GBM.....	93
Figure 26 High APLN/low ANGPT2 expression levels in GBM are associated with prolonged survival.	95
Figure 27 Functions of TAMEP in GBM-angiogenesis.	100

Content

List of tables

Table 2.1 Devices.....	23
Table 2.2 Consumables.....	25
Table 2.3 Cell culture materials.....	26
Table 2.4 Reagents and Chemicals	26
Table 2.5 Primary antibodies.....	28
Table 2.6 Secondary antibodies	29
Table 2.7 Streptavidin conjugates	29
Table 2.8 Mouse strains.....	30

Abbreviations

Abbreviations

Ang1	Angiopoietin-1
Ang2	Angiopoietin-2
<i>APLN</i>	Human apelin gene
AQP4	Aquaporin4
BBB	Blood-brain barrier
BM	Base membrane
BMDMs	Bone marrow-derived macrophages
BSA	Bovine Serum Albumin
CT	Computed tomography
DC101	VEGFR2-blocking antibody
DEX	Dexamethasone
DMEM	Dulbecco's Modified Eagle's Medium
ECs	Endothelial cells
EphA3	Ephrin A3
EGFR	Epidermal growth factor receptor
FITC	Fluorescein-isothiocyanate
GBM	Glioblastoma
Glut1	Glucose transporter 1
IDH	Isocitrate dehydrogenase
IntDen	Integrated density
iDTA	Inducible diphtheria toxin A
MSCs	Mesenchymal stem cells
MW	Molecular weight

Abbreviations

MET	Mesenchymal–epithelial transition factor
MRI	Magnetic resonance imaging
NG2	Nerve-glia antigen 2
OPCs	Oligodendrocyte precursor cells
PBS	Phosphate-buffered saline
PC	Pericyte
PDGFRA	Platelet-derived growth factor receptor α
PDGFRB	Platelet-derived growth factor receptor β
PFA	Paraformaldehyde
RGS-5	Regulator of G protein-5
RTKs	Receptor tyrosine kinases
SVZ	Subventricular zone
TAMEP	Tumor-associated cells with a myeloid-like expression profile
TAMs	Tumor-associated microglia/macrophages
TME	Tumor microenvironment
VEGF	Vascular endothelial growth factor
α -SMA	α -smooth muscle actin

1. Introduction

1.1 Glioma

Glioma is one of the most prevalent intracranial malignancies. It has a poor prognosis and can be refractory to chemotherapy and radiotherapy^{1,2}. The therapeutic outcomes of glioma are highly variable, with median survival ranging from one to seven years^{3,4}. Accurate diagnosis and classification are important for subsequent therapies. Gliomas are classified as grade I to IV by the World Health Organization (WHO) based on clinical, genetic, and histopathological criteria. WHO grade I includes pilocytic astrocytoma and astroblastoma. WHO grade II includes diffuse astrocytoma and oligodendroglioma. WHO grade III includes anaplastic astrocytomas and oligodendrogliomas. WHO grade IV includes glioblastoma (GBM). GBM is the most common malignant brain tumor⁵ and the most aggressive primary brain tumor among all glioma subtypes, accounting for 54% of all gliomas and 16% of all primary brain tumors⁶. Survival rate of GBM patients remains poor, at a median overall survival of 14.6 months⁷, despite advances in its molecular characterization. Therefore, GBM treatment remains a global challenge for society and public health systems.

1.2 GBM

1.2.1 Angiogenesis of GBM

The contribution of angiogenesis to tumor development was first recognized in 1971⁸. Since then, the impact of angiogenesis on tumor growth has been extensively studied.

Introduction

The collective data have established that tumor angiogenesis boosts tumor development and influences the invasion and metastasis of tumors⁹. A major pathological feature of GBM is the extensive vascularization¹⁰. Consequently, inhibition of angiogenesis has been proposed as a treatment for GBM. Despite promising preclinical data and findings in early clinical trials, randomized clinical trials of patients with GBM anti-angiogenic agents have failed to bestow a survival benefit¹¹. Only bevacizumab (a monoclonal antibody targeting vascular endothelial growth factor [VEGF]) in combination with conventional therapies has proven effective, with a two-month increase in disease-free survival reported¹². However, the study did not find evidence of improved overall mortality. Bevacizumab was approved by the United States Food and Drug Administration (FDA) for the treatment of recurrent GBM. However, it failed to get approval from the European Medicines Agency (EMA)¹³. Hence, there remains an unmet need to develop alternative treatments that aim to inhibit angiogenesis.

1.2.2 Pericytes in GBM

The tumor blood vessels of GBM are tortuous, disorganized, highly permeable, and characterized by abnormalities in their endothelial cell and basement membrane (BM)¹⁴.¹⁵. In the healthy brain, cerebral microvessels have a higher ratio of pericytes to endothelial cells than other tissues¹⁶. The contribution of perivascular cells like pericytes and smooth muscle cells to GBM angiogenesis has attracted a great deal of research interest in recent years. Anatomically, pericytes wrap around the endothelial

Introduction

cells of cerebral microvessels^{17,18}. Classically, pericytes are identified based on their unique location, morphology, and molecular markers. Three markers that are often used to identify pericytes include: platelet-derived growth factor receptor beta (PDGFRB), alpha-smooth muscle antigen (α -SMA), and nerve-glia antigen 2 (NG2)¹⁹. Under physiological conditions, pericytes contribute to the vascular formation, maturation, and maintenance^{20, 21}. In GBM, pericytes are also crucial for neovascularization and invasion²². Angiogenesis is a major hallmark of GBM growth²³. Direct contact and crosstalk between endothelial cells and pericytes tightly regulate blood vessel homeostasis²⁴. Cytokine release from pericytes stimulates endothelial tip-cell sprouting from existing blood vessels and stabilizes newly formed vessels²⁵. In addition, pericytes within GBM maintain a certain degree of vessel stabilization and maturation in some regions of tumors. However, GBM may be characterized by strong intratumoral heterogeneity and other tumor regions.

Poor and disorganized pericyte coverage is often observed in GBM, which allows the tumor to spread²⁶. Very leaky blood vessels in GBM have been hypothesized to enhance tumor invasion and peritumoral edema by increasing intratumoral fluid pressure²⁷. Intratumoral pressure also causes hypoxic microenvironments in GBM by attenuating blood circulation and stimulating the invasion of GBM cells²⁸. GBM-activated pericytes release interleukin-10 (IL-10) and transforming growth factor (TGF). The resulting suppression of antitumor immunity augments tumor growth²⁹. Therapeutically targeting pericytes to inhibit angiogenesis and invasion may thus

Introduction

provide a mechanism to restrict tumor growth and warrants further research³⁰.

To evaluate the function of pericytes in GBM, we employed a pericyte lineage tracing transgenic mouse line (*PDGFRB::CreERT2*, R26-RFP, abbreviated as PDGFRB-WT)³¹ and a pericyte lineage depletion model that features the conditional expression of diphtheria toxin-A (*PDGFRB::creERT2*, R26-RFP, R26-iDTA, abbreviated as PDGFRB-iDTA). Lineage tracing is one of the most reliable methods to reveal cell fate in vivo³².

1.2.3 GBM microenvironment

The brain tumor microenvironment (TME) serves as a critical regulator of tumor progression in malignant brain tumors³³. The GBM microenvironment contains both non-immune and immune cells. Non-immune cells include vascular cells, astrocytes, and neurons³⁴. GBM-associated immune cells include tumor-infiltrating lymphocytes, tumor-associated myeloid cells, and natural killer cells³⁵. Among these, particular attention has been paid to cells involved in the innate immune response, which include tumor-associated microglia/macrophages (TAMs), the most abundant infiltrating non-malignant cell cluster^{36, 37} that comprise up to 30% of the tumor mass in GBM³⁸. Microglia are unique resident macrophages³⁹ of the central nervous system (CNS). During embryonic day E8.5 to E9.5, microglia progenitors migrate from the yolk sac into the primitive brain and generate microglia cells⁴⁰. In GBM, microglia are attracted by tumor cell-derived factors and mostly reside in the peritumoral area⁴¹. Bone marrow-

Introduction

derived macrophages (BMDMs) are derived from hematopoietic stem cells. BMDMs are preferentially located in the main tumor mass and also in the perivascular region of glioma⁴¹. TAMs promote tumor cell proliferation and invasion, modify the extracellular matrix, and induce an immunosuppressive environment^{42, 43}.

The TME also contains different types of stem and progenitor cells, such as neural progenitor cells (NPC)⁴⁴, mesenchymal stem cells^{45, 46}, and oligodendrocyte and progenitor cells (OPCs)⁴⁷. Stem and progenitor cells play different roles in tumor development. NPCs secrete endovanilloids to promote tumor cell death and the tumor suppressive capacity of NPCs declines with age⁴⁴. The TME can also recruit MSCs from the bone marrow or brain perivascular stem cell niche^{46, 48}. Bone marrow mesenchymal stem cells have a strong tropism for tumor cells and inhibit tumor growth by downregulating tumor angiogenesis⁴⁹. OPCs may promote tumor growth by enhancing tumor stemness, chemoradioresistance, and neovascularization in GBM^{50, 51}. However, it has not been determined yet whether other types of stem and progenitor cells exist in GBM.

1.2.4 TAMEP in the GBM microenvironment

Earlier studies in our laboratory discovered a previously unknown short-lived avascular population of tumor-associated cells with a myeloid-like expression profile (TAMEP) in GBM development⁵². These progenitors were traced in a transgenic mouse model, allowing cre-recombinase-mediated lineage tracing under the control of the *Nestin* gene

Introduction

promoter and expression of the stem cell marker SOX2⁵³. Single-cell RNA-Seq data revealed an aberrant myeloid-like expression profile in TAMEP, including the markers PU.1, CD11b, F4/80, and CX3CR1. Moreover, we confirmed that TAMEP do not origin from the myeloid lineage in transgenic lineage-tracing models (*CCR2*-reporters⁴¹ or *Flt3*-based tracing model⁵⁴) and with bone marrow transplantation. In a *Cx3cr1*-creER2 model⁵⁵ in which the microglia and other CNS resident macrophages were identified, we found that the microglia lineage never expressed Sox2. The finding ruled out the possibility that TAMEP are derived from brain macrophages. In our previous study, the co-expression of SOX2 and PU.1 was used to identify TAMEP⁵². To date, SOX2 and PU.1 co-expression has been reported only in certain leukemia subtypes, but not in other diseases⁵⁶. Thus, we concluded that the combined detection of SOX2 and PU.1 is a feasible strategy for the identification of TAMEP. The collective data supports the view that TAMEP and its progenitors are novel cell populations that originate from the CNS and have a myeloid-like expression profile. In this study, we aimed to determine the exact function of TAMEP in GBM progression in more detail and to further explore the molecular mechanisms mediating the pathological effects of TAMEP.

1.2.5 Diagnosis of GBM

In general, the clinical management of GBM includes diagnosis, assessment of disease progression, and prospective treatment efficacies⁵⁷. Accurate diagnosis is important for optimal clinical management. The clinical diagnosis of GBM is usually based on a

Introduction

combination of clinical signs and symptoms, and radiological evaluation⁵⁸. The most typical clinical signs and symptoms of GBM include progressive neurological deficits, motor weakness, headache, and seizure⁵⁹. Imaging assessment includes computed tomography (CT), positron emission tomography (PET), and magnetic resonance imaging (MRI), among others^{60,61}. MRI is the most frequently used diagnostic modality in clinical practice, and its spatial and temporal resolution and tissue contrast have steadily improved⁶². For typical GBM, the conventional T1 sequence of MRI often shows a heterogeneous core (necrosis or hemorrhage) surrounded by a hypointense mass, contrast-enhanced T1-weighted sequence demonstrates a ring-enhancing mass, and the T2/FLAIR sequence reveals a hyperintense mass and indicates the edema⁵⁹. T2/Flair sequence intensity has a strong positive correlation with vascular permeability in glioma⁶³. In glioma patients, high permeability of tumor vessels promotes the diffusion of contrast agents and leads to a stronger signal in the T2/FLAIR sequence. Therefore, peritumoral edema can reflect the vascular permeability of GBM⁶⁴.

1.2.6 Radiogenomic analysis in GBM

The development of high-throughput whole-genome GBM analysis has provided insight into the practical genetic and cellular point-of-origin of GBM^{65,66}. Advances in genomic assays continue to provide new diagnostic tools for more precise and personalized treatment. In a more conventional approach, MRI permits the non-invasive diagnosis, prognostic analysis, and treatment planning of GBM patients⁶⁷. In

Introduction

MRI, GBM tumors exhibit pronounced phenotypic features, such as peritumoral edema, tumor contrast enhancement, tumor necrosis, and tumor mass⁶⁸. If these phenotypic features of GBM obtained from MRI can be associated with specific gene expression, imaging phenotypes will serve as non-invasive surrogates for cancer genomic events and will supply vital information for diagnosis, prognosis, and treatment. Complementary opportunities for high-throughput whole-genome GBM analysis and MRI have led to the emergence of a field called “radiogenomics.” In this study, I investigated the potential function of the vascular regulatory molecules Apelin (APLN) and Ang2 (ANGPT2) in the vasogenic edema of GBM using radiogenomic data from The Cancer Genome Atlas (TCGA) and the Chinese Glioma Genome Atlas (CGGA) genomic databases, and corresponding MRI data from The Cancer Imaging Archive (TCIA).

1.2.7 Role of APLN in the angiogenesis of GBM

APLN is an endogenous ligand of the G protein-coupled receptor APJ (APLNR)⁶⁹. Apelin-77, an APLN precursor peptide, consists of 77 amino acids and is post-processed by endopeptidases to generate different active APLN isoforms, including APLN-12, APLN-13, APLN-17, APLN-19, APLN-26, and APLN-36⁷⁰. The role of APLN in promoting angiogenesis is well established under physiological conditions⁷¹. In addition, APLN is also involved in pathological blood vessel sprouting (angiogenesis) in many diseases, including cerebral ischemic stroke, cardiac ischemia, and tumors⁷².

Introduction

Especially in cancer, a growing body of evidence shows that APLN could be an essential regulator of angiogenesis^{73, 74}. Overexpression of APLN and its receptor has been observed in clinical GBM biopsies⁷⁵. Targeting APLN/APLNR can improve the efficiency of the inhibition of angiogenesis and reduce the pro-invasive side effects of bevacizumab in GBM⁷⁴. The association between APLN and angiogenesis has made APLN a popular topic in GBM research^{76, 77}. Moreover, a correlation between peritumoral edema and vascular permeability has been described in GBM⁶⁴. Given the close relationship between the APLN and tumor angiogenesis, we hypothesized that there is a correlation between APLN and peritumoral edema in GBM patients.

1.2.8 Role of ANGPT2 in the angiogenesis of GBM

Angiopoietins (ANGPTs) and Tie2 form a specific-angiogenic ligand-receptor complex, which has a crucial function in tumor angiogenesis⁷⁸. Three ANGPTs have been described in humans: angiopoietin-1 (ANGPT1), angiopoietin-2 (ANGPT2), and angiopoietin-4 (ANGPT4)⁷⁹. Among these, ANGPT1 and ANGPT2 are well characterized as human Tie2 ligands. ANGPT1 is widely expressed in perivascular cells and maintains the integrity of blood vessels^{80, 81}. ANGPT2 is an angiogenic growth factor that drives vessel angiogenic sprouting, co-option and remodeling^{82, 83, 84}. ANGPT2 is highly expressed in GBM and is absent in normal human brain endothelium⁸⁵. ANGPT2 expression reduces pericyte coverage and destabilizes the tumor vasculature by partially antagonizing ANGPT1 in GBM^{85, 86}. Given the close

Introduction

relationship between ANGPT2 and tumor vessel destabilization⁸⁷, we explored whether ANGPT2 is associated with peritumoral edema in GBM patients. This thesis study combined mRNAseq data and MRI data obtained from public databases to explore the correlation between peritumoral edema of GBM patients with APLN and ANGPT2 mRNA expression levels.

1.3 Objectives

The aims of this thesis are:

- a) To investigate the different functions of host-derived pericytes in the early and advanced stages of GBM using a pericyte-depletion, transgenic mouse model.
- b) To evaluate the effects of TAMEP on GBM expansion and angiogenesis using a TAMEP specific depletion model.
- c) To assess the roles of APLN and ANGPT2 in GBM using radiogenomics data from the TCGA and CGGA databases.

Materials

2. Materials

2.1 Devices

Table 2.1 Devices

Equipment / Software	Company
Axiovision rel. 4.8 / 4.9 software	Carl Zeiss
AngioTool software	NIH
Balances-AG204	Mettler Toledo
Balances-monoBloc	Mettler Toledo
Centrifuge	Thermo Fisher Scientific/Eppendorf
Clamp mount micromanipulators	ADInstruments
Countess II FL automated cell counter	Thermo Fisher Scientific
Digital vortex mixer	VWR
Electrophoresis system	Bio-RAD
Electrophoresis tank	multiSUB
Fridge (4°C, -20°C)	Liebherr
Freezer (-80°C)	Thermo Fisher Scientific
Hera safe hood	Thermo Fisher Scientific
Incubator	Thermo Fisher Scientific
LAS X software	Leica Microsystems
Leica SP8X wll upright confocal microscope	Leica Microsystems
Leica DMI8 inverted confocal microscope	Leica Microsystems
Magnetic hotplate stirrer	VWR

Materials

Microliter syringe	Hamilton
Micropipette (10 µl, 20 µl, 100 µl, 200 µl, 1000 µl)	Eppendorf
Microscope axioskop 2	Carl Zeiss
Microscope axiovert 25	Carl Zeiss
Microscope camera axiocam	Carl Zeiss
Microtome slide 2003	PFM medical AG
Microwave	Siemens
Mastercycler nexus gradient	Eppendorf
Olympus-BX53-microscope	Olympus Europe
Perfusion system dose IT P910	Integra Biosciences AG
pH meter WTW multical bench	Sigma Aldrich
Pipette boy	Eppendorf
Photoshop online version	Adobe
Shaker	Biozyme Scientific
Infinite® 200 PRO	Tecan
Stereotactic frame	Stereotactic Frame
Surgical instruments	Aesculap
Water bath	Memmert

2.2 Consumables

Materials

Table 2.2 Consumables

Product	Supplier	Cat No.
Alzet brain infusion Kit 3	ALZET	125-1613
Alzet osmotic pump model 1002	ALZET	NC0551767
Cell culture flask (T25)	TPP	90026
Cell culture flask (T50)	TPP	90076
Cell culture flask (T75)	TPP	90151
Centrifuge tubes (0.5 ml)	Eppendorf	0030121.023
Centrifuge tubes (1 ml)	Eppendorf	0030121.694
Centrifuge tubes (2 ml)	Eppendorf	0030121.094
Centrifuge tubes (15 ml)	TPP / Falcon	91015
Centrifuge tubes (50 ml)	TPP / Falcon	91051
Cover slips	Gerhard Menzel	9.160829
Ethibond excel (5-0) sutures	Ethicon	389065
Microtome blade A35	Feather	36-099-2334
Pap-pen	Dako	S2002
Pipette tips (10 µl, 100 µl, 200 µl, 1000 µl)	Eppendorf	3123000020/3123000047/ 3123000055/ 3123000063
Plate (6wells)	TPP	Z707775
Scalpel (#15)	Feather	504172
Syringe (1 ml)	B. Braun Melsungen AG	9166017

Materials

Syringe needle (30G)	B. Braun Melsungen AG	305400
Tissue-tek-cryomold (15 mm × 15 mm × 5 mm)	Sakura Finetek	25608-924

2.3 Cell culture materials

Table 2.3 Cell culture materials

Material	Catalog Number	Supplier
DMEM	FG0415	Biochrom
Fetal bovine serum	10270-106	Life Technologies
Penicillin-streptomycin	15140-122	Life Technologies
Trypan-blue Solution 0.4%	T8154	Sigma Aldrich
Trypsin/EDTA	L2153	Merck Millipore

2.4 Reagents and Chemicals

Table 2.4 Reagents and Chemicals

Product	Supplier	Catalog Number
Acetone 100%	Sigma Aldrich	67-64-1
Agarose	Sigma Aldrich	9012-36-6
Aqua	B. Braun Melsungen AG	67240920000
Aquatex mounting medium	DAKO	S3023
Bepanthen	Bayer	82290583
Bull serum albumin	Sigma Aldrich	9048-46-8

Materials

CaCl ₂ · 2H ₂ O	Sigma Aldrich	10035-04-8
Citric acid monohydrate	Sigma Aldrich	77-92-9
DAPI	Fluka	32670
DC101	Eli Lilly	293VE
Donkey serum	Jackson ImmunoResearch	017-000-121
Dextran, biotin, 70,000 MW	Invitrogen	D1957
Dextran, fluorescein, 2,000,000 MW	Invitrogen	D7137
Evans Blue	Sigma	314-13-6
Eosin solution	Sigma Aldrich	15086-94-9
Ethanol 100%	Carl Roth	64-17-5
Ethanol 70%	Carl Roth	64-17-5
Ethanol 96%	Carl Roth	64-17-5
Ethylene glycol	Sigma Aldrich	107-21-1
Glycerol	Sigma Aldrich	56-81-5
HCl	Sigma Aldrich	7647-01-0
Isopropanol	Sigma Aldrich	67-63-0
KCl	Sigma Aldrich	7447-40-7
Ketamin 10%	Zoetis Deutschland GmbH	4025270000
MgCl ₂ · 6H ₂ O	Sigma Aldrich	7791-18-6
Na ₂ HPO ₄ · 7H ₂ O	Sigma Aldrich	7782-85-6
NaCl 0.9%	B. Braun Melsungen AG	69488220000
NaH ₂ PO ₄ · H ₂ O	Sigma Aldrich	10049-21-5
Paraformaldehyde (PFA)	Sigma Aldrich	30525-89-4

Materials

PBS	Apotheke Klinikum der Universität München	-
Pentobarbital (Narcofen®)	Merial	798-594
Povidone iodine solution 7.5%	B. Braun Melsungen AG	1588716
Protein block serum-Free	Dako	X0909
Rompun 2%	Bayer	PZN-1320422
Roti® Histol	Carl Roth	6640.1
Sucrose	Sigma Aldrich	84100-250G
Tri-natriumcitrat-dihydrat	Sigma Aldrich	6132-04-03
Tris base	Sigma Aldrich	77-86-1
Triton X-100	Roche Diagnostics	93418
Tween-20	Sigma Aldrich	2001-0250

2.5 Primary antibodies

Table 2.5 Primary antibodies

Antigen	Host Species	Isotype	Dilution	Catalog number	Provider
GFP	Goat	IgG	1:500	R1091P	Acris
CD31	Rat	IgG	1:50	550274	B & D
PDGFR- β	Goat	IgG	1:200	AF1042	R&D
Humanin	Rabbit	IgG	1:100	PA1-41325	Thermo Fisher
Iba1	Goat	IgG	1:400	ab5076	Abcam
Ki67	Rabbit	IgG	1:200	ab16667	Abcam
vWF	Rabbit	IgG	1:400	A0082	Dako

Materials

Aquaporin4	Rabbit	IgG	1:400	AB2218	Millipore
Glut1	Rabbit	IgG	1:400	Ab652	Abcam
Collagen4	Rabbit	IgG	1:200	148826	Bio-Rad

2.6 Secondary antibodies

Table 2.6 Secondary antibodies

Conjugate	Antigen	Host Species	Dilution	Catalog number	Provider
Alexa fluor 488	Goat IgG	Donkey	1:500	705-545-147	Jackson Immuno Research
Alexa fluor 594	Rabbit IgG	Donkey	1:500	711-585-152	Jackson Immuno Research
Alexa fluor 647	Goat IgG	Donkey	1:500	705-605-147	Jackson Immuno Research
Biotinylated	Goat IgG	Horse	1:200	BA9500	Vector
Biotinylated	Rabbit IgG	Donkey	1:200	711-065-152	Jackson ImmunoResearch

2.7 Streptavidin conjugates

Table 2.7 Streptavidin conjugates

Conjugation	Dilution	Catalog number	Provider
Alexa fluor 488- streptavidin	1:500	016-540-084	Jackson ImmunoResearch

Materials

conjugate			
Alexa fluor 594-streptavidin conjugate	1:500	016-580-084	Jackson ImmunoResearch
Alexa fluor 647-streptavidin conjugate	1:500	016-600-084	Jackson ImmunoResearch

2.8 Mouse strains

Table 2.8 Mouse strains

Mouse Strains	Abbreviated as:
PDGFRB::CreERT2, Ai9-tdTomato mice	PDGFRB-WT
PDGFRB::CreERT2, R26 LSL diphtheria toxin subunit alpha (DTA), Ai9-tdTomato mice	PDGFRB-iDTA
Nestin::CreERT2, Ai9-tdTomato mice	Nes-RFP or Sox2-WT
Nestin::CreERT2, SOX2 ^{fl/fl} , Ai9-tdTomato mice	Sox2-KO
APLN knockout mice	APLN-KO
APLN wild type mice	APLN-WT

3. Methods

3.1 Cell culture

The GL261 glioma cell line derived from C57BL/6 mice was obtained from the NCI (Frederick, MD, USA). GL261 cells were cultured in DMEM medium and supplements with 10% FBS, 1X MEM non-essential amino acids, 1% penicillin-streptomycin. These cells were maintained in a 37°C humidified incubator with a 5% CO₂ atmosphere.

3.2 Animal experiments

3.2.1 Animal care

All animal experiments were approved by the Institutional Animal Care and Use Committee of the Regierung von Oberbayern and were performed according to the Animal Protection Guidelines of Germany. All animals were kept at Walter-Brendel Experimental center in standard cages under conventional laboratory conditions (12 h/12 h light/dark cycle, 22°C) with water and food ad libitum.

3.2.2 Tamoxifen sensitivity of Nestin-creERT2 mouse-strains

Genetic lineage tracing is the most effective and commonly used method for studying the origin and fate of specific cell types. Tamoxifen-induced nuclear accumulation of Cre-recombinase (Cre-ERT2) activating the inheritable expression of a fluorescent reporter (R26-lsl-tdTomato) allows tracing different cell populations under the control of gene-promoters⁸⁸. We worked with two different *Nestin::CreERT2* models^{89,90}. For

Methods

comparing the sensitivity of cre-recombinase to tamoxifen between two models, we divided the comparison into two groups, low dose tamoxifen (75 mg/kg) treatment group and high dose tamoxifen (180 mg/kg) treatment group. Tamoxifen (75mg/kg or 180mg/kg) was injected intraperitoneally for three consecutive days and the brains were collected at 6 h after the last injection.

3.2.3 Tumor implantation

Mice were anesthetized with 7 μ l/g body weight using an anesthetic containing 0.36 ml 2% Rompun, 1.02 ml 10% Ketamine and 4.86 ml 0.9% NaCl (intraperitoneal injection). Then mice were immobilized in a stereotaxic mouse frame. Bepanthen cream was applied to keep the eyes moist and protected. A sagittal skin incision was made along the head's midline, and a hole was drilled on the skull 1.0 mm anterior and 1.5 mm lateral (right) to bregma. Then 1 μ l of glioblastoma cell suspension (1×10^5 , GL261, in cell-culture medium with serum) was injected by a 30G Hamilton syringe over a time-course 2 min. The Hamilton syringe was perpendicularly inserted to a depth of 4 mm and then retracted to a depth of 3mm to create a cavity for the injection cells. After the injection, the needle was removed at the rate of 1 mm/min. Finally, complete hemostasis was confirmed, and the wound was cleaned and sutured carefully. For cre activation in all experimental paradigms, tamoxifen was administered i.p. to mice 75 (mg/kg daily) for three consecutive days.

Methods

3.2.4 Intracerebral application of substances

The day before implantation, Alzet osmotic pumps were loaded with appropriate substances (DC101, aCSF) and allowed to prime overnight at 37°C until the time of implantation. Osmotic minipumps were implanted subcutaneously in the dorsal midline of the animals under anesthesia. The pumps and brain infusion equipment (Brain infusion kit 3) were connected following the manufacturer's instructions. Then infusion tips were at the site of tumor cell implantation.

3.2.5 Mice cerebral ischemic stroke model

After anesthesia transient cerebral ischemia was induced by a simplified protocol blocking the right middle cerebral artery (MCA) for one hour with a silicone-coated 8-0 Doccoc monofilament. For sham surgery controls, the filament was shortly advanced to the MCA and retracted immediately. During the operation procedures, body temperature was kept at physiological levels with a heating pad. One hour after the occlusion, the filaments were withdrawn to restore blood flow. For cre activation, tamoxifen was administered i.p. to mice 75 (mg/kg daily) at days 0, 1, 2, and the brain tissues were collected on day 7 for further analysis.

3.2.6 Analysis of vascular permeability by Evans Blue assay

The Vessel permeability was assessed by leakage of the Evans Blue dye after intravenous injection of Evans Blue: Tumors were allowed to grow for three weeks,

Methods

Evans Blue dye (200 μ l of 2% (w/v)) was intravenously administered 2 h before the mice were sacrificed. The brains were then extracted and the cerebellum removed, the cerebral were dissected into the tumor and tumor-free hemisphere along the sagittal midline. Brain hemispheres were weighed and homogenized in dimethylformamide (DMF) (150g: 400ul, weight-to-volume ratio). The homogenate was incubated in a 37°C oven for 30 min and placed at 4°C overnight, then centrifuged at 16,000 g for 45 min. After centrifugation, the supernatants were collected. In addition, the absorbance was measured at a wavelength of 620 nm. The concentrations of Evans Blue were calculated by comparing the absorbance to an Evans Blue standard curve. Absolute values for absorbance are represented per samples or values of the tumor hemispheres normalized to each model's average tumor volume.

3.2.7 Dextran leakage assay

To study the local vessel permeability, a 100 μ l fixable dextran mixture containing 50 μ l fluorescein-isothiocyanate (FITC)-labeled 2 MDa (Million Dalton) dextran and 50 μ l biotin-conjugated 70 KDa (Kilo Dalton) dextran dissolved in saline were administered via tail vein injection. At three weeks after tumor cell implantation, mice were injected with 100 μ l dextran mixture (as described previously) 15 min before perfusion. Brains were carefully removed from the skulls and placed in 4% PFA for post-fixation (4°C, 48 h) followed by 30% sucrose until the tissues sank to the bottom of the container. Frozen brains were cut into 40 μ m horizontal sections with a cooled

Methods

sliding microtome. After immunostaining, brain sections were inspected obtained by confocal laser scanning microscopy (TCS SP8, Leica). All images were acquired at identical laser/gain settings between experimental groups and they were processed using the same intensity thresholds. For quantification of 2 MDa Fluorescein-dextran, four images (40x vision) located within the tumor per section on three sections per mouse (12 in total) were acquired. ImageJ software was used to measure the areas of interest.

For quantification of the 70 KDa biotin-dextran leakiness, the sections were scanned with the tile scan function (40x magnification, 16 fields) of the confocal microscope (TCS SP8, Leica) after immunostaining for biotin. The tile scan module allows the user to automatically assemble an image from multiple smaller images. The total area of the 70 KDa biotin-dextran (stained with Cy5-streptavidin) in the tumor parenchyma was assessed by ImageJ. 70 KDa biotin-dextran leakage into the tumor parenchyma was obtained by subtracting the 2 MDa Fluorescein-dextran area from the 70 KDa biotin-dextran (Cy5-stained) area.

3.3 Histology

3.3.1 Perfusion and tissue processing

Animals were deeply anesthetized, followed by PBS and PFA (4%) perfusion. After continuous perfusion, brains were harvested and post-fixed by PFA for 48 h, followed by 30% sucrose dehydration. Next, the brains were embedded in OCT compound and

Methods

frozen. Frozen brains were cut into 40 μm horizontal sections by a frozen sliding microtome. All sections were collected and consecutively sampled into cryoprotectant (Glycerol, Ethylene glycol, and 0.01 M PB at a volume ratio of 1:1:2). Samples were stored at -20°C .

3.3.2 H&E staining

The tissues were stained with hematoxylin and eosin (H&E) to allow histopathological inspection and to calculate the tumor volume. The sections were washed in PBS and then mounted onto slides before being allowed to air dry for 30 min. Subsequently, slides are dehydrated in 100% ethanol for 30 seconds followed by hematoxylin solution for 2 min; then the slides were washed in running tap water for 5 min and stained with 0.5% Eosin solution for 30 seconds, and then rinsed with distilled water. After staining, all slides were dehydrated in graded ethanol (70%, 96%, and 100% ethanol, one min each) and histol and then cover slides with Entellan® mounting medium. Pictures for H&E staining of each tissue were acquired by a Carl Zeiss Microscope Axioskop 2 with AxioCam MRm and Axiovision Rel. 4.9 software.

3.3.3 Cresyl-violet (Nissl) staining

To determine the exact final position of the ischemia and visualize neuronal cells, we performed Nissl staining. The slides were washed with 0.01 M PBS, five min with three repetitions, and stained with 0.5% cresyl violet solution for 15 min. The slides were

Methods

then washed with distilled water. After staining, all slides were dehydrated in graded ethanol (70%, 96%, and 100% ethanol, one min each) and histol and then cover slides with Entellan® mounting medium. Pictures for Nissl staining of each tissue were acquired by a Carl Zeiss Microscope (Axioskop 2).

3.3.4 Quantification of tumor volume

Tumor volume was measured as described in a previous study⁴⁴. 21 days after implantation of GL261 cells, brains were consecutively cut into 40 µm-thick horizontal sections. In 1.24 to 5.02 mm from dural surface, every 6th axial sections were collected and mounted on slices. According to the Cavalieri principle, tumor volume was quantified by determining the tumor area in every sampled brain sections⁴⁴. The height of the tumor on the Z-axis was determined by the highest and lowest sections containing GBM. This Z-axis was multiplied with the average tumor volume per section to get the tumor size.

3.4 Immunofluorescence staining

3.4.1 Immunofluorescence staining of mouse brain sections

The free-floating sections were usually stored at 24-well plates filled with cryoprotectant at -20°C. Firstly, 3-5 floating sections were collected from the stored 24-well plates to a 12-well plate with PBST (0.1% Tween-20 in 1× PBS) and washed the sections with PBST three times (5 min each time) at room temperature (RT) on an

Methods

orbital shaker. Subsequently, the sections were blocked with protein blocking buffer (5% normal donkey serum and 0.3% Triton X-100 in 1× PBS) at room temperature (RT) for one hour. Sections were then incubated with primary antibodies in blocking buffer at 4°C overnight. Primary antibodies and working dilutions that were used in this study are listed as follows: rat anti-CD31 (1:50), goat anti-PDGFRb (1:200), goat anti-Sox2 (1:400), and rabbit anti-Pu.1 (1:100), rabbit anti-glut1 (1:200), rabbit anti-collagenIV (1:400), rabbit anti-Aquaporin4 (1:400). The following day, sections were washed 3 times for 5 min with PBST and incubated with the secondary antibodies (fluorescent conjugated secondary antibody or streptavidin-conjugated secondary antibody) for two hours at RT. For the streptavidin-conjugated secondary antibodies, sections were washed again with PBST and incubated with third antibody (anti-streptavidin antibody), 1 hour at RT. After three washes in PBST, DAPI (1:10,000) was added to stain the nuclei, 5 min at RT. Sections were mounted on slides and covered with fluorescent mounting medium (DAKO). Pictures were taken by confocal microscopy (TCS SP8, Leica) and quantified by ImageJ software.

3.4.2 Quantification of tumor microvascular pattern

A software AngioTool was used to analyze the tumor area vessels following CD31 staining to reveal the vasculature network in different experimental groups⁹¹. Pictures were obtained by confocal microscopy (TCS SP8, Leica), and performed angiogenesis assessments in AngioTool, which computed the branching index and several other

Methods

morphometric parameters such as total analysis area, total vessel length, number of endpoints, number of junctions and vessel density. Total vessel length means the sum of Euclidean distances between the pixels of all the vessels in the image; total number of endpoints means the number of open-ended segments in the image; total number of junctions is the total number of vessel junctions in the image⁹¹.

3.5 Bioinformatics analysis on clinical data from public database

3.5.1 Data collection and preprocessing

TCGA-GBM Illumina HiSeq (RSEM normalized) mRNA dataset and patients' clinical data were obtained from the FIREHOSE Broad GDAC (<https://gdac.broadinstitute.org/>). The MRI imaging data were collected from TCIA (<http://cancerimagingarchive.net/>) database and measured by OHIF Viewer TCIA ALPHA (<https://www.cancerimagingarchive.net/viewer/>). We used two sequences for this study: T2-Flair and T1 weighted contrast (T1C), T1C for segmentation enhancement (defined as the tumor) and necrosis, and T2-Flair sequences in GBM patients for tumor edema and infiltration^{92,93}. Since the tumor volume showed apparent differences between patients, we used edema index⁹⁴, T2-Flair tumor volume, and T1C volume ratio to eliminate tumor size and get a more accurate reflection for peritumoral edema. For validation, the CGGA-GBM Illumina HiSeq (RSEM normalized) mRNA dataset and clinical data of survival were obtained from the CGGA data portal (<http://www.cgga.org.cn/>).

3.5.2 Pan-cancer gene expression analysis in TIMER2.0

Gene differential expression (Gene-DE) module of TIMER2.0 (cistrome.shinyapps.io/timer)⁹⁵ was used to analyze APLN expression levels in TCGA pan-cancer datasets. Gene-DE module allows users to study the differential expression between tumor and adjacent normal tissues for any gene of interest across all TCGA tumors.

3.5.3 Gene correlation analysis in LinkedOmics

In this study, co-expression genes of APLN and ANGPT2 were assessed for the TCGA GBM dataset using LinkedOmics⁹⁶ (<http://www.linkedomics.org/login.php>). LinkedOmics is an online platform for exploring and visualizing multi-dimensional genomics datasets in 32 types of TCGA cancer⁹⁶. Pearson's correlation coefficient was used to assess APLN and ANGPT2 co-expression genes. Heatmaps were used to visualize the associated genes.

3.5.4 Kaplan–Meier plots

Kaplan–Meier plots were generated to demonstrate the correlation between overall survival and APLN and/or ANGPT2 gene expression levels. The relationship was tested by log-rank test. $P < 0.05$ was considered significant. The normalized expression data for each gene was divided into high and low groups. High or low expressions were

Methods

defined as gene expressions higher or lower than their mean expression (RSEM genes normalized data) in the TCGA and CGGA databases.

3.5.5 Gene set enrichment analysis

Gene set enrichment analysis was performed using Metascape (<https://metascape.org>)⁹⁷ with GO biological processes and pathway enrichment analysis. We performed enrichment analysis on APLN and ANGPT2-associated genes in GBM.

3.6 Statistics

All statistical analysis was performed by GraphPad Prism 6 software (GraphPad Software, Inc. CA. USA). Statistical significance of survival curves was calculated using the log-rank test. Differences between two groups were assessed using Student's t-test and the differences among more than two groups were examined by one-way ANOVA. P values less than or equal to 0.05 were used as a criterion for a statistically significant difference.

4. Results

4.1 Different roles of pericytes in early and advanced GBM

4.1.1 Pericyte lineage-tracing and -depleting models

In this experiment, a pericyte lineage tracing model (*PDGFRB::creERT2*, R26-RFP mice, abbreviated as PDGFRB-WT) and pericyte lineage depletion model conditionally expressing diphtheria toxin-A (*PDGFRB::creERT2*, R26-RFP, R26-iDTA, abbreviated as PDGFRB-iDTA) were used to evaluate the functions of pericytes in the different stages of GBM. The experiment contained three groups: a control group (PDGFRB-WT) and two pericyte-depletion groups (PDGFRB-iDTA Group-1 and PDGFRB-iDTA Group-2). In PDGFRB-iDTA Group-1, tamoxifen was administered on days 0, 1, and 2 after tumor inoculation to deplete the pericytes in the early stage of tumor formation. The PDGFRB-iDTA Group-1 was an early pericyte-depletion GBM model. In PDGFRB-iDTA Group-2, tamoxifen was administered on days 10, 11, 12, 16, 17, and 18 after tumor inoculation to deplete the pericytes in the advanced stage tumor expansion. PDGFRB-iDTA Group-2 was a pericyte-depletion model for advanced GBM. Confocal microscopy of the control group (PDGFRB-WT) showed that PDGFRB-RFP+ cells were located along vessels and were negative for the CD31 endothelial cell marker. (Figure 1D). PDGFRB-RFP+ cells were identified as pericytes based on their location, morphology, and protein expression profile. In the PDGFRB-iDTA Group-1 early pericyte-depletion GBM model, the number of PDGFRB-RFP+ cells was much lower than in the PDGFRB-WT control group (Figure 1B, C). The

Results

findings indicate that using PDGFRB-iDTA model successfully reduced the number of pericytes in the GBM environment. Interestingly, no significant alteration in the number of PDGFRB-RFP⁺ cells and pericyte coverage was found between the advanced pericyte-depletion GBM model and control group (Figure 1B-D, F).

Results

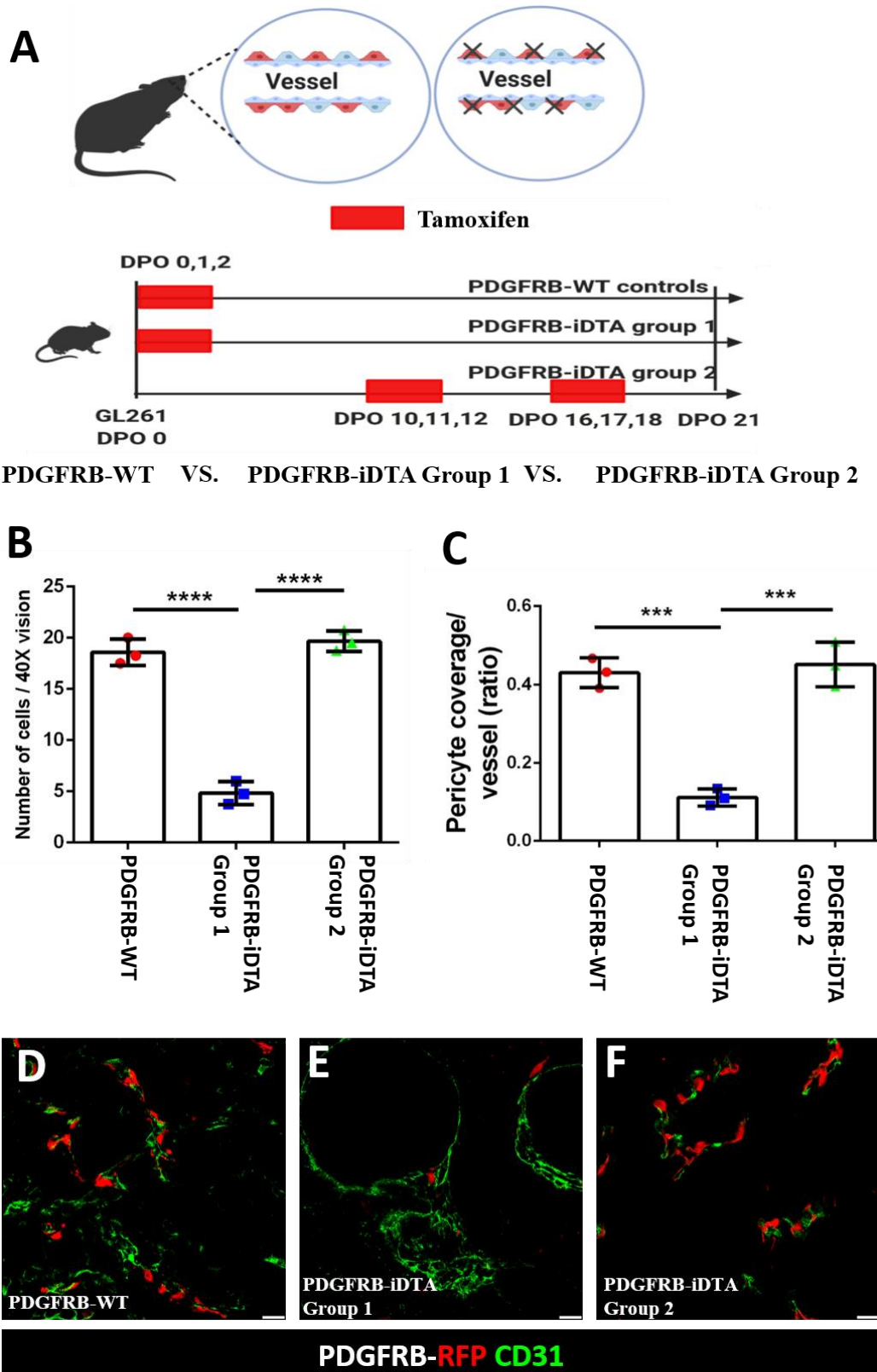


Figure 1 | Pericyte lineage-tracing and -depletion models.

(A) Schematic diagram of the experimental procedure in PDGFRB-WT (control), PDGFRB-iDTA Group-1, and PDGFRB-iDTA Group-2. Tamoxifen indicates

Results

tamoxifen injection days. Brains were harvested in all groups at day 21. (B) PDGFRB-RFP+ cells were observed by confocal microscopy and the number of RFP+ cells was quantified. (C) Quantification of PDGFRB-RFP+ pericyte-coverage on CD31+ microvessels in the tumor area. (D) Representative image of CD31 (green) immunostaining in the tumor areas of the PDGFRB-WT group shows the traced vascular PDGFRB-RFP+ (red) cells. (E) Representative image of CD31 (green) immunostaining shows successful depletion of PDGFRB-RFP (red) cells in the tumor area of the PDGFRB-iDTA Group-1. (F) Representative image of CD31 (green) immunostaining shows traced vascular PDGFRB-RFP (red) cells in the tumor area of the PDGFRB-iDTA Group-2. Statistical significance according to one-way ANOVA with post-hoc test is expressed as * $P < 0.05$, ** $P < 0.01$, *** $P < 0.001$, and **** $P < 0.0001$. Each dot shows the average data acquired from a single mouse. Values are presented as mean \pm SD. Scale bar, 20 μm .

4.1.2 Pericyte reduction in pericyte-depletion advanced GBM model

The previous section showed that the number of PDGFRB-RFP+ cells covering GBM blood vessels did not differ between the advanced pericyte-depletion GBM model and the control group. Hence, we investigated the number of PDGFRB-RFP+ cells in GBM at DPO14 to determine whether the numbers of pericytes were reduced rapidly and transiently in the pericyte-lineage-depletion model groups after the addition of tamoxifen at DPO10, 11, and 12. A schematic of the experiment is presented in Figure 2A. The number of PDGFRB-RFP+ cells in the tumor-free area and GBM region was markedly decreased in PDGFRB-iDTA mice compared to PDGFRB-WT controls (Figure 2A, B; middle panel). Moreover, leakage of the 2 MDa FITC-dextran vascular intra-luminal tracer was increased in PDGFRB-iDTA mice compared to PDGFRB-WT controls (Figure 2B, C; lower right panels). These results confirmed the depletion of pericytes in the depletion models and indicated an increased vascular permeability in the advanced GBM model.

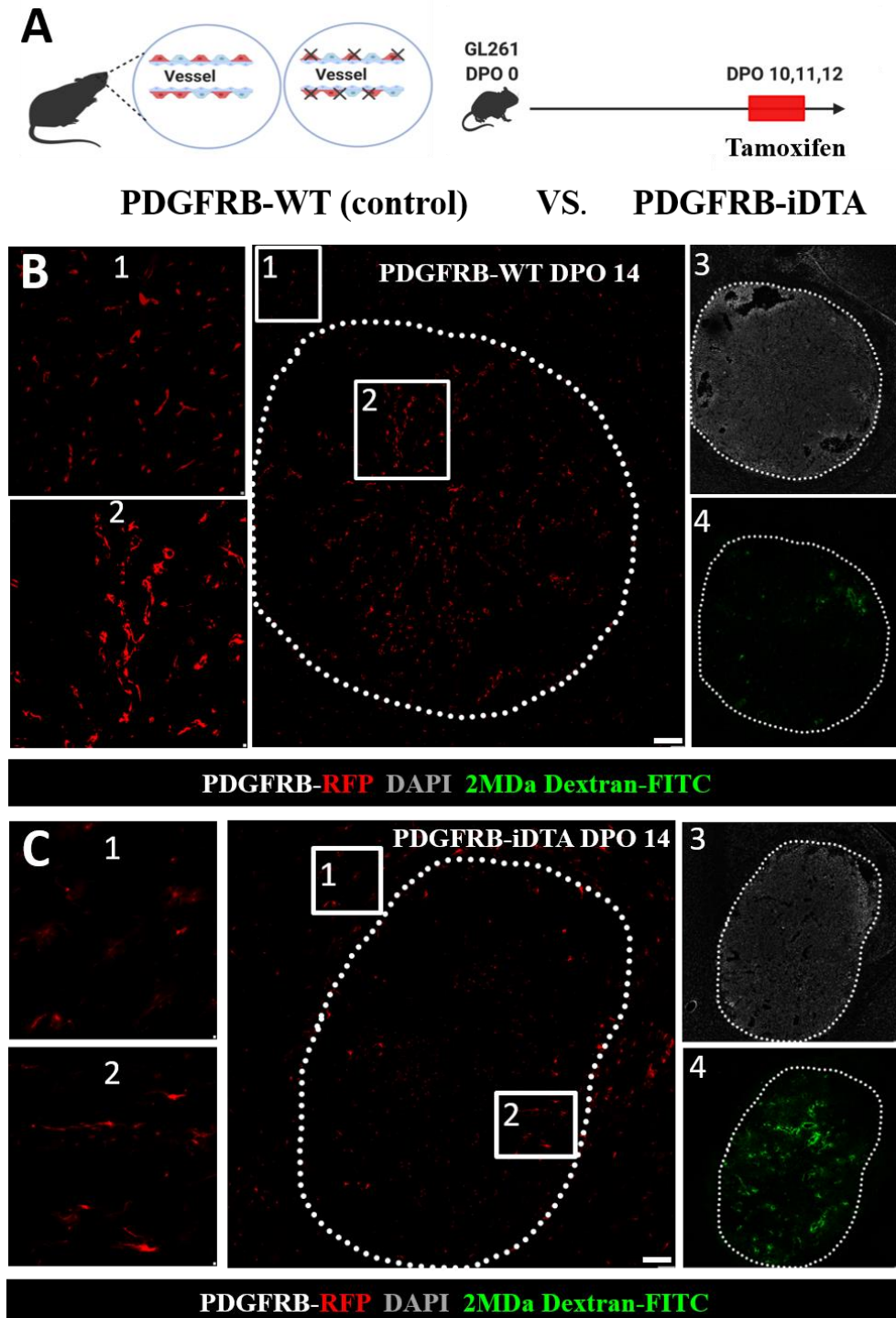


Figure 2 | Pericyte reduction in pericyte-depletion models.

(A) Schematic diagram of the orthotopic transplantation procedure in PDGFRB-WT controls and PDGFRB-iDTA mice. Brains were harvested in all groups at day 14. (B) The middle panel displays the representative distribution of PDGFRB-RFP+ cells in tumors and adjacent tumor-free tissue of PDGFRB-WT controls. Left panels (1, 2) are

Results

enlarged images from the corresponding regions (1, 2) of the middle panel. The result of the DAPI stained nuclei of cells is shown in the right upper panel (3). 2 MDa FITC-dextran staining is shown in the right lower panel (4) (n = 3). Dashed lines delineate the tumor margin. (C) The middle panel displays the representative distribution of PDGFRB-RFP+ cells in tumors and adjacent tumor-free tissue of PDGFRB-iDTA mice. Left panels (1, 2) are enlarged images from the corresponding regions (1, 2) of the control image. Nuclear DAPI staining is shown in the right upper panel. 2 MDa FITC-dextran staining is shown in the right lower panel (n = 1). Dashed lines delineate the tumor margin. Scale bar, 200 μ m.

4.1.3 Replenishment of pericytes in tumor-free areas

The results in the preceding section indicate that GBM has a rapid compensatory mechanism that may replenish pericytes shortly after their transgenically induced ablation. This possibility was formally investigated in an experiment summarized in Figure 3A. At day 4 following the addition of tamoxifen, PDGFRB-RFP+ cells of the tumor-free brain were markedly decreased in the PDGFRB-iDTA group compared to the PDGFRB-WT controls (Figure 3B-D). In contrast, at 21 days after tamoxifen administration, the number of RFP+ cells did not differ between pericyte-depleted models and the control group. (Figure 3E-G). The findings indicate that pericyte replenishment also occurred in the tumor-free brain.

Results

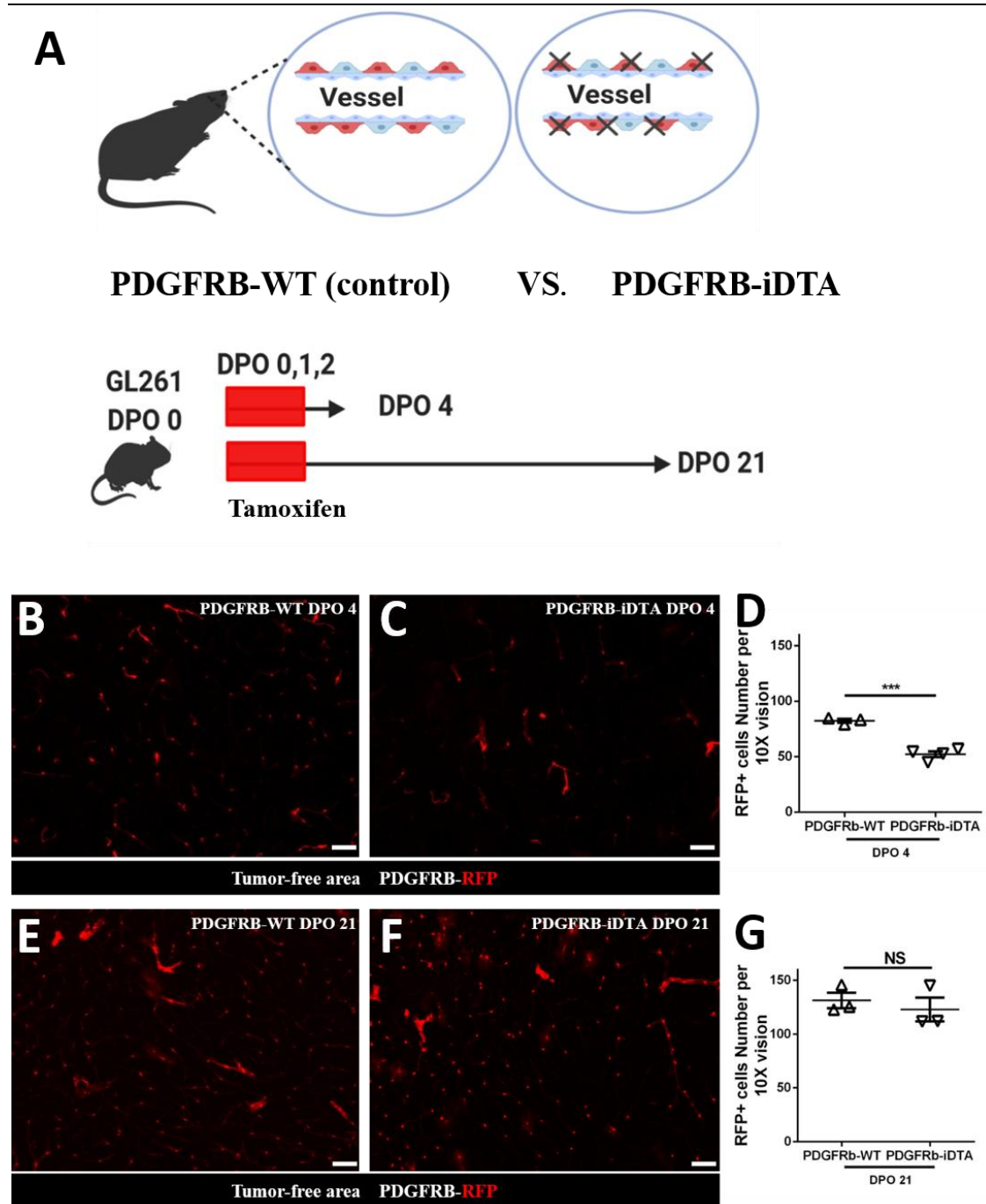


Figure 3 | Pericytes are replenished in tumor-free areas.

(A) Schematic diagram of the orthotopic transplantation procedure in the PDGFRB-WT controls and PDGFRB-iDTA mice. Brains were harvested on DPO 4 or DPO 21. (B) The representative distribution of PDGFRB-RFP+ cells in tumor-free tissue of PDGFRB-WT mice. (C) The representative distribution of PDGFRB-RFP+ cells in tumor-free tissue of PDGFRB-iDTA mice. (D) Quantification of PDGFRB-RFP+ cells at 10 \times magnification at day 4 in the PDGFRB-WT and PDGFRB-iDTA groups. (E, F) Representative PDGFRB-RFP+ cell distribution in tumor-free tissue at day 21 of PDGFRB-WT and PDGFRB-iDTA groups. (G) Quantification of PDGFRB-RFP+ cell

Results

at 10× magnification at day 21 in the PDGFRB-WT and PDGFRB-iDTA groups. Statistical significance using unpaired two-tailed Student's t-test (in B and C), * P<0.05, ** P<0.01, *** P<0.001. Each dot shows average data acquired from a single mouse. Values are presented as mean ± SEM. Scale bars, 200 μm.

4.1.4 Pericyte ablation inhibits the expansion of GBM

To determine the role of pericytes in the development of GBM, their effects on tumor growth were analyzed. The experiment is summarized in Figure 4A. In PDGFRB-iDTA Group-1, tamoxifen was administered on days 0, 1, and 2 after tumor inoculation to deplete the number of pericytes in the early stage of tumor development. In the PDGFRB-iDTA Group-2, tamoxifen was administered on days 10, 11, 12, 16, 17, and 18 after tumor inoculation to deplete the number of pericytes in the advanced stage of tumor growth. The tumor volume was significantly decreased in the PDGFRB-iDTA Group-1 group compared to the control group (Figure 4B, C, E). A less pronounced reduction in tumor size was observed in the PDGFRB-iDTA Group-2 compared to the control group (Figure 4B, D, E). The findings indicate a crucial role of pericytes in the development of GBM. The cell-biological mechanisms underlying the anti-tumorigenic effect of pericyte depletion in experimental GBM were investigated next.

Results

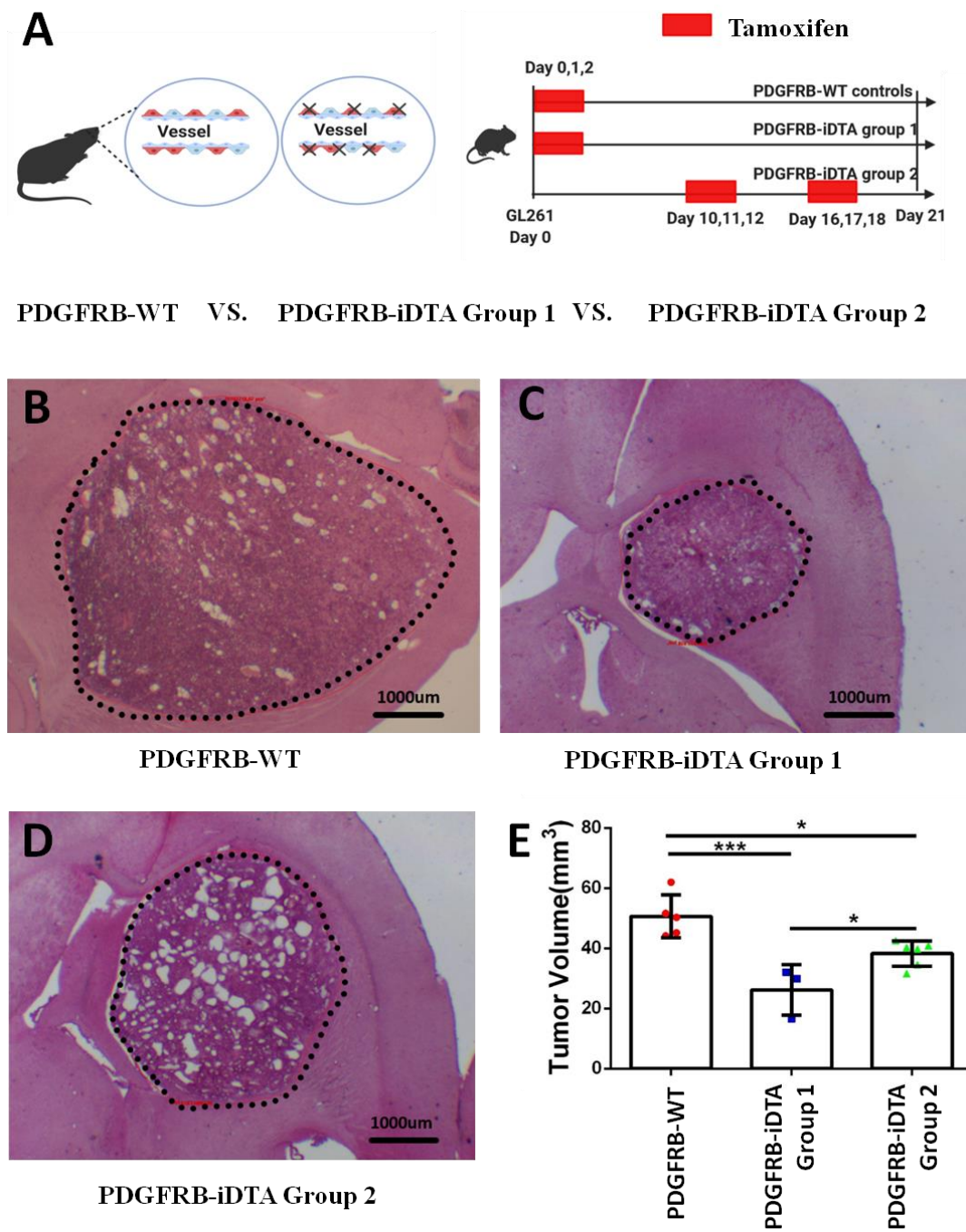


Figure 4 | Pericyte ablation inhibits the expansion of GBM.

(A) Schematic diagram of the orthotopic transplantation procedure in PDGFRB-WT controls and PDGFRB-iDTA Group-1 and Group-2. Brains were harvested in all groups at day 21. (B-D) Representative H&E staining in PDGFRB-WT and PDGFRB-iDTA Group-1 and Group-2 mice. (E) Quantification of tumor volume in PDGFRB-WT, PDGFRB-iDTA Group-1, and PDGFRB-iDTA Group-2. Statistical significance according to one-way ANOVA with post-hoc test, * $P < 0.05$, ** $P < 0.01$, *** $P < 0.001$. Each dot shows average data acquired from a single mouse. Values are presented as mean \pm SD. Scale bar, 1000 μ m.

4.1.5 Pericyte ablation inhibits the angiogenesis of GBM

Since there is a close relationship between pericytes and angiogenesis in tumors^{98, 99}, we wanted to determine whether pericyte depletion would interfere with angiogenesis in GBM. Alterations in angiogenesis are evident as changes in the total vessel length, vascular endpoints, and the number of vessel junctions⁹¹. Total vessel length is defined as the sum of Euclidean distances between the pixels of all the vessels in an image. The total number of endpoints corresponds to the number of open-ended vascular segments in an image and the total number of junctions is the total number of vessel junctions in the image⁹¹. Experiments were performed as shown in Figure 5A. CD31 staining routinely revealed fewer but larger vessels in the early pericyte-depletion GBM model compared to that in the control group (Figure 5B, C). A similar morphology of tumor vessels was observed between the control group and the advanced pericyte-depletion GBM group (Figure 5B, D). Numerical values of total vessel length, vessel end points, and vessel junctions were markedly decreased in the early pericyte-depletion GBM model compared to the control group (Figure 5E, F). In the advanced pericyte-depletion GBM group, the total vessel length and number of vessel junctions were significantly reduced compared with the control group (Figure 5E, F). These results may explain why the tumor volume was much smaller in PDGFRB-iDTA Group-1 than in controls and significantly decreased compared to PDGFRB-iDTA Group-2. Interestingly, we observed a drastic change in the tumor vessel morphology in PDGFRB-iDTA Group-1

Results

(Figure 5C) as compared to the control group and PDGFRB-iDTA Group-2 (Figure 5B, D). The findings prompted the subsequent examination of whether abnormal vessel morphology would result in detrimental vessel function.

Results

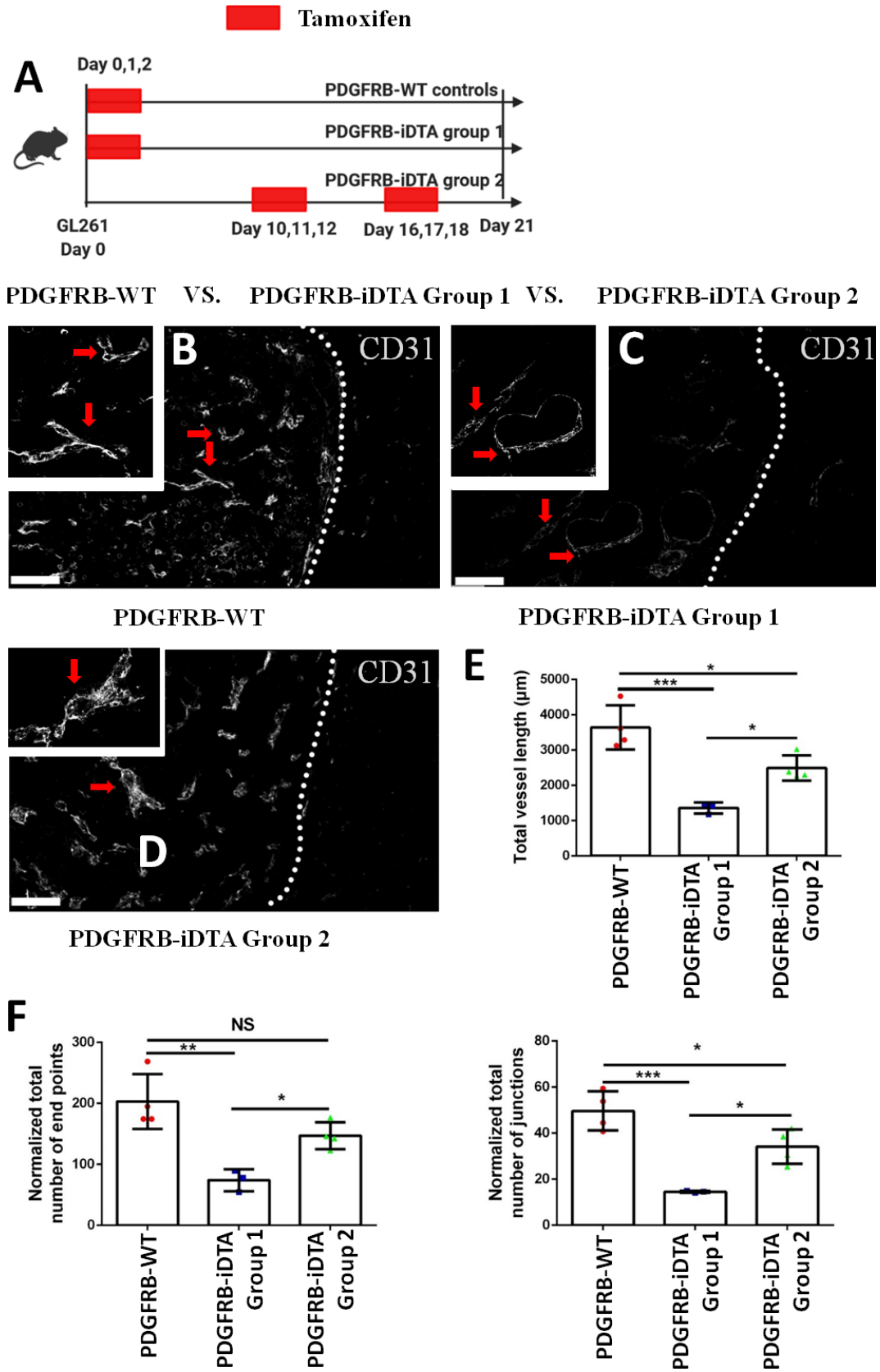


Figure 5 | Pericyte ablation inhibits GBM angiogenesis.

Results

(A) Schematic diagram of the orthotopic transplantation procedure in PDGFRB-WT, PDGFRB-iDTA Group-1, and PDGFRB-iDTA Group-2 mice. Brains were harvested in all groups at day 21. (B) Representative confocal images of staining of vessels for the CD31 endothelial cell marker in PDGFRB-WT controls. Dotted lines delineate the boundary between tumor (left) and adjacent non-tumor (right). Inset shows an example of long and torturous vessels (arrows). (C) Representative confocal images of vessels stained for CD31 (gray) in PDGFRB-iDTA Group-1. Dotted lines delineate the boundary between tumor (left) and adjacent non-tumor tissues (right). Inset shows an example of a large vessel lumen indicated by the arrowheads. (D) Representative confocal images of vessels with CD31 (gray) staining for endothelia cell in PDGFRB-iDTA Group-2 group. Dotted lines delineate the boundary between tumor (left) and adjacent non-tumor tissues (right). The inset shows an example of a short tumor vessel indicated by the arrowhead. (E-F) Quantification of total vessel length, normalized endpoints, and junctions among PDGFRB-WT, PDGFRB-iDTA Group-1, and PDGFRB-iDTA Group-2. Statistical significance according to one-way ANOVA with post-hoc test, * $P < 0.05$, ** $P < 0.01$, *** $P < 0.001$). Each dot shows average data acquired from a single mouse, and values are presented as mean \pm SD. Scale bars, 100 μm .

4.1.6 Pericyte ablation in early, but not advanced GBM, boosts Evans Blue extravasation

Pericytes play a crucial role in regulating vascular integrity¹⁰⁰. Thus, we evaluated whether pericyte depletion interferes with the permeability of tumor vessels, as determined by the extent of Evans Blue extravasation from the tumor parenchyma¹⁰¹. The results showed that the Evans Blue extravasation was significantly increased in the early pericyte-depletion GBM model. Remarkably, vascular leakiness was decreased in the advanced pericyte-depletion GBM model when raw (non-normalized) Evans Blue values were compared with those of the PDGFRB-WT control (Figure 6A, B). In the tumor-free hemispheres, the Evans Blue extravasation was close to the detection limit in the control group and the early and advanced pericyte-depletion groups (Figure 6A,

Results

B). The results confirmed that, as expected, the Evans Blue dye leaked into the tumor, but not the tumor-free area containing an intact blood–brain barrier. To account for the varying tumor sizes in the two different pericyte-depletion models, we normalized the Evans Blue extravasation value according to the average tumor volume. The normalized Evans Blue extravasation results revealed a more pronounced increase in the early pericyte-depletion GBM model. No significant difference in the normalized Evans Blue extravasation was found in the advanced pericyte-depletion GBM model compared to the control group (Figure 6A, C). These results suggest that intratumoral pericytes in advanced GBM (represented by PDGFRB-iDTA Group-2) do not efficiently maintain a blood-tumor barrier function (since pericyte depletion at this stage does not accelerate vascular leakiness). In contrast, the depletion of pericytes at early stages of glioma growth has drastic and persistent consequences, since reduced pericyte numbers in early GBM result in smaller tumors with strongly increased vascular leakiness in the tumor area.

Results

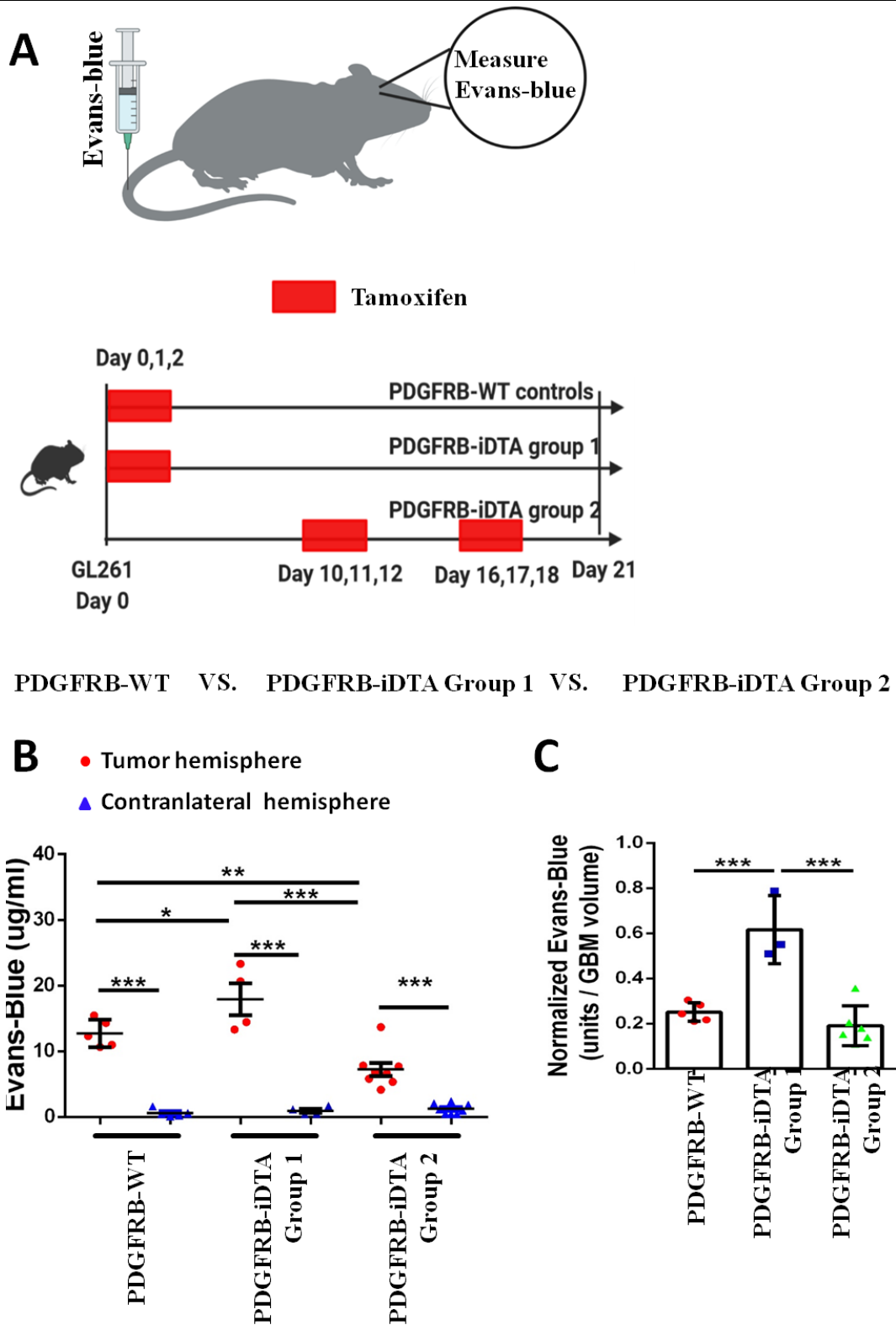


Figure 6 | Pericyte ablation in early, but not advanced GBM, boosts Evans-Blue extravasation.

(A) Schematic diagram of the orthotopic transplantation procedure in PDGFRB-WT

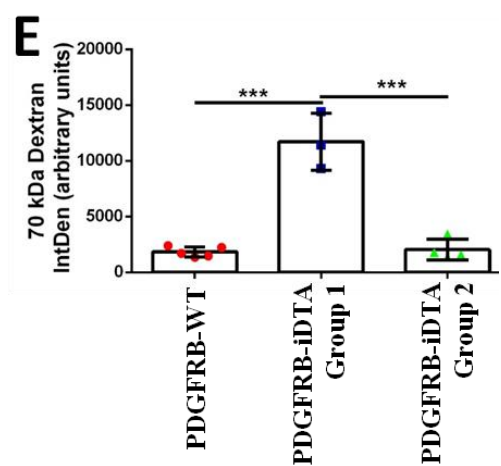
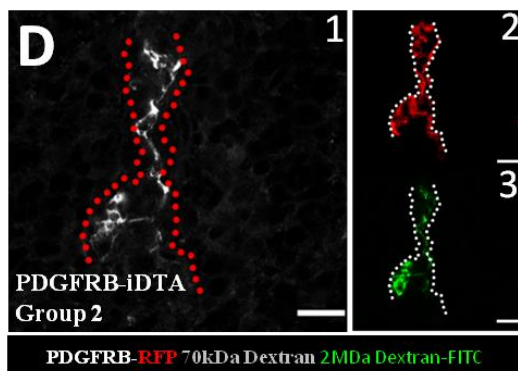
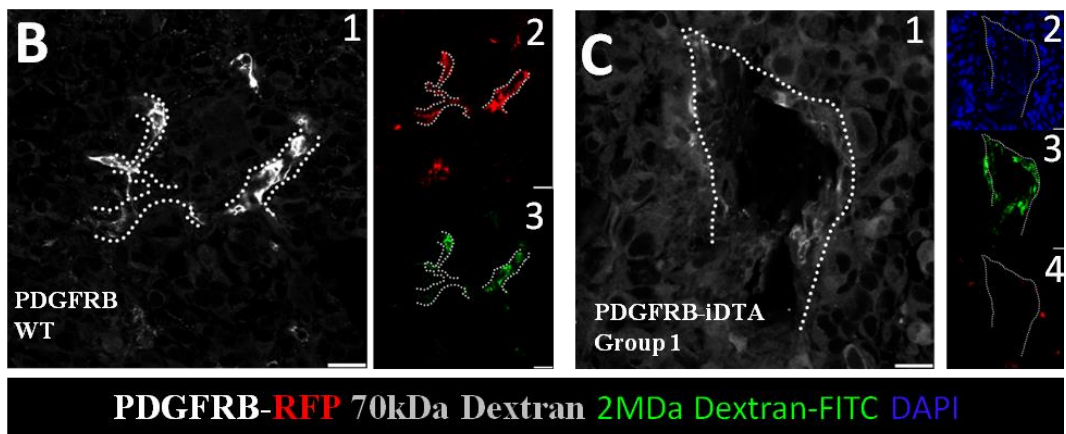
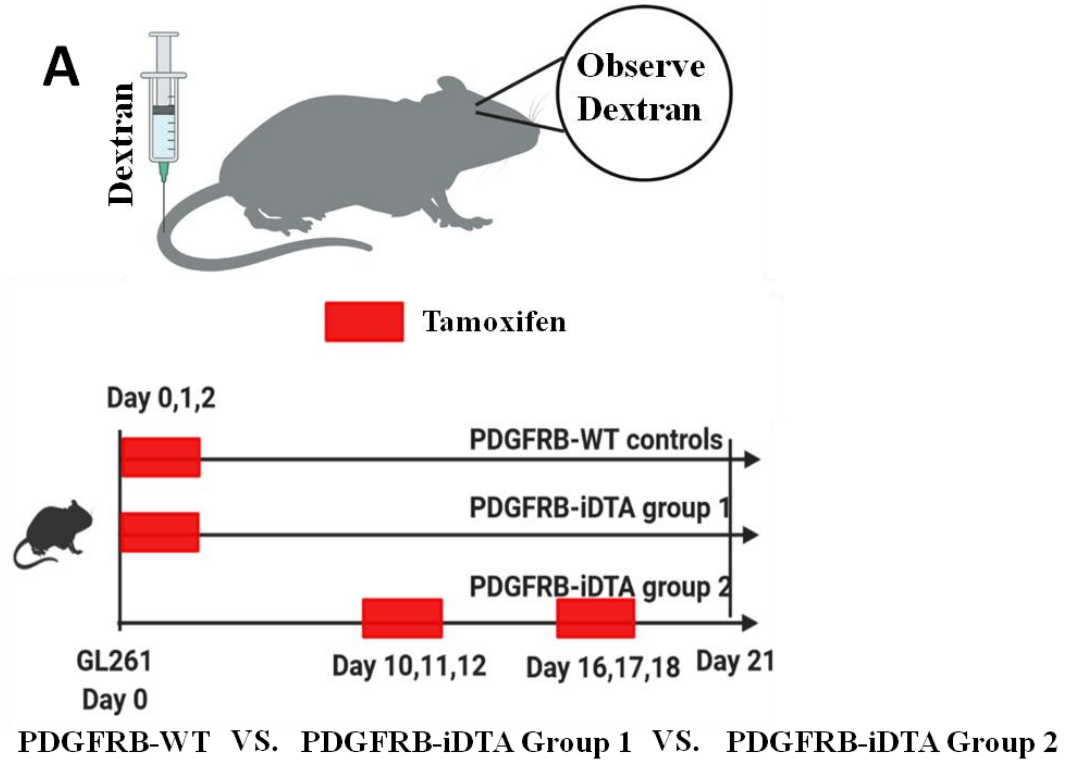
Results

(control), PDGFRB-iDTA Group-1, and PDGFRB-iDTA Group-2 models. Mice were injected intravenously with administered Evans-Blue 2 h before sacrifice in all models at day 21. (B) Vascular permeability of the Evans Blue dye extravasation is expressed in $\mu\text{g/ml}$ of brain homogenates. (C) Values for Evans-Blue uptake in tumor hemispheres were normalized to the average GBM volume of the respective experimental group. Statistical significance according to one-way ANOVA with post-hoc test, * $P < 0.05$, ** $P < 0.01$, *** $P < 0.001$. Each dot shows average data acquired from a single mouse; values are presented as mean \pm SD.

4.1.7 Pericyte ablation in early, but not advanced GBM, boosts 70 KDa dextran leakiness

To determine vessel permeability within the morphological context of the brain tissue, we performed a dextran leakage assay. Supporting the findings with Evans Blue, the use of fixable dextrans provided direct evidence of local vascular leakiness at defined intra-tumoral vascular structures¹⁰². Dextran (70 KDa) has a similar molecular weight as Evans Blue albumin complexes¹⁰³. The extravasation value of 70 kDa dextran in the tumor parenchyma was significantly increased in the early pericyte-depletion GBM model (Figure 7E) as compared to that when pericytes were depleted in advanced GBM or to the control group (Figure 7E). The results of the dextran experiments confirmed our observations with the Evans Blue dye and showed that pericyte depletion in the early stage of tumor formation, but not at later stages, leads to an apparent increase in leakage of tumor vessels.

Results



Results

Figure 7 | Pericyte ablation in early, but not advanced GBM, boosts 70 KDa dextran leakiness.

(A) Schematic diagram of the orthotopic transplantation procedure in PDGFRB-WT mice (control), PDGFRB-iDTA Group-1, and PDGFRB-iDTA Group-2 GBM models. All mice were administered a dextran mixture (70 KDa and 2 MDa dextran) 15 min before sacrifice at day 21. (B) Representative pictures of 70 KDa dextran (gray, 1), PDGFRB-RFP (red, 2), and 2 MDa dextran (green, 3) in PDGFRB-WT (controls). Dotted lines (based on morphological criteria) indicate vessel walls. (C) Representative pictures of 70 KDa dextran (gray, 1), DAPI (blue, 2), 2 MDa dextran (green, 3), and PDGFRB-RFP (red, 4) in PDGFRB-iDTA Group-1. Dotted lines indicate vessel walls. (D) Representative pictures of 70 KDa dextran (gray, 1), PDGFRB-RFP (red, 2), and 2 MDa dextran (green, 3) in PDGFRB-iDTA Group-2. The dotted lines indicate vessel walls. Integrated Density (IntDen) directly represents the extent of 70 KDa dextran uptake into the GBM parenchyma. Statistical significance according to one-way ANOVA with post-hoc test, * $P < 0.05$, ** $P < 0.01$, *** $P < 0.001$. Each dot shows average data acquired from a single mouse. Values are given as mean \pm SD. Scale bar, 20 μm .

4.1.8 Pericyte ablation in early, but not advanced GBM, inhibits collagen IV synthesis

The basement membrane (BM) is essential in maintaining the integrity of vessels^{104, 105}. In addition, collagen IV makes up approximately 50% of all BM components¹⁰⁶. Therefore, to further understand the mechanisms underlying the alterations of vascular permeability, we investigated the positive vascular basement in PDGFRB-WT, PDGFRB-iDTA Group-1, and PDGFRB-iDTA Group-2 GBM models. Collagen IV was significantly decreased after early depletion of pericytes in GBM (Figure 8B, C, E). No significant difference in collagen IV expression was found after depletion of pericytes in advanced GBM model compared to that in the control group (Figure 8B, D, E).

Results

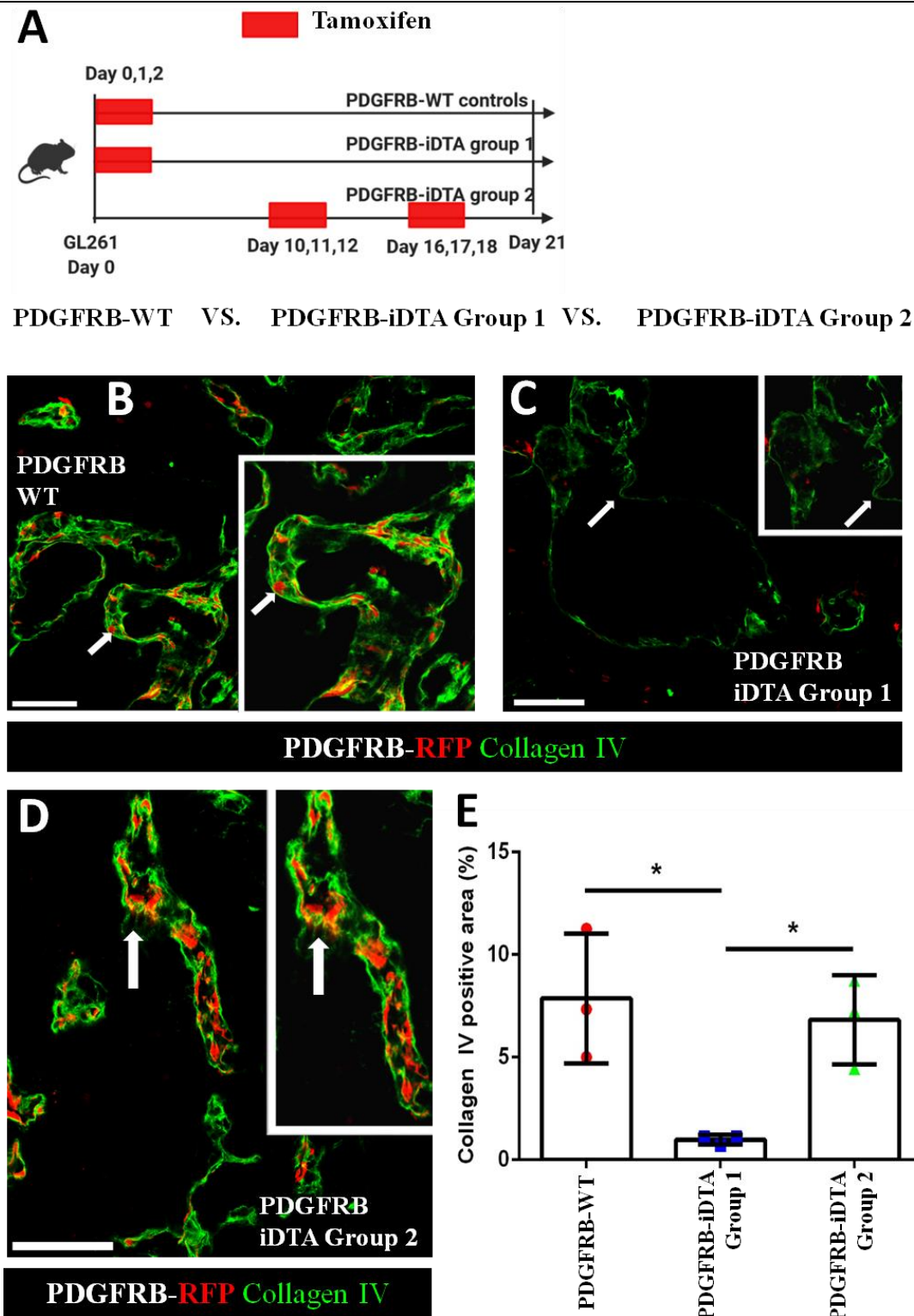


Figure 8 | Effect of pericytes on collagen IV production.

(A) Schematic diagram of the orthotopic transplantation procedure in PDGFRB-WT (control), PDGFRB-iDTA Group-1, and PDGFRB-iDTA Group-2 GBM models. Brains were harvested in all models at day 21. (B) Representative fluorescence

Results

photomicrographs from the tumor area of collagen IV (green) and PDGFRB-RFP in PDGFRB-WT mice. Inset shows an example of collagen IV staining in the basement membrane of vessels in the tumor area (indicated by the arrow). (C) Representative fluorescence images from tumor areas of collagen IV (green) and PDGFRB-RFP in the PDGFRB-iDTA Group-1 GBM models. Inset shows a representative example for scarce collagen IV deposition at intratumoral vessels (indicated by the arrow). (D) Representative fluorescence images from tumor areas of collagen IV (green) and PDGFRB-RFP in PDGFRB-iDTA Group-2 mice. Inset shows an example of strong collagen IV immunofluorescence from the area indicated by the arrow. (E) Quantification of the collagen IV positive area at the vascular basement membrane in the three GBM models. Statistical significance according to one-way ANOVA with post-hoc test, * $P < 0.05$, ** $P < 0.01$, *** $P < 0.001$). Each dot shows average data acquired from a single mouse, and values are presented as mean \pm SD. Scale bars, 100 μm .

4.1.9 Pericyte ablation in early GBM promotes transcytosis in tumoral endothelial cells

When vascular disruption is severe, high-molecular-weight (2 MDa) FITC-dextran accumulates in areas of basal lamina disruption, endothelial cells¹⁰⁷, and in the brain parenchyma. Intravenously injected 2 MDa FITC-dextran does not normally penetrate the vessels of the healthy brain¹⁰⁸ and remains restricted to the tumor vessel-lumen¹⁰⁹. Accumulation of 2 MDa FITC-dextran in endothelial cells suggests that transcytosis of this fluorescence tracer is increased in these cells¹⁰⁷. In the control (PDGFRB-WT) and PDGFRB-iDTA Group-2 GBM models, we observed that 2 MDa FITC-dextran was restricted to the vessel lumen (Figure 9B, D). Interestingly, the co-staining of 2 MDa FITC-dextran and CD31 (endothelial cell marker) was markedly increased in PDGFRB-iDTA Group-1 (Figure 9C). Therefore, we quantified the co-stained area of 2 MDa FITC-dextran and CD31 in all three groups to determine the level of transcytosis

Results

in brain endothelial cells. Uptake of 2 MDa FITC-dextran in the endothelium was significantly increased in the early pericyte depletion GBM model (PDGFRB-iDTA Group-1) compared to the control group (PDGFRB-WT) and when pericyte depletion occurred in advanced GBM model (PDGFRB-iDTA Group-2) (Figure 9E). These results suggest that the depletion of pericytes in the early stage of tumors promotes transcytosis in intratumoral endothelial cells.

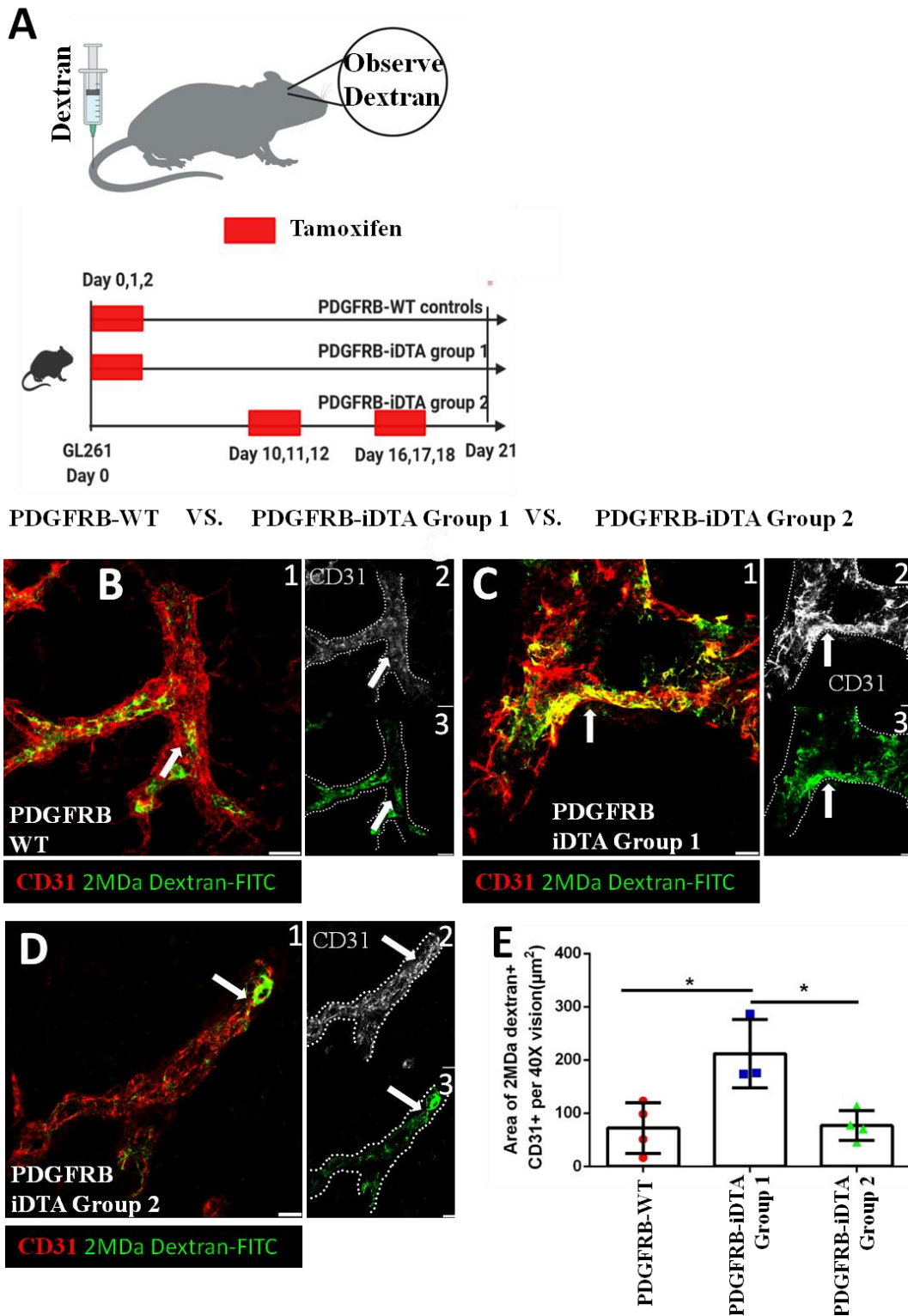


Figure 9 | Pericyte ablation in early GBM promotes transcytosis in tumoral endothelial cells.

(A) Schematic diagram of the orthotopic transplantation procedure in PDGFRB-WT mice (control), PDGFRB-iDTA Group-1, and PDGFRB-iDTA Group-2 GBM models.

Results

TAM indicates the days of tamoxifen injection. All mice were administered the dextran mixture 15 min before sacrifice at day 21. (B) Representative pictures of 2 MDa dextran (green) and CD31 in PDGFRB-WT mice. 2 MDa dextran was distributed in the vessel lumen (arrow). The dotted lines indicate vessel walls. (C) Representative immunostaining pictures of 2 MDa dextran (green) and CD31 in PDGFRB-iDTA Group-1. Endothelial cells containing 2 MDa dextran are indicated by the arrow. The dotted lines indicate vessel walls. (D) Representative pictures of 2 MDa dextran (green) and CD31 in PDGFRB-iDTA Group-2 mice. 2 MDa dextran was distributed in the vessel lumen (arrow). The dotted lines indicate vessel walls. Statistical significance according to one-way ANOVA with post-hoc test, * $P < 0.05$, ** $P < 0.01$, *** $P < 0.001$. Each dot shows data acquired from a single mouse; values are presented as mean \pm SD. Scale bars, 20 μm .

4.2 Functions of TAMEP in GBM

A recent study from our laboratory reported the pronounced impact of TAMEP on GBM vascularization and intratumoral pericytes in GBM⁵². In the present study, we determined the role of pericyte-coverage on vascular permeability in GBM. We hypothesized that TAMEP and pericytes interact and control vascular permeability in GBM. Hence, we aimed to determine the exact function of TAMEP GBM progression and intratumoral vessel function.

4.2.1 Nes-RFP model traces two different cell types in GBM

Genetic lineage tracing is a practical method to study the origin and fate of specific cell types in complex organs¹¹⁰. To investigate CNS resident progenitors in GBM, we established two *Nestin::CreERT2* R26-RFP lineage tracing models that allow the lineage tracing of nestin-positive cells after injection tamoxifen. In a previous study, we inspected orthotopic gliomas in two *Nestin::CreERT2* R26-RFP mouse-strains⁵². We

Results

found large numbers of glial fibrillary acidic protein (GFAP) negative, RFP+ cells in the tumor-core that were visualized with the NesERT2 R26-RFP model-1 (abbreviated as Nes-RFP), whereas in the NesERT2 R26-RFP model-2, cells of GFAP+ cells were preferentially observed in the tumor rim⁵².

The experiment is summarized in Figure 10A. In the Nes-RFP GBM model, many traced (RFP+) cells were present in the tumor area (Figure 10C, D). As shown in the schematic diagram in Figure 11B, the RFP+ cells comprised vascular and avascular RFP+ cells. Vascular RFP+ cells expressing the PDGFRB pericyte marker, were negative for SOX2, and displayed extended processes along the CD31+ vessels (Figure 10C, yellow arrows). Avascular RFP+ cells were negative for PDGFRB expression and portion of these cells expressed the transcription factor SOX2 (Figure 10C, D; white arrows, known as TAMEP⁵²). SOX2 was expressed in 42% of TAMEP. Loss of SOX2 expression in Nes-RFP Sox2^{fl/fl} mice resulted in a decrease of SOX2+ TAMEP and led to a very pronounced reduction in the traced TAMEP⁵². Hence, we concluded that SOX2+ TAMEP were the source for all TAMEP. Accordingly, SOX2+ TAMEP were termed TAMEP progenitors⁵². SOX2 expression in Nes-RFP+ cells was exclusively detected in TAMEP and was never observed in vascular RFP+ cells. These findings imply that conditional SOX2-knockout in our Nes-RFP mouse strain selectively modulated TAMEP, but not any other cell type.

Results

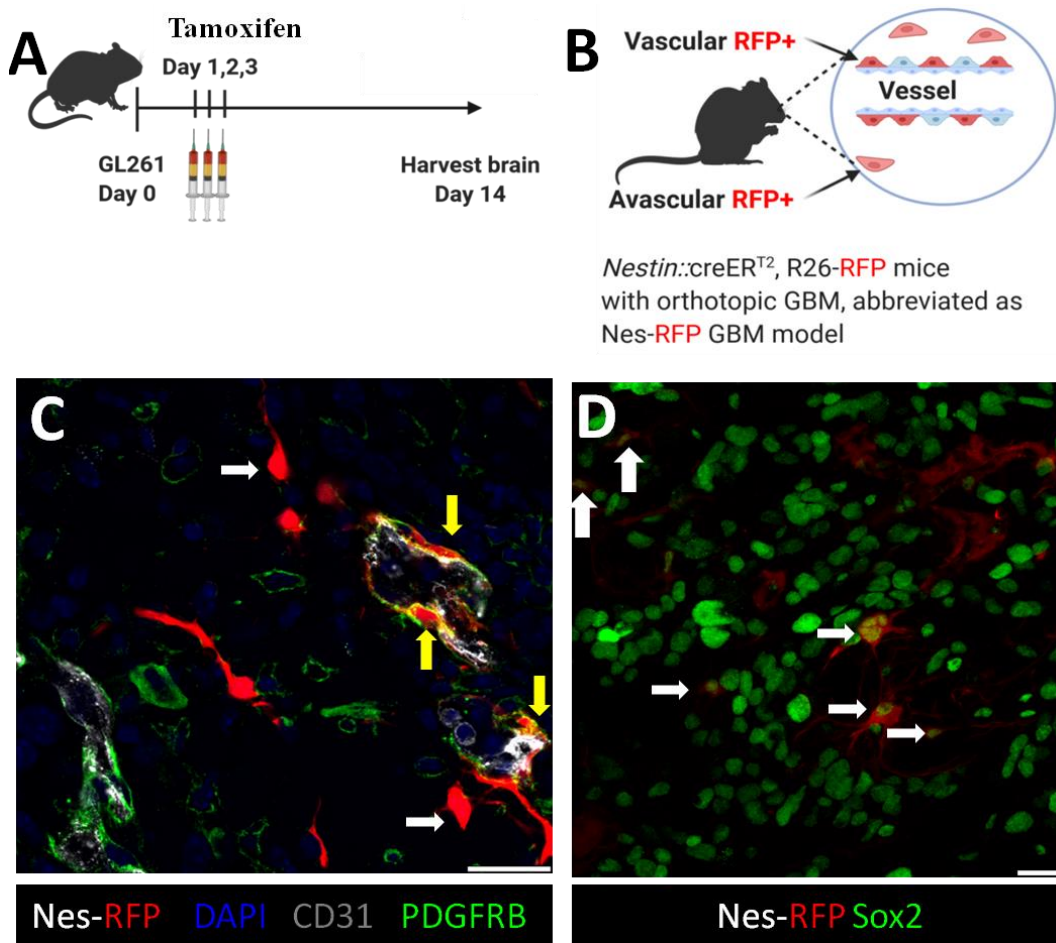


Figure 100 | Vascular RFP+ and avascular RFP+ cells in the Nes-RFP GBM model.

(A) Schematic diagram of time points for GBM inoculation, tamoxifen injections, and brain removal. (B) Schematic diagram of two populations, vascular RFP+ and avascular RFP+, in the Nes-RFP GBM model. (C) Representative image of CD31 (gray), PDGFRB (green) immunostaining, and Nes-RFP (red) in the Nes-RFP GBM model. Yellow arrows show vascular RFP+/PDGFRB+ cells. The white arrowheads indicate avascular RFP+/PDGFRB- cells. DAPI was used to stain nuclei (blue). (D) Representative image of Sox2 (green) immunostaining and Nes-RFP (red) in Nes-RFP GBM model. Avascular Nes-RFP+ (red) cells with Sox2 (green) expression (white arrow). Scale bars, 20 μ m.

4.2.2 Nes-RFP model exhibits higher sensitivity to tamoxifen than NesERT2 R26-RFP model-2

We also compared the sensitivity of cre-recombinase to tamoxifen between the two

Results

Nestin::creERT2 R26-RFP models in this study. The comparisons involved a 75 mg/kg tamoxifen treatment group (low-dose group) and 180 mg/kg tamoxifen treatment group (high-dose group). In the low-dose group, Nes-RFP displayed more cre-recombinase expression in cell nuclei than in the NesERT2 R26-RFP model-2 group (Figure 11A, B). In the NesERT2 R26-RFP model-2 group, mice treated with 180 mg/kg tamoxifen showed more cre-recombinase expression in cell nuclei than mice treated with 75 mg/kg tamoxifen (Figure 11B, C). Thus, the Nes-RFP model was more sensitive to tamoxifen than the NesERT2 R26-RFP model-2. While the NesERT2 R26-RFP model-2 was also effective in tracing nestin⁺ cells, it required a higher dose of tamoxifen. Therefore, the Nes-RFP model involving 75 mg/kg tamoxifen was chosen for subsequent experiments.

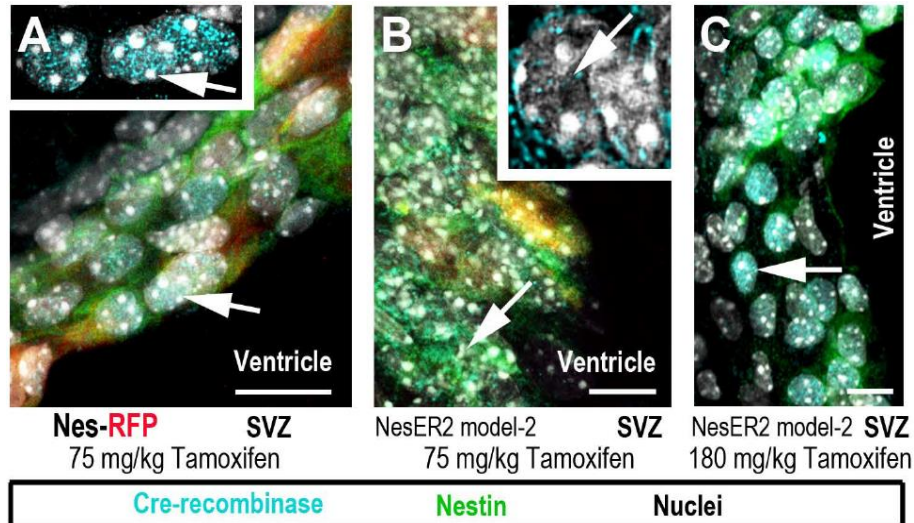


Figure 111 | Differences in tamoxifen sensitivity in two Nes-RFP mouse strains.

(A-B) Immunofluorescence staining of Cre-recombinase (blue) and nestin (green) on SVZ area in Nes-RFP and NesER2 model-2 mice treated with a lower dose of tamoxifen (75 mg/kg). Cre-recombinase nuclei localization is indicated by arrows and boxes. DAPI counterstained nuclei are shown in gray. (C) Staining of Cre-recombinase (blue) and nestin (green) in NesER2 model-2 treated with a higher dose of tamoxifen (180

Results

mg/kg). Arrowhead indicates the Cre-recombinase nuclei localization. DAPI counterstained nuclei are shown in gray. N = 3 per group. Scale bars, 10 μ m.

4.2.3 TAMEP promote GBM growth

Next, we investigated whether TAMEP have a particular function in GBM progression. We established nestin::creER2, R26-RFP, Sox2^{fl/fl} (abbreviated as Sox2-KO) mice. The Sox2-KO GBM model allowed us to selectively deplete TAMEP. The tumor volume was significantly reduced in the Sox2-KO mice compared to the volume in Nestin-RFP (hereafter, Sox2-WT) mice⁵². H&E staining consistently revealed a difference in tumor volume between the Sox2-WT and Sox2-KO groups (Figure 12B, C). The findings suggest the importance of TAMEP in tumor progression.

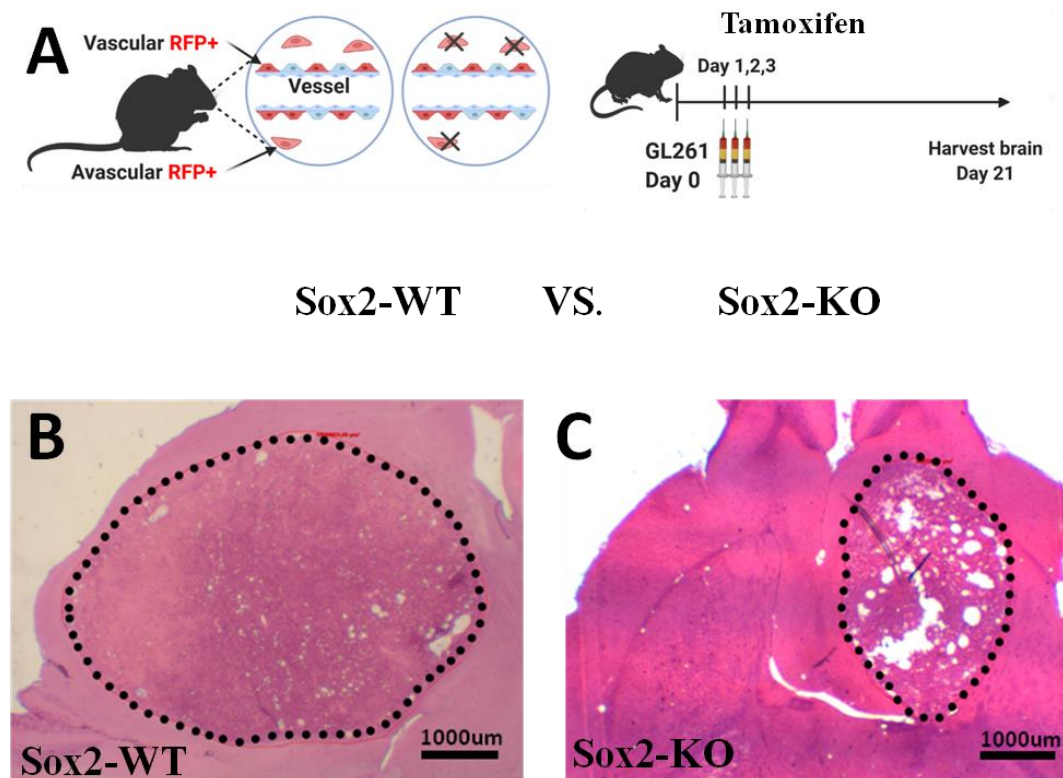


Figure 12 | TAMEP promote the expansion of GBM.

(A) Schematic diagram of the orthotopic transplantation procedure in Sox2-WT mice (control) and Sox2-KO mice. Brains were harvested in both models at day 21. (B-C)

Results

Representative images of tumor sections stained with H&E for histological analysis in Sox2-WT (**B**) and Sox2-KO (**C**) mice. Scale bars, 1000 μm .

4.2.4 TAMEP promote and shapes GBM angiogenesis

Next, we investigated the mechanism of TAMEP-promoted tumor growth. The morphology of tumor vessels was changed in Sox2-KO mice. Representative images revealed tumor vessels with large lumens in SOX2-KO mice, but not in mice in the control group (Figure 13D, E). In the Sox2-KO mice, the total vessel length and pericyte coverage were noticeably decreased compared to the Sox2-WT group (Figure 13B, C). These results indicate the profound effect of TAMEP on angiogenesis in GBM.

Results

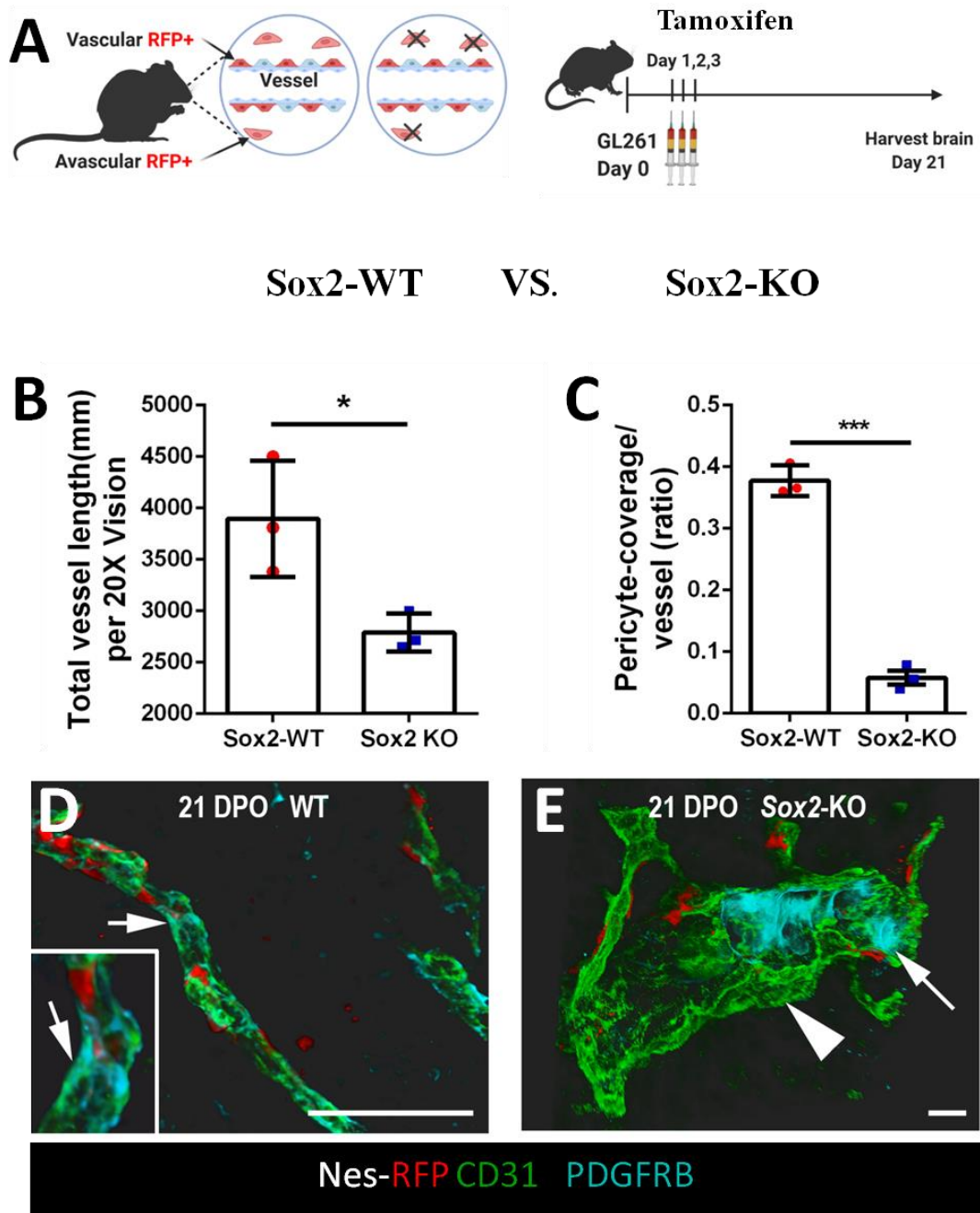


Figure 13 | TAMEP control the angiogenesis of GBM.

(A) Schematic diagram of the orthotopic transplantation procedure in Sox2-WT mice (control) and Sox2-KO mice. Brains were harvested in both models at day 21. (B) Quantification of total vessel length in Sox2-WT and Sox2-KO groups. (C). Quantification of pericyte-coverage in the Sox2-WT and Sox2-KO groups. (D) Representative three-dimensional reconstruction of the tumor area CD31 (green), PDGFRB (cyan) immunostaining and Nes-RFP (red) in Sox2-WT mice. Arrow indicates the magnified area. (E) Representative 3D reconstruction of tumor area CD31 (green), PDGFRB (cyan) immunostaining and Nes-RFP (red) in Sox2-KO mice. Enlarged tumor vessel lumen with a patchy association of pericytes (arrow) and

Results

pericyte-free areas (arrowhead). Statistical significance using unpaired two-tailed Student's t-test (in B and C), * $P < 0.05$, ** $P < 0.01$, *** $P < 0.001$. Each dot shows data acquired from a single mouse. Values are presented as mean \pm SD. Scale bars, 100 μm .

4.2.5 TAMEP maintain the tumoral vascular permeability of GBM

Changes in vessel morphology may impact vascular function¹¹¹. Therefore, we assessed the changes in tumor vascular permeability in the Sox2-WT and Sox2-KO GBM tumors in the Evans Blue extravasation and dextran (70 kDa dextran and 2 MDa dextran) leakage assay¹¹² are shown in Figure 14A. In the tumor hemispheres of Sox2-KO mice, Evans Blue leakage was significantly increased compared to Sox2-WT mice (Figure 14E). Notably, in the tumor-free hemispheres, the leakage of Evans Blue was close to the detection limit in both Sox2-KO and Sox2-WT mice (Figure 14E). Therefore, we concluded that most of the Evans Blue leaked from the tumor tissues in both Sox2-WT and Sox2-KO GBM models. Hence, we normalized the values of Evans Blue extravasation by the average tumor volume to account for the differences in tumor volume in our different GBM models. The normalized Evans Blue leakiness data corroborated the increased vascular permeability of the Sox2-KO group as compared to the Sox2-WT group (Figure 14F). In the Sox2-KO group, the leakiness of 70 Da dextran was also significantly increase compared to the leakiness in the Sox2-WT group (Figure 14D, G).

While 2 MDa dextran was restricted to the tumor vessel lumen in Sox2-WT tumor and occasionally accumulated in some structures, including branch points of tumor vessels (Figure 14B), the accumulation and penetration of 2 MDa dextran into the tumor

Results

parenchyma was much more pronounced and widespread in Sox2-KO tumors (Figure 14C). The 2 MDa dextran leakiness in the tumor parenchyma was significantly elevated in the Sox2-KO group compared to the Sox2-WT group (Figure 14H).

Results

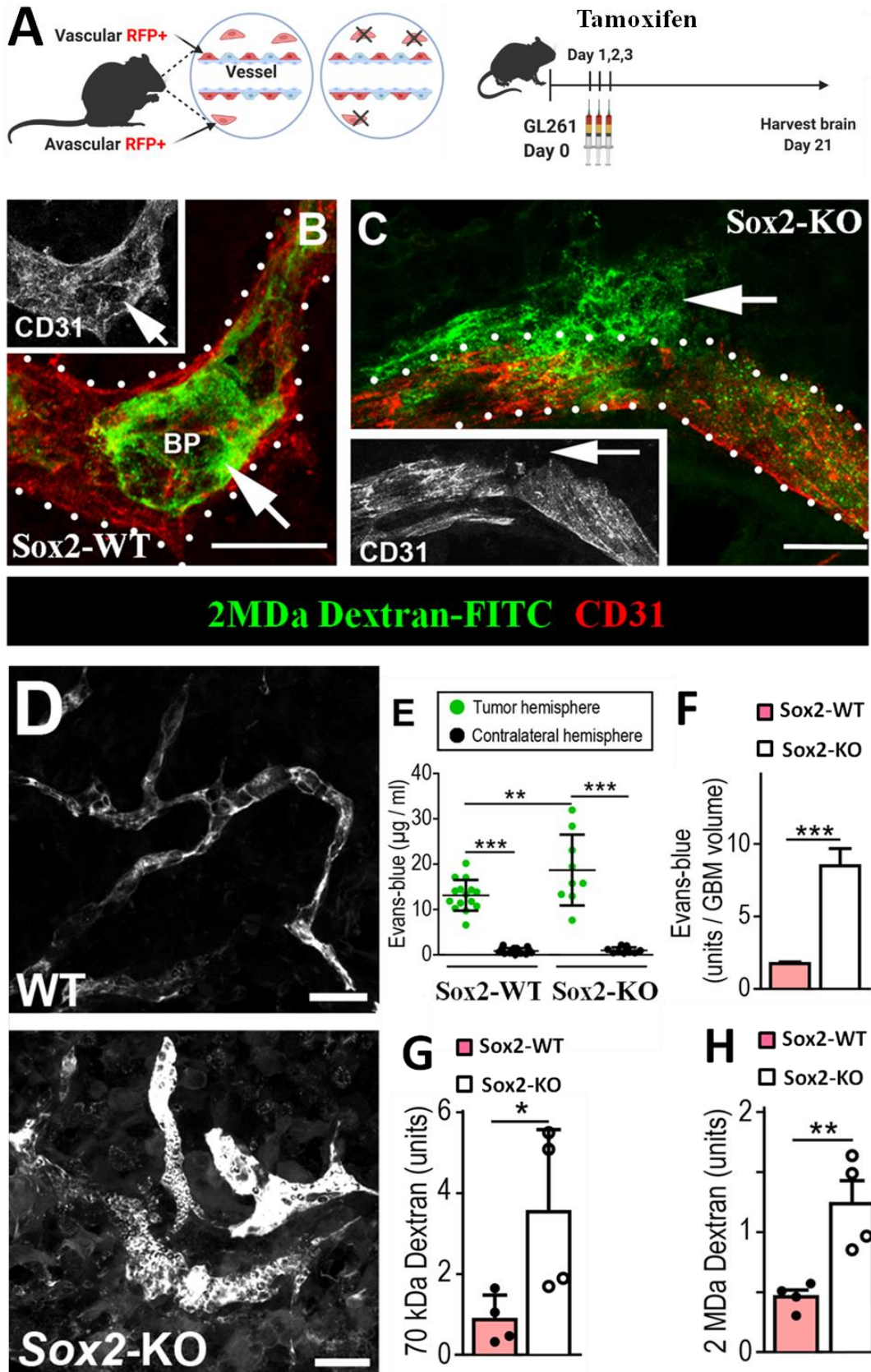


Figure 14 | TAMEP maintain the vascular tightness of GBM.

Results

(A) Schematic diagram of the orthotopic transplantation procedure in Sox2-WT (control) and Sox2-KO mice. Mice were administered Evans Blue (or dextrans mixture) 2 h (or 15 min) before sacrifice in both models at day 21. (B) Representative fluorescence photomicrographs of 2 MDa dextrans (green) and CD31 staining (red) in Sox2-WT (control) mice, 2 MDa dextran distributed in the branch point (BP) of the vessel (arrow). The white dotted lines indicate vessel walls. Rectangular box denotes the staining of CD31 (gray). (C) Representative fluorescence photomicrographs of 2 MDa dextran (green) and CD31 staining (red) in Sox2-KO mice, part of 2 MDa dextran through vessel breach into the parenchyma (arrow). Vessel walls are indicated by the white dotted line. Rectangular box denotes CD31 (gray) staining. (D) Representative pictures of 70 KDa dextran (gray) in Sox2-WT mice (top) and Sox2 KO groups (bottom). (E) Vascular permeability of the Evans Blue dye expressed as micrograms (μg) of Evans Blue per milliliter (ml) of brain homogenates. (F) The degree of permeability in tumor hemispheres was normalized to the average GBM volume (Sox2-WT ($n = 14$) and Sox2-KO ($n = 9$)). (G-H) Quantification of 70 KDa and 2 MDa dextran leakiness in Sox2-WT (G) and Sox2-KO (H) groups. Statistical significance according to one-way ANOVA with post-hoc test (E) or t-test (F, G, and H), * $P < 0.05$, ** $P < 0.01$, *** $P < 0.001$. Each dot shows data acquired from a single mouse. Values are presented as mean \pm SD. Scale bars, 30 μm .

4.2.6 Effects of TAMEP on collagen IV production in GBM

To investigate the molecular mechanisms underlying the changes in tumor vascular permeability in TAMEP-deficient GBM, we evaluated the expression of a panel of markers for the neuro-vascular unit, including collagen IV, AQP4, and Glut1¹¹³, in Sox2-WT and Sox2-KO mice. The expression of collagen IV was decreased in the tumor area of Sox2-KO mice compared to that in the Sox2-WT mice. However, no difference in collagen IV distribution was observed in the tumor-free regions between the Sox2-WT and Sox2-KO groups (Figure 15A, B). In addition, the expression of AQP4 and Glut1 also did not vary between the Sox2-WT and Sox2-KO groups (Figure 15C-F). These results suggest that TAMEP maintain the integrity of tumor vessels by controlling the level of collagen IV in the vascular basement membrane.

Results

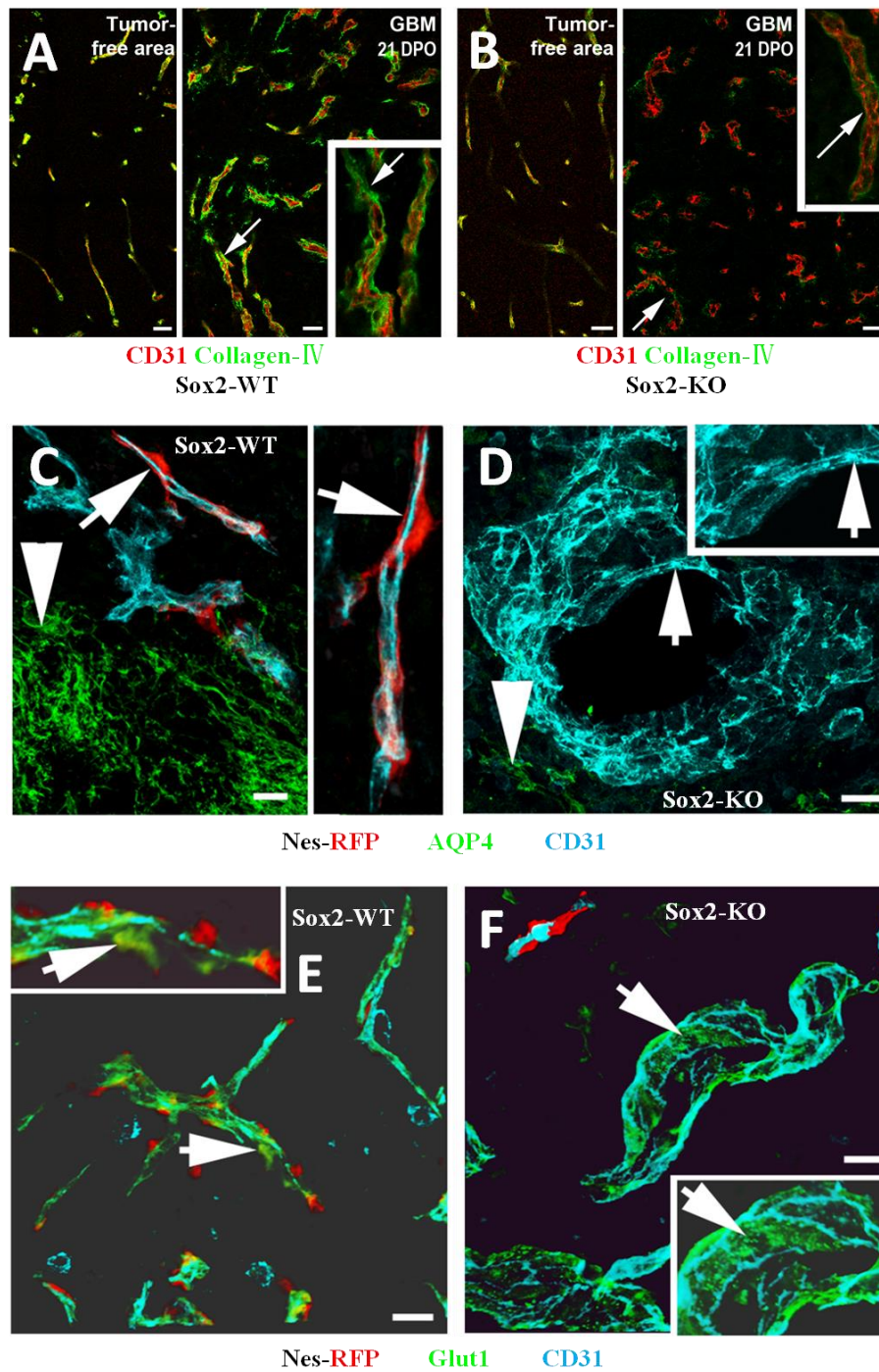


Figure 15 | TAMEP promote the production of collagen IV in GBM.

(A) Representative fluorescence photomicrographs from tumor-free and tumor areas of collagen IV (green) and CD31 (red) staining in Sox2-WT mice. Inset shows an example of thick and strong collagen IV from the tumor area indicated by the arrow. (B) Representative fluorescence images from tumor-free and tumor areas of collagen IV (green) and CD31 staining (red) in Sox2-KO mice. Inset shows an example of thin and

Results

weak collagen IV from the area indicated by the arrow. (C-D) Representative micrographs of astrocytic endfeet marker AQP4 (green) and CD31 (cyan) staining at the border of Sox2-WT (C) and Sox2-KO (D) groups. AQP4 positive vessels are found outside the tumor (arrowheads), negative tumor vessels (arrows) are found in the tumor area in both genotypes. (E-F) Representative micrographs showing equal expression of endothelial glucose transport Glut1 (green) on the tumor vessels (CD31, cyan) in Sox2-WT (E) and Sox2-KO (F) groups, Glu1-positive tumor vessel (arrows). Rectangular boxes are magnifications of the areas indicated by the arrows. Scale bars, 30 μm .

4.2.7 Angiogenesis of GBM does not affect the number of TAMEP

We demonstrated that TAMEP promote angiogenesis in GBM. However, it still remained unclear whether angiogenesis affects the number of TAMEP in GBM. To address this issue, we compared the number of TAMEP in brain tumor angiogenesis under control conditions (vehicle treatment; aCSF) versus anti-angiogenic treatment with DC101 in our Sox2-WT GBM model. DC101 is a monoclonal antibody targeting mouse VEGFR-2¹¹⁴. The treatment reduces tumor vascularization¹¹⁵. To confirm the therapeutic effect of DC101 in our Sox2-WT GBM model, we inspected the changes of tumor volume and vascular network between the DC101 and aCSF treatment groups at DPO21. Tumor volume was significantly decreased in the DC101 treatment group compared to the aCSF treatment group (Figure 16A, C, D). The representative staining of the CD31 endothelial cell marker revealed an obviously reduced number of vessels in DC101 treated tumors compared to the number of vessels in aCSF controls (Figure 16E, F). The average number of TAMEP markedly declined from approximately 11 cells per frame to approximately 3 cells per frame in the Sox2-WT GBM model⁵². The findings are the first confirmation of the therapeutic effect of DC101 at DPO 21 of

Results

Sox2-WT GBM and corroborate the anti-angiogenic efficacy of DC101. In the same model, we observed that the average number of TAMEP were not significantly different between the DC101 treated and aCSF control groups at DPO14 (Figure 16B). These results indicate that the extent of angiogenesis in GBM does not affect the number of TAMEP. Rather, TAMEP uni-directionally control GBM angiogenesis.

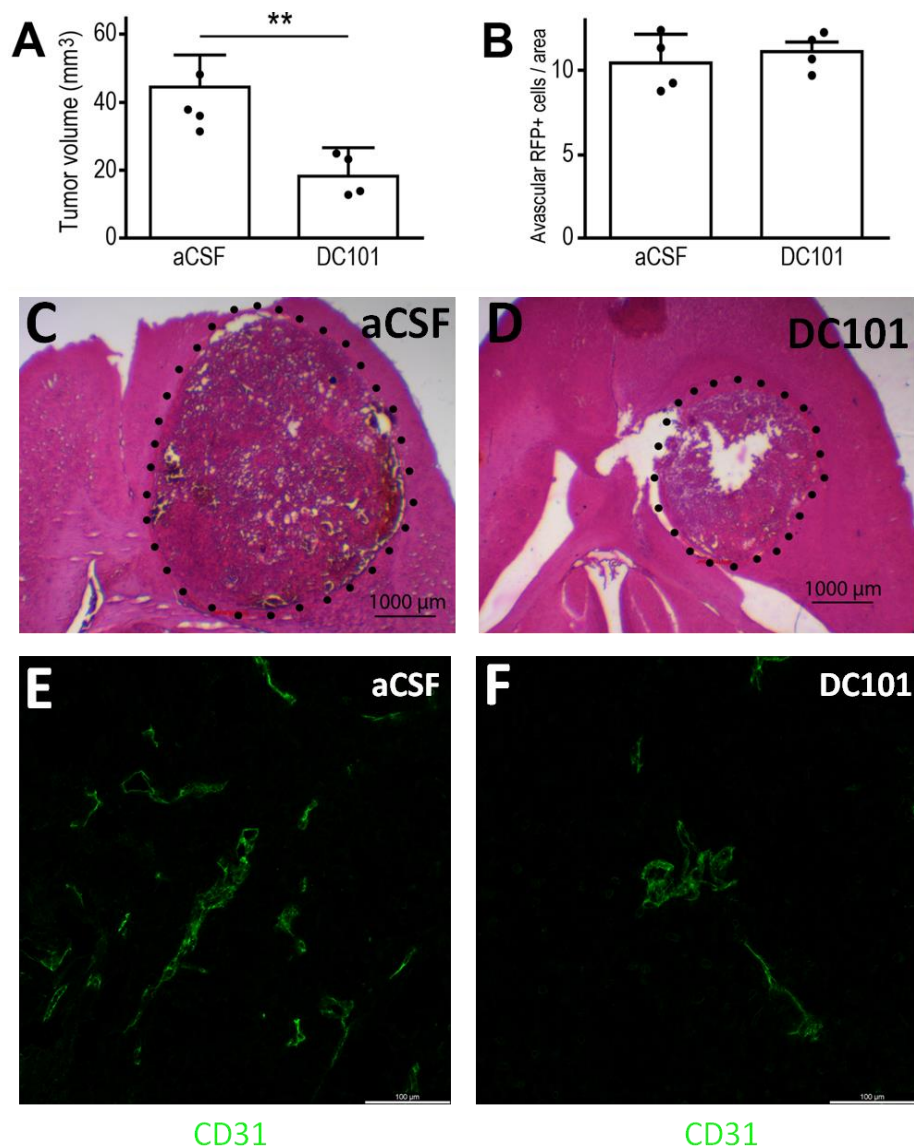


Figure 16 | Inhibition of angiogenesis does not affect the number of TAMEP.

(A) Quantification of tumor volume in the GL261 model with DC101 or aCSF treatment at day 21 after implantation. (B) Quantification of the number of avascular RFP+ cells (TAMEP) at day 14 after tumor implantation. (C-D) Representative H&E

Results

staining of aCSF and DC101 treated tumors. (E-F) Representative confocal microscopy images of vessels with CD31 (green) staining in endothelial cells in aCSF and DC101 treated tumors. Statistical significance was determined by Student's t-test (** $P < 0.01$). Each dot represents averaged data from one animal. Values are presented as mean \pm SD. Scale bars, 1000 μm (C and D) and 100 μm (E and F).

4.2.8 TAMEP do not accumulate in cerebral ischemia

Finally, we investigated whether TAMEP exist in other neuropathologies. Transient MCA occlusion (tMCAo), as a model for stroke, was established in Sox2-WT mice together with researchers at the Department of Neurosurgery at Kiel University. Nissl staining was performed to confirm the area of the tMCAo model (Figure 17B-D; arrows). More than 1000 RFP+ traced cells were inspected in the tMCAo model. SOX2/PU.1 double-positive RFP+ cells were not evident in the ischemic area (Figure 17F-G). The finding indicates the absence of TAMEP in the cerebral ischemia model.

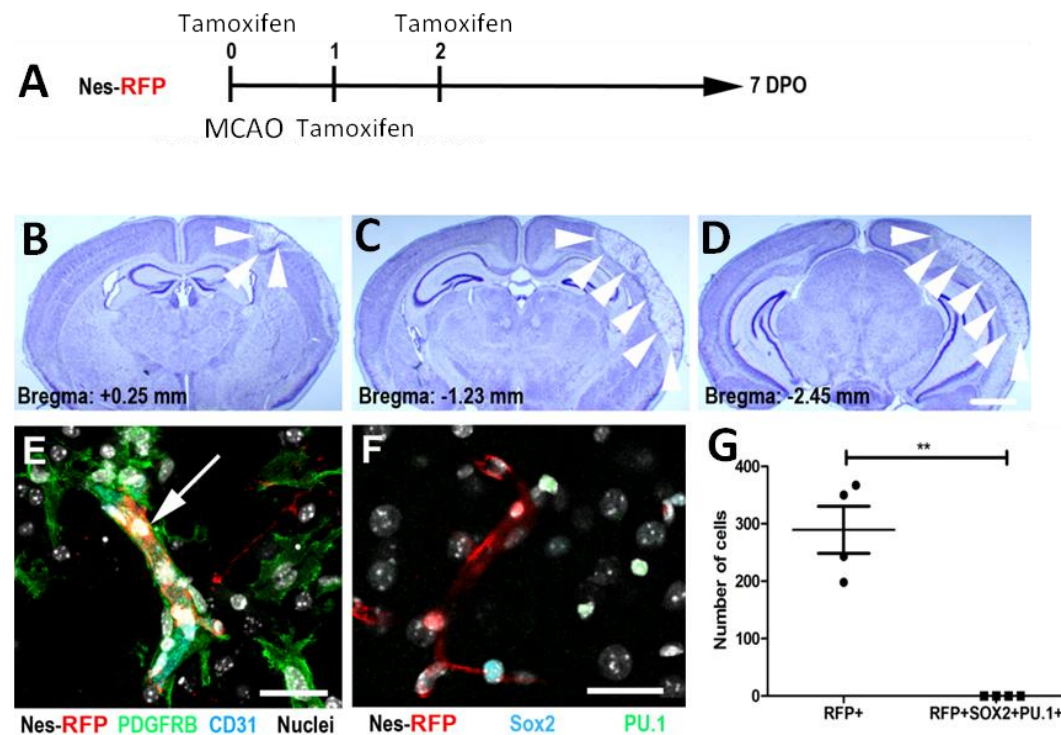


Figure 17 | TAMEP do not accumulate in cerebral ischemia.

Results

(A) Schematic diagram of transient middle cerebral artery occlusion (tMCAO) model procedure in Nes-RFP (Sox2-WT) mice. Tamoxifen was injected at days 0, 1, and 2. Brain tissues were harvested at day 7. (B-D) Representative images of Nissl staining performed on coronal mouse brain sections showing areas of ischemia (arrowheads; positions of images correspond to the bregma). (E) Nes-RFP tMCAO model traced the PDGFRB- (green) positive and CD31- (cyan) negative mural cells (arrow) in the stroked area. (F) Representative confocal image of Sox2 (cyan), Pu.1 (green), and Nes-RFP (red) in the area of stroke. Nuclei (gray) are stained with DAPI. (G) Quantification of the number of RFP+ cells and TAMEP in the infarction area of the tMCAO model. Statistical significance was determined using Student's *t*-test (** P<0.01). Each dot represents averaged data from one mouse. Values are presented as mean \pm SD. Scale bars, 1000 μ m (B-D) and 40 μ m (E and F).

1.3 Role of APLN and ANGPT2 mRNA in GBM

Previous studies from our group revealed that APLN is vital for tumor angiogenesis in GBM and that the APLN/APLNR signaling pathway plays a critical role in the resistance to anti-angiogenic treatment^{74,76}. Thus, it was appropriate to explore whether the loss of APLN in mouse GBM models could lead to increased vascular leakage. To ascertain the function of APLN in controlling vascular permeability, APLN knockout transgenic mice (APLN-KO) and APLN wild-type mice (APLN-WT) inoculated with GL261 tumor cells were used as experimental models. APLN expression cannot be detected in the murine GL261 glioma cell-line⁷⁶. Thus, the APLN-KO GL261 GBM mouse model constitutes an APLN-deficient microenvironment that can better elucidate the functions of APLN in GBM.

4.3.1 Loss of APLN increases the tumoral vascular permeability in GL261

Results

experimental glioma

We assessed the changes in tumor vascular permeability in the APLN-WT and APLN-KO GBM tumors using Evans Blue extravasation. A significant increase in Evans Blue extravasation was observed in the APLN-KO GBM model compared to the control (APLN-WT GBM model, Figure 18A). Representative images highlighted the difference in Evans Blue leakiness between the APLN-WT and APLN-KO GBM models (Figure 18B, C). The findings suggest the importance of APLN in controlling tumor vascular permeability. This finding from our experimental glioma model prompted us to investigate the role of APLN in vascular leakiness and edema formation with peritumoral edema in GBM patients using bioinformatics analysis of GBM data.

Results

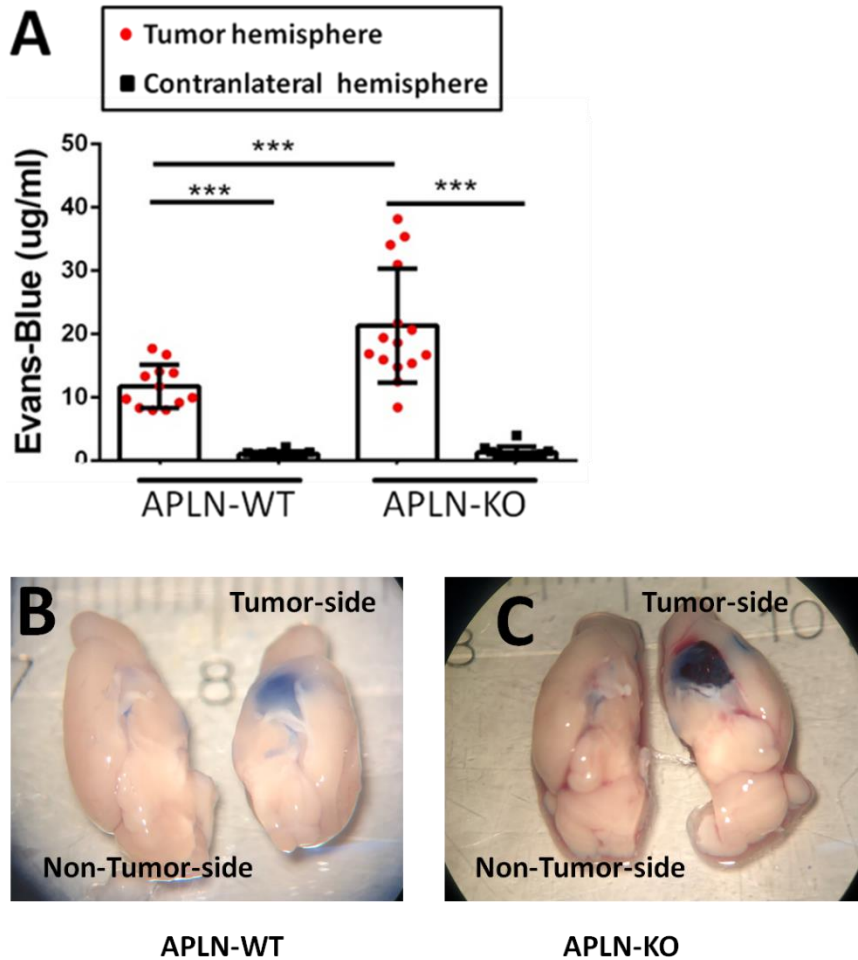


Figure 18 | Loss of APLN expression increases the tumoral vascular permeability in the GL261 mouse model.

(A) Vascular permeability of the Evans Blue dye extravasation is expressed as $\mu\text{g/ml}$ of brain homogenates. (B) Representative image shows extravasation of Evans Blue dye in APLN-WT GBM model mouse brain hemispheres. (C) Representative image shows extravasation of Evans Blue dye in APLN-KO GBM model mouse brain hemispheres.

4.3.2 Expression levels of APLN mRNA in the TCGA pan-cancer datasets

APLN expression levels in human cancer specimens (TCGA database)¹¹⁶ was explored.

The APLN expression level was significantly increased in different cancers as compared to the levels in the normal groups, including bladder urothelial carcinoma,

Results

cholangiocarcinoma, colon adenocarcinoma, glioblastoma, head-neck squamous cell carcinoma, kidney chromophobe, kidney renal papillary cell carcinoma, liver hepatocellular carcinoma, lung adenocarcinoma, lung squamous cell carcinoma, and stomach adenocarcinoma (Figure 19). Notably, the highest average expression of APLN in TCGA pan-cancer datasets was observed in the TCGA GBM dataset (Figure 19; red box).

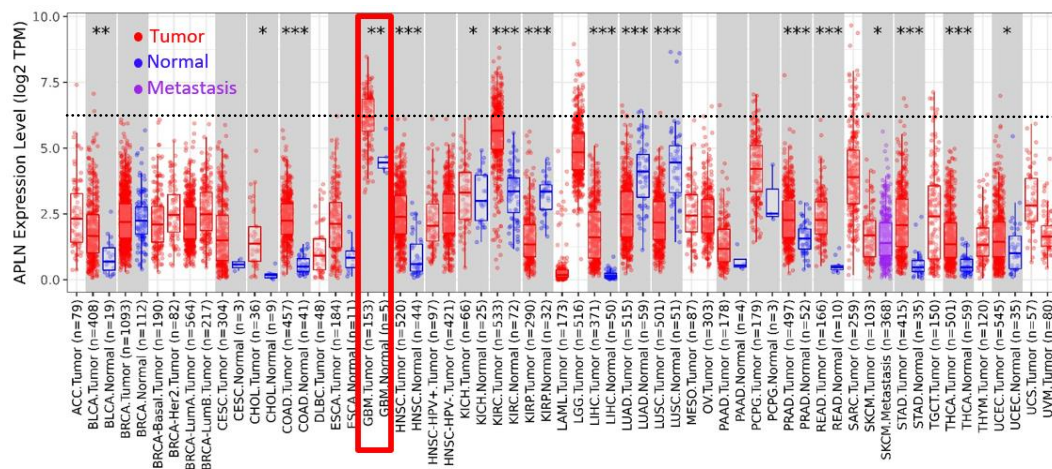


Figure 19 | Expression of APLN in TCGA pan-cancer database.

TCGA mRNA-seq data visualization using TIMER2.0 showing the expression of APLN in different types of tumors. The red frame highlights APLN mRNA expression in GBM. The distributions of the gene expression levels are shown using box plots. The statistical significance calculated by differential analysis (edgeR) on RNA-Seq raw counts was annotated by the number of asterisks (* P < 0.05, ** P < 0.01, *** P < 0.001). Each dot represents sample expression. Red denotes tumor samples, blue denotes normal samples, and violet denotes a metastatic tumor. As shown in the gray columns, normal data are available.

4.3.3 APLN-associated genes in the TCGA-GBM database

To explore the potential biological function of APLN in GBM, the genes correlated with APLN expression were examined in the TCGA-GBM dataset. A Volcano plot showed

Results

genes with significant positive and negative associations with APLN (Figure 20A). The top 50 genes that positively correlated with APLN expression are shown in the heat map in Figure 20B.

Results

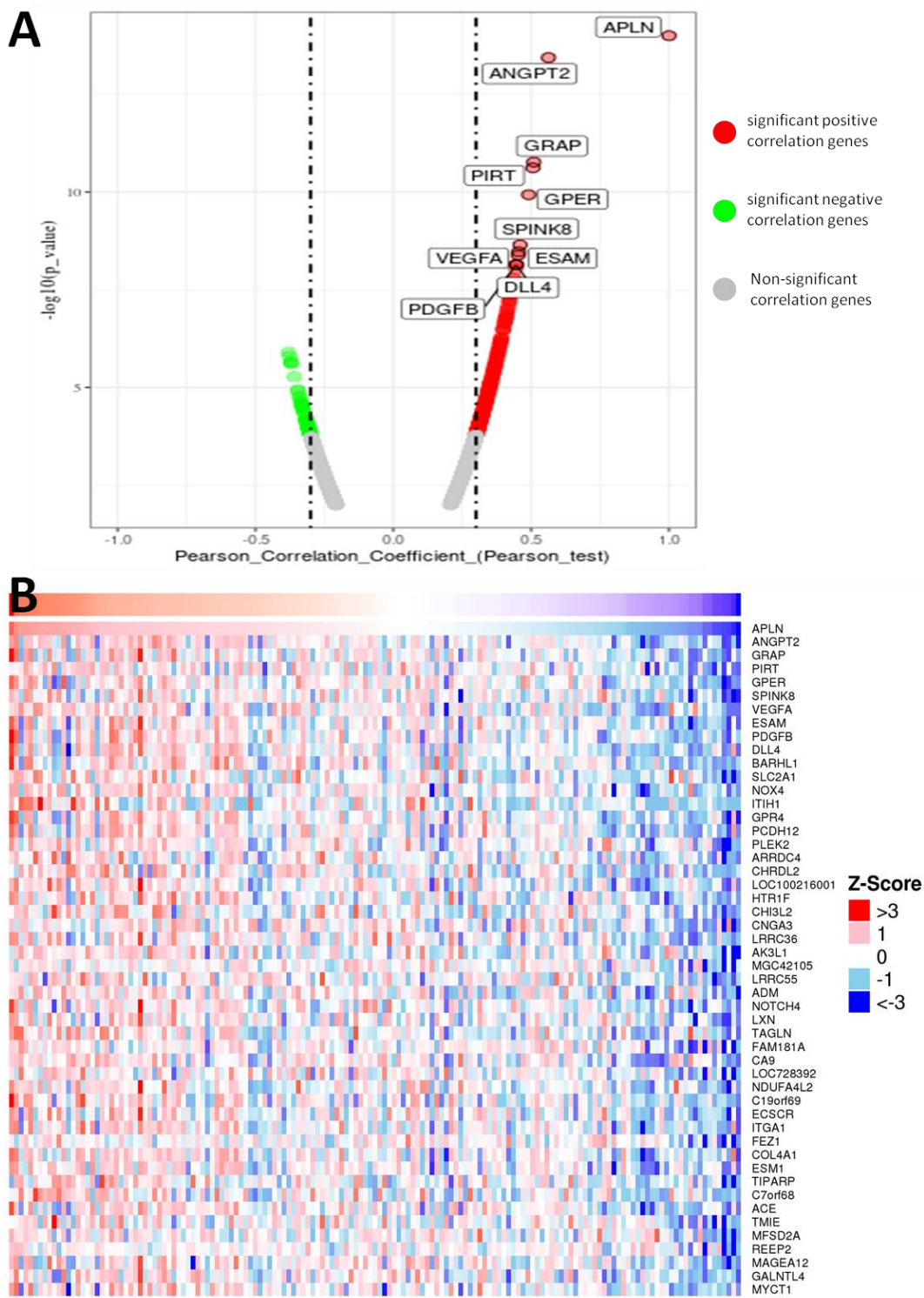


Figure 20 | APLN-associated genes in TCGA-GBM database.

(A) Volcano plot depicting the association between APLN and association genes. This plot was created using VolcanoSeR¹¹⁷ (<https://huygens.science.uva.nl/VolcanoSeR/>)
 (B) Heatmap of the top 50 positive correlated genes of APLN in TCGA-GBM.

4.3.4 Gene ontology (GO) annotations of APLN-associated genes in GBM

GO biological process and Kyoto Encyclopedia of Genes and genomes (KEGG) pathway enrichment analyses⁹⁷ were performed on the top 50 APLN-associated genes. APLN-associated genes were involved in blood vessel development, vascular processes in the circulatory system, blood vessel branching morphology, and maintenance of blood–brain barrier permeability (Figure 21A). This functional enrichment agreed with our Evans Blue extravasation experiment in the APLN-KO GL261 model, in which loss of APLN led to increased vessel permeability. Thus, we questioned whether the APLN expression level is also associated with tumoral vascular permeability in GBM patients. A previous study showed that peritumoral edema in the GBM is associated with the vascular permeability of the tumor¹¹⁸. The extent of peritumoral edema could be assessed by edema index (ratio of T2/FLAIR tumor volume and T1 contrast-enhanced tumor volume of MRI)⁹⁴. In the present study, we used this edema index to compute the peritumoral edema of GBM patients. There was no significant association between APLN expression levels and peritumoral edema in GBM patients (Figure 21B).

Results

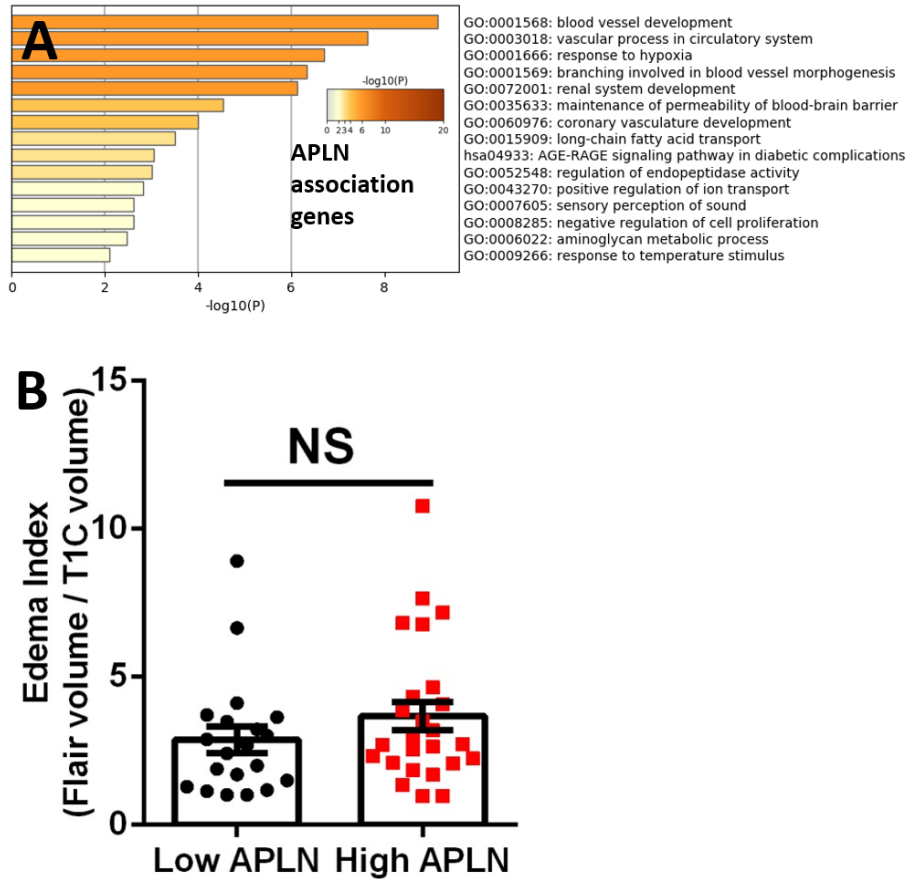


Figure 21 | Potential functions of APLN-associated genes in GBM.

(A) Analyses of GO- and KEGG-enriched terms were performed in Metascape using the top 50 ANGPT2-associated genes, colored by $-\log(p\text{-value})$. (B) The edema index was used to represent the extent of edema-formation in GBM with high or low APLN expression levels. Statistical significance according to Student's t -test, * $P < 0.05$, ** $P < 0.01$, *** $P < 0.001$, NS, No significant difference. Each dot shows data acquired from a single patient. Values are presented as mean \pm SEM.

4.3.5 Strong positive correlation between APLN and ANGPT2 expression levels in GBM

Clinically, *MGMT* methylation¹¹⁹, and the *IDH1 R132H* mutation¹²⁰ are candidates for predicting the prognosis of GBM. These predictions are more reliable than those based on morphological methods. However, in most cases, using a single gene is insufficient

Results

to predict the prognosis of highly heterogeneous GBM. The combination of *IDH1* mutations and *MGMT* methylation to predict the prognosis of GBM is more reliable than the use of either of the single gene alone¹²¹. Thus, we wondered if we could also combine APLN with other genes to predict peritumoral edema in GBM. The TCGA database was screened for additional genes that also controlled angiogenesis. ANGPT2 was the most significant APLN-association gene in the TCGA-GBM dataset (Figure 20A, B and Figure 22A). This strong correlation was confirmed in the CGGA-GBM database (Figure 22B). Also, APLN and ANGPT2 are highly expressed by endothelial tip cells and both are essential in angiogenesis^{122, 123}. GBM had the second-highest average expression level of ANGPT2 in the TCGA database (Figure 22C). Therefore, we chose to combine APLN and ANGPT2 to explore the association between peritumoral edema of GBM with these both gene expression levels.

Next, TCGA-GBM patients were classified into high APLN/high ANGPT2 expression and low APLN/low ANGPT2 expression groups. The extent of peritumoral edema of patients was not different between patients with high APLN/high ANGPT2 expression levels and patients with low APLN/low ANGPT2 expression levels (Figure 22E). We also assessed if ANGPT2 expression levels were associated with peritumoral edema in GBM patients. The extent of patients' peritumoral edema level was also not different in patients with high or low ANGPT2 expression levels (Figure 22D).

Results

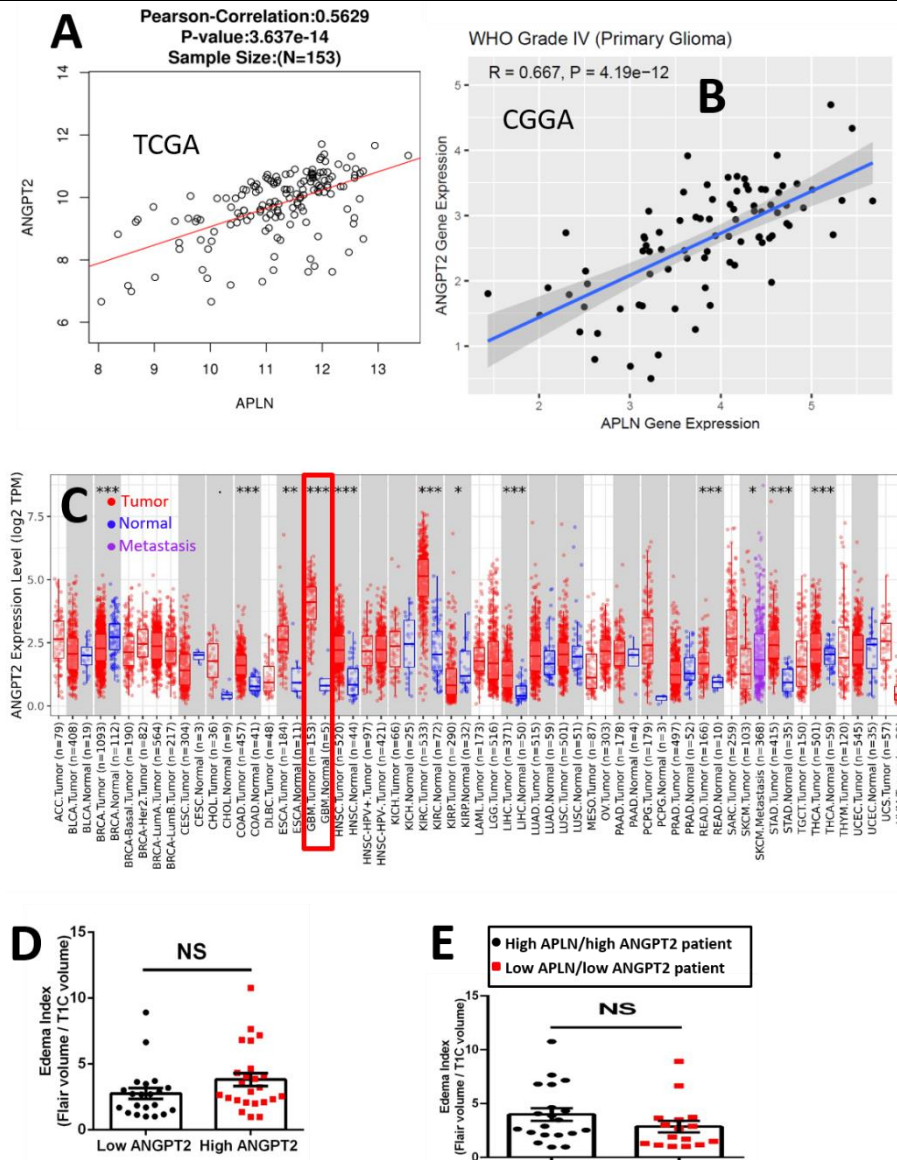


Figure 22 | Strong positive correlation between APLN and ANGPT2 expression levels in GBM.

(A) Association between APLN and ANGPT2 gene expression in TCGA-GBM database. (B) Association between APLN and ANGPT2 gene expression in CGGA database. (C) The expression of ANGPT2 in different types of cancers. The red frame highlights the ANGPT2 expression in GBM. The distribution of the gene expression levels is shown with box plots. The statistical significance was calculated by differential analysis (edgeR) on RNA-Seq raw counts (* $P < 0.05$, ** $P < 0.01$; *** $P < 0.001$). Each dot represents a single sample. Red symbols indicate tumor samples, and violet denotes metastatic tumor. Values were highlighted with a gray background when tumor-free controls were available. (D) The edema index was used to represent the extent of edema-formation in GBM with low or high level of ANGPT2. (E) The edema index was used to represent the extent of edema-formation in GBM with low level of

Results

APLN/ANGPT2 or high level of APLN/ANGPT2. Statistical significance according to Student's *t*-test (D, E), * $P < 0.05$, ** $P < 0.01$, *** $P < 0.001$. NS, No significant difference. Each dot shows data acquired from a single patient. Values are presented as mean \pm SEM.

4.3.6 High APLN/low ANGPT2 expression levels are associated with milder peritumoral edema

Interestingly, patients with high mRNA levels of APLN and low expression levels of ANGPT2 showed milder edema than patients with low mRNA levels of APLN and high expression levels of ANGPT2 (Figure 23A). The ratio of T2/FLAIR volume (tumor + edema) and T1C volume (tumor) was calculated as the tumor edema index and used to evaluate peritumoral edema⁹⁴. Representative T2/FLAIR and T1C sequences of MR images from patients with high mRNA levels of APLN and low expression levels of ANGPT2 showed milder peritumoral edema (Figure 23 B, C). Representative T2/FLAIR and T1C sequences of MR images from patients with low mRNA levels of APLN and high expression levels of ANGPT2 showed prominent peritumoral edema (Figure 23 D, E).

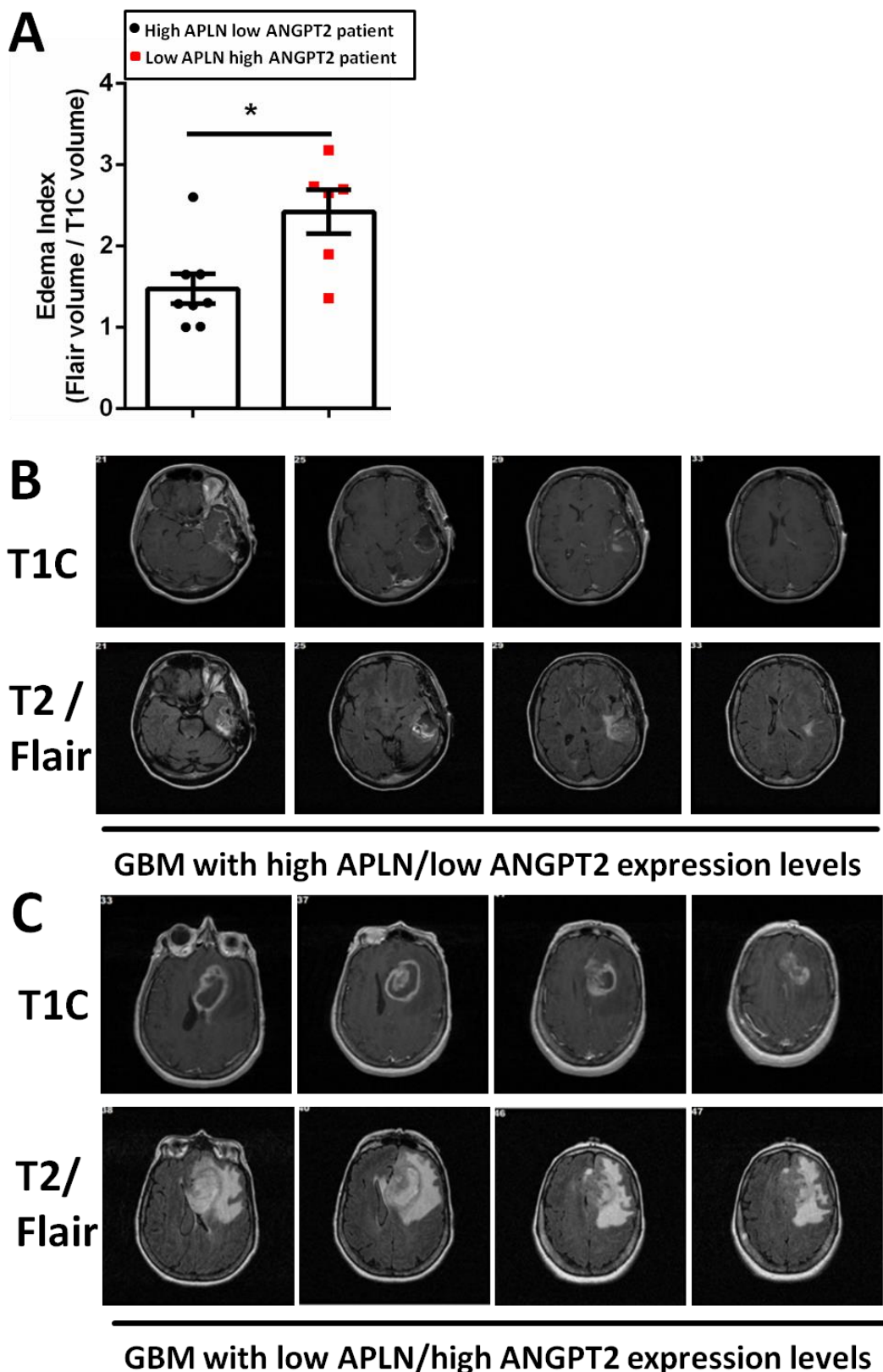


Figure 23 | High APLN/low ANGPT2 expression levels are associated with milder

peritumoral edema.

(A) The edema index was used to represent the extent of edema-formation in GBM with high APLN/low ANGPT2 or low APLN/high ANGPT2 expression levels. (B) Representative post-contrast T1-weighted (upper panel) and T2-FLAIR (lower panel) brain MRI scans of GBM patient with high APLN/low ANGPT2 expression levels. (C) Representative post-contrast T1-weighted (upper panel) and T2-FLAIR (lower panel) brain MRI scans of GBM patient with low APLN/high ANGPT2 expression levels. Statistical significance according to Student's *t*-test (A), * $P < 0.05$. Each dot shows data acquired from a single patient. Values are given as mean \pm SEM.

4.3.7 Potential roles of ANGPT2-associated genes in TCGA-GBM dataset

Next, we explored why high APLN/low ANGPT2 expression levels are associated with milder peritumoral edema in GBM. From the functional enrichment analysis on APLN-associated genes in the TCGA-GBM dataset (4.3.4), we already concluded that APLN-associated genes were associated with vascular development in GBM. Next, we also investigated the potential roles of ANGPT2-associated genes using the TCGA-GBM repository. Here, we identified the top 50 ANGPT2-associated genes (Figure 24A). Functional enrichment analysis of these genes included GO and KEGG annotations connecting these genes with response to hypoxia, regulation of blood vessel endothelial cell migration, and the HIF2 pathway (Figure 24B). Response to hypoxia results in stimulation of angiogenesis¹²⁴ and endothelial cell migration. The hypoxia inducible factor 2 (HIF2) pathway is also involved in the initial stage of angiogenesis^{125,126}. These suggested that ANGPT2-associated genes in GBM correlate with the initial stage of tumor angiogenesis development.

Results

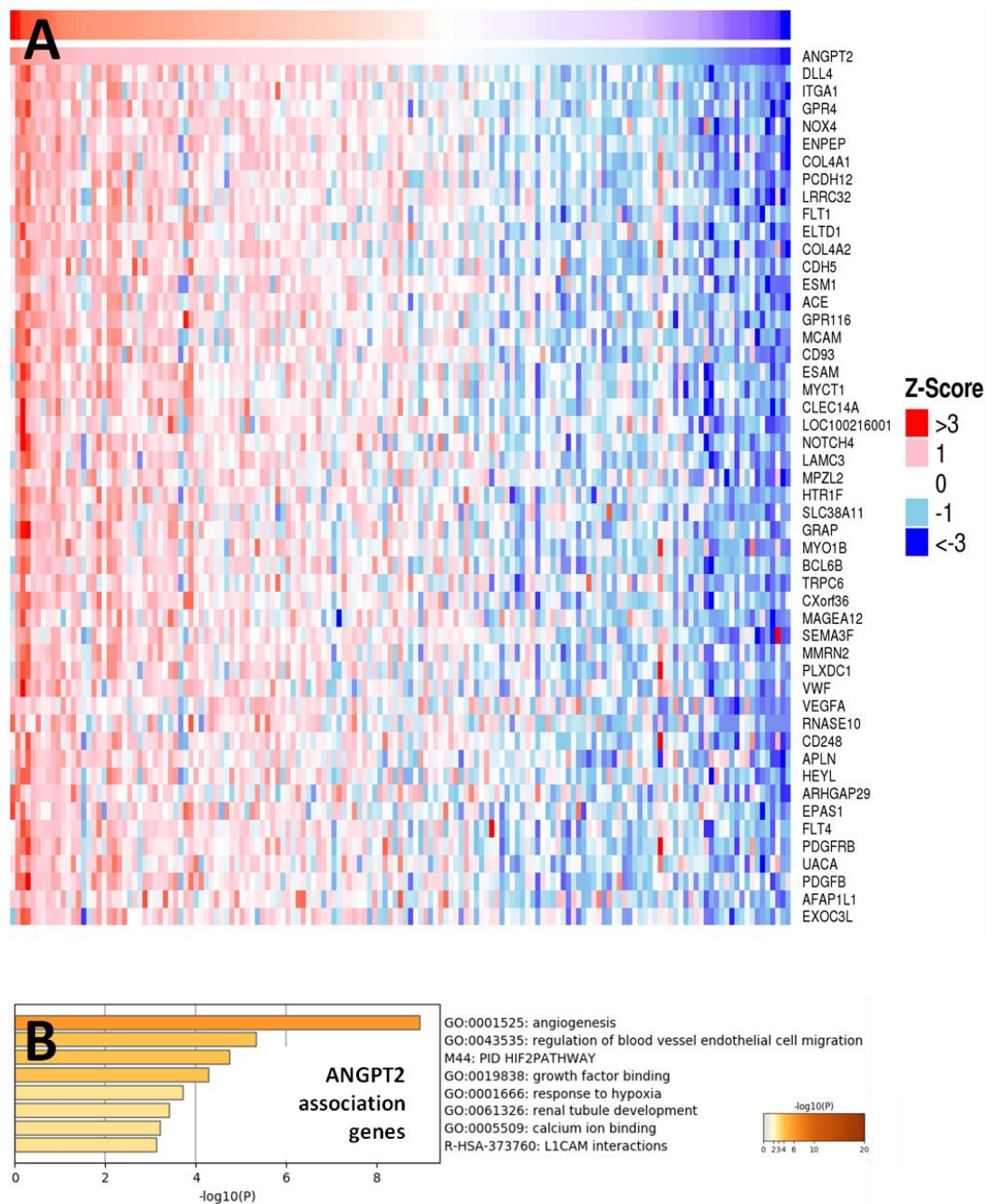


Figure 24 | Potential roles of ANGPT2-associated genes in GBM.

(A) Heat map showing top 50 genes positively correlated with ANGPT2 in GBM. (B) GO-enriched and KEGG-enriched terms analysis were performed in Metascape using the top 50 ANGPT2-associated genes, colored by $-\log(p\text{-value})$.

4.3.8 Different roles of APLN- and ANGPT2-associated genes in angiogenesis of

Results

GBM

To further explore the different functions of APLN- and ANGPT2-associated genes in GBM, Metascape was used to depict top enriched clusters and their enrichment patterns across APLN- and ANGPT2-associated gene lists as a clustered heatmap (Figure 25). APLN- and ANGPT2-associated genes in GBM shared some GO terms that included response to hypoxia, blood vessel branching morphogenesis, and blood vessel development (Figure 25; blue box). Response to hypoxia¹²⁴ and blood vessel branching morphogenesis¹²⁷ both have important early roles in the angiogenesis of GBM. These results might indicate that the activity of both APLN- and ANGPT2-associated genes are orchestrated in the early stages of tumor vessel development in GBM.

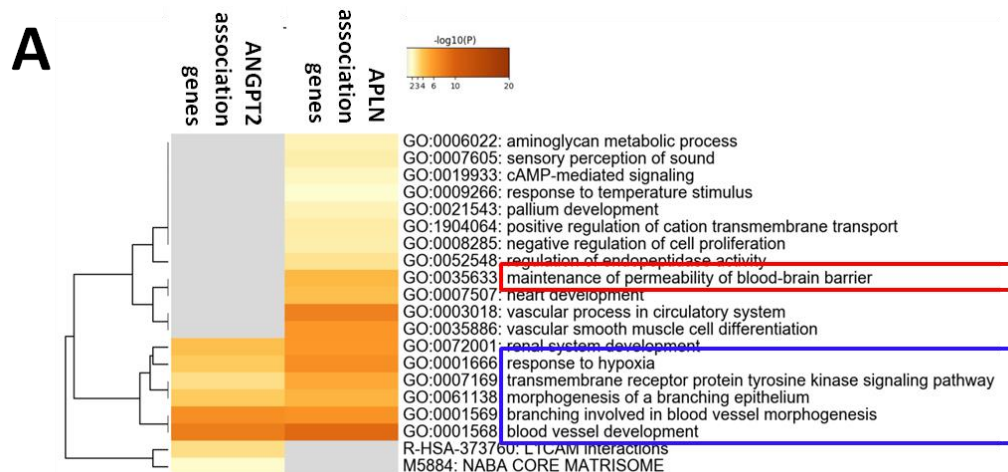


Figure 25 | Different roles of APLN- and ANGPT2-associated genes in angiogenesis of GBM.

(A) Metascape analysis shows the top 20 clusters with their representative GO-enriched and KEGG-enriched terms across the APLN-association, and ANGPT2-association gene lists, colored by colored by $-\log_{10}(p\text{-value})$.

4.3.9 High APLN/low ANGPT2 expression levels in GBM are associated with

Results

prolonged survival

A potential association between APLN and (or) ANGPT2 expression levels with overall survival in GBM patients was investigated using a Kaplan–Meier plot¹²⁸. No significant correlation between APLN or ANGPT2 expression levels alone with overall survival of GBM patients was evident in the TCGA and CGGA GBM datasets (Figure 26A, B, E, F). There was also no difference in overall survival between the patients with “high APLN”/“high ANGPT2” expression levels and the patients with “low APLN”/“low ANGPT2” expression levels in both TCGA-GBM and CGGA-GBM datasets (Figure 26C, G). Interestingly, significant longer survival was observed in the patients with high APLN/low ANGPT2 expression levels compared to that in the patients with “low APLN”/“high ANGPT2” expression level in the TCGA-GBM and CGGA datasets (Figure 26D, H). Peritumoral edema may cause severe neurological signs and symptoms in GBM patients⁵⁹. A number of studies reported that the higher peritumoral edema is associated with a worse clinical prognosis in GBM patients^{129, 130, 131}. This may partially account for the longer survival in GBM patients with “high APLN”/“low ANGPT2” expression levels compared to the patients with “low APLN”/“high ANGPT2” expression levels.

Results

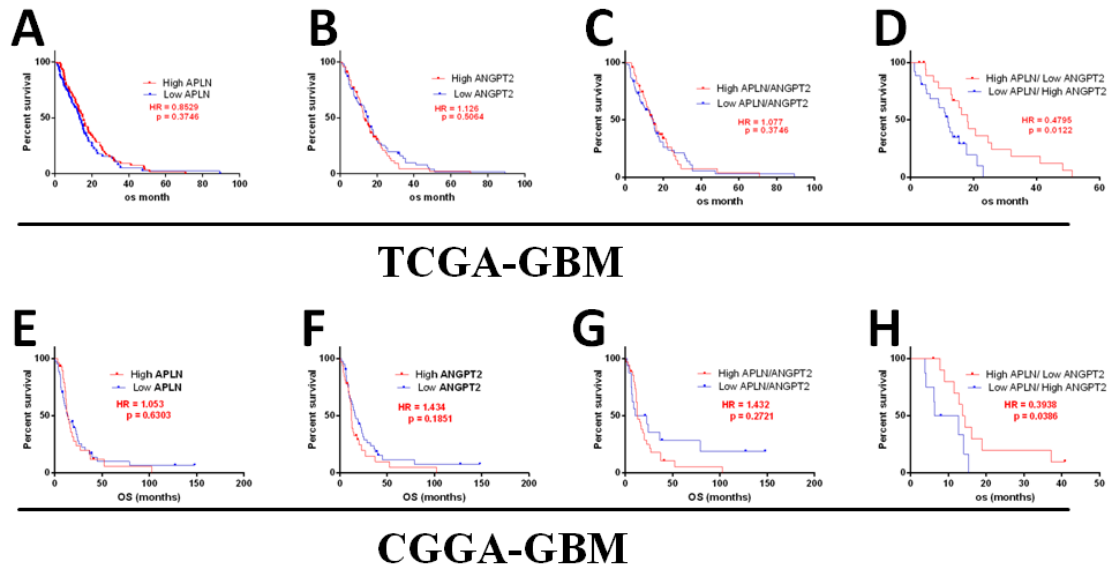


Figure 26 | High APLN/low ANGPT2 expression levels in GBM are associated with prolonged survival.

(A) Kaplan–Meier analysis was used to assess the overall survival rates of high (n=75) or low (n=76) APLN expression in TCGA-GBM. (B) Kaplan–Meier analysis was used to assess the cumulative survival rates of high (n=75) or low (n=76) ANGPT2 expression in TCGA-GBM. (C) Kaplan–Meier analysis for the patients between high APLN, ANGPT2 expression (n=45), and low APLN, ANGPT2 expression (n=60) in TCGA-GBM. (D) Kaplan–Meier analysis for the patients between high APLN, low ANGPT2 expression (n=20), and low APLN, high ANGPT2 expression (n=25) in TCGA-GBM. (E) Kaplan–Meier analysis was used to assess the overall survival rates of high (n=29) or low (n=44) APLN expression in CGGA-GBM. (F) Kaplan–Meier analysis was used to assess the cumulative survival rates of high (n=32) or low (n=41) ANGPT2 expression in CGGA-GBM. (G) Kaplan–Meier analysis for the patients between high APLN, ANGPT2 expression (n=35) and low APLN, ANGPT2 expression (n=19) in CGGA-GBM. (H) Kaplan–Meier analysis for the patients between high APLN, low ANGPT2 expression (n=11), and low APLN, high ANGPT2 expression (n=8) in CGGA-GBM. Log-rank (Mantel-Cox) test was used to determine statistical significance, *P<0.05, **P<0.01.

5. Discussion

In the first part of this thesis, the function of pericytes in tumor vascular permeability was investigated in a GBM mouse model. In the second part of the thesis, the function of a previously unknown cell population, TAMEP, in tumor vascular permeability was investigated *in vivo*. In the third part of the thesis, bioinformatics analysis and analyses in transgenic mice were performed to assess the function of APLN and ANGPT2 in vascular permeability.

5.1 The role of pericytes in early and advanced GBM

The results demonstrate that pericytes play a critical role in maintaining vascular integrity and GBM expansion. Moreover, advanced GBM features rapid compensatory mechanisms to repair pericyte loss. Tumor volumes were significantly reduced in both the early and advanced pericyte-depletion GBM models. In the early pericyte-depletion GBM model, there was a reduced vascular network and decreased collagen IV production. Moreover, tumor vascular permeability was markedly increased when pericytes were depleted early in GBM. These results indicate that pericytes play a critical role in the formation, development, and maturation of GBM vessels. A previous study using the same GL261 mouse GBM model also indicated the critical role of host-derived pericytes in GBM development¹³². Consequently, pericytes play a decisive role in regulating the angiogenesis of GBM, especially in the early phase of GBM formation.

One major obstacle in the treatment of GBM is the presence of the blood–brain

Discussion

barrier. Due to their relatively high molecular weight, most therapeutic drugs fail to cross this barrier from the blood circulation¹³³. Consistent with this knowledge, our results in wild-type controls demonstrated that most of the high molecular weight dextran (2 MDa) stayed inside the vessel lumen. Interestingly, in the early pericyte-depletion GBM model, more 2 MDa dextran was located inside the endothelial cells. These results suggest that pericyte depletion markedly upregulates the transcytosis of endothelial cells and increases the uptake of high molecular drugs into the brain. To date, of all drugs in the medicinal chemistry database, only approximately 5% are capable of entering the CNS¹³⁴. This significantly influences the medical efficacy of treatment for diseases of the CNS. Modulating pericytes and increasing endothelial transcytosis may be a feasible way to improve the delivery of high molecular antitumor agents for brain cancer therapy. Hence, combining pericyte-modulating drugs (increasing blood-tumor barrier permeability) with antitumor agents is an interesting possibility, which merits further evaluation in preclinical models.

The vascular network and tumor volume were only mildly decreased after pericyte depletion in advanced GBM compared to wild-type controls. Interestingly, pericyte depletion in advanced GBM, vascular permeability, PDGFRB⁺ pericytes, and collagen IV production were not significantly different from controls. We confirmed the efficiency of pericyte depletion in the advanced GBM and observed a decrease in PDGFRB⁺ pericytes and an increase in vascular permeability with pericyte depletion in the advanced GBM model. Pericyte loss in early GBM could be completely repaired

Discussion

in tumor-free regions. Interestingly, in the early pericyte-depletion GBM model, the number of PDGFRB+ pericytes and vascular integrity was dramatically and persistently decreased in tumors compared to that in the wild-type controls. These results suggest that pericyte loss can be completely repaired in tumor-free regions and partially repaired in advanced GBM. However, pericyte loss cannot be compensated for in the early stage of GBM formation. In the tumor-free brain and advanced GBM, the pre-existing damage of blood vessels and endothelial cells remain after pericyte depletion. These pre-existing endothelial cells can secrete growth factors, such as sphingosine-1-phosphate-1¹³⁵, PDGF-B¹³⁶, VEGF-A, and TGF- β ¹³⁷, to repair pericyte loss by promoting the proliferation and migration of pericytes. Notably, VEGF-A and TGF- β are highly expressed in endothelial cells of GBM¹³⁷. Hence, we supposed that pre-existing endothelial cells and blood vessels could promote the reversal of pericyte loss after the depletion of pericytes in advanced GBM and tumor-free brains.

In contrast, in the early phase of GBM, we observed a relatively small number of intratumoral blood vessels, compared with the vascular network of advanced GBM, which may suggest that the “angiogenic switch” had not started at this early GBM stage. vessels¹³⁸. Therefore, pericyte-depletion in early GBM, which might induce the “angiogenic switch off” in the early stage of GBM, could lead to the abnormal development of the tumoral vascular network. This might explain why the vessels had a large lumen and high vascular permeability compared to the wild-type controls in the early pericyte-depletion GBM model.

Discussion

Hyperplasia of pericytes is an established pathological feature of malignant gliomas^{139, 140}. Moreover, in the CNS and retina, the approximate ratio of pericytes to endothelial cells is 1:1, which is much higher than the ratio in other organs (e.g., 1:10 in the skin and lung 1:100 in striated muscle)¹⁴¹. These hyperplastic pericytes in GBM and high pericytes/ECs ratio in the brain may contribute as cell-reservoir compensatory for the loss of pericyte in advanced GBM and tumor-free brain.

In summary, the collective findings confirm the crucial role of pericytes in GBM growth, especially in the early stages of GBM. In advanced GBM, there may be rapid compensatory mechanisms to repair the loss of pericytes. This is a reminder that different tumor stages require a combination of multi-therapeutic approaches, which must also consider the rapid pericyte-loss repair capability in advanced GBM. However, the underlying molecular mechanisms of rapid replenishment of pericytes are still unclear and are worthy of further study.

5.2 Depleting TAMEP disrupt angiogenesis of GBM

Our study showed that TAMEP could regulate angiogenesis, contribute to collagen IV synthesis, and maintain vascular permeability in GBM (Figure 27). Moreover, TAMEP were only present in the TME but not in tumor-free CNS regions and other neuropathologies, including cerebral ischemia. Avascular cells, such as avascular MSCs, often promote the formation of vessels, maintain vascular permeability, and repair damaged vessels¹⁴². TAMEP also displayed an avascular location. Thus, we wondered

Discussion

whether TAMEP can also regulate angiogenesis in GBM. The observation of significantly decreased tumor vessel density in TAMEP-defective GBM compared to TAMEP-containing GBM controls support the conclusion that TAMEP participates in GBM angiogenesis. This may explain the tumor reduction in the GBM model featuring TAMEP depletion. The relationship between TAMEP and angiogenesis is unidirectional, as demonstrated by the number of TAMEP that were not reduced compared to the control after administration of the anti-angiogenic agent (DC101 VEGF-A antibody). The VEGF-A neutralizing antibody bevacizumab was approved in 2009 by the FDA for the treatment of recurrent glioblastoma¹⁴³. The observation that VEGF-A antibody did not affect the number of TAMEP indicates the suitability of VEGF-A antibody and TAMEP-modulating molecule for GBM patients.

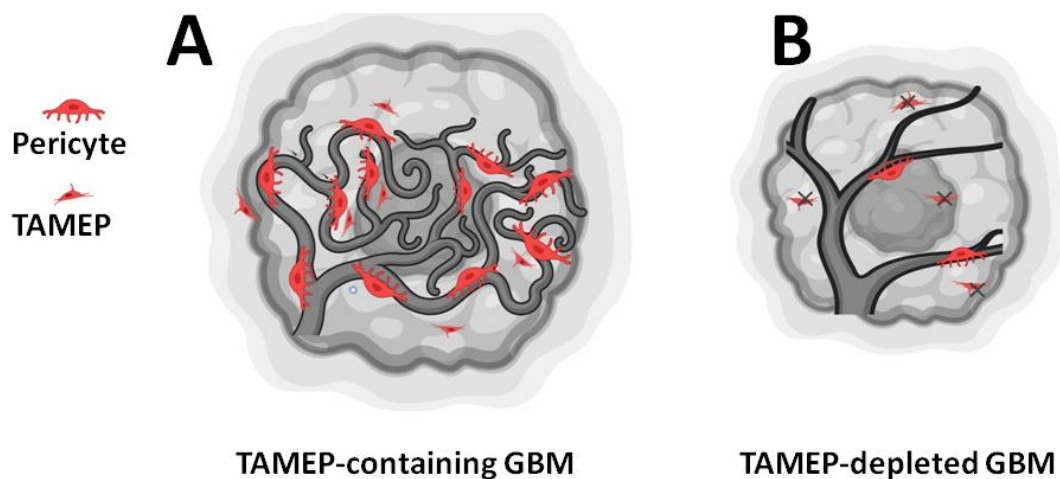


Figure 27 | Functions of TAMEP in GBM-angiogenesis.

(A) Wild-type GBM with rich vessels and high pericyte-coverage. (B) TAMEP-depletion GBM model with fewer vessels, low pericyte-coverage, and smaller volume. This figure was created using BioRender (<https://biorender.com/>).

Discussion

Pericyte-coverage in the TAMEP-depleted GBM group was significantly lower than that in the control group. Pericytes can promote collagen IV synthesis^{144, 145} and maintain vascular integrity^{146, 147, 148}. Thus, speculating that the loss of pericytes might decrease the production of collagen IV, we assessed collagen IV production and demonstrated a dramatic decrease within the tumor but not in the tumor-free region. Since TAMEP are only traced within the tumor, increased vascular permeability was only evident in the tumor. Additionally, TAMEP were not detected in the cerebral ischemic stroke model. These results suggest that TAMEP modulate pericyte proliferation and collagen IV synthesis, affecting vascular permeability. Moreover, TAMEP are only found in tumor tissue and are not present in tumor-free regions or in regions with non-neoplastic neuropathology. Taken together, these results indicate that TAMEP are tumor-specific cells required for the formation and maturation of GBM vessels. The data implicate TAMEP as a novel and promising therapeutic target in neuro-oncology.

5.3 High APLN/low ANGPT2 mRNA expression levels are associated with vascular tightness and prolonged survival

In this part of my study, the use of a mouse GBM model demonstrated that the loss of APLN leads to an increase in tumoral vascular permeability. Moreover, the ratio of high APLN/low ANGPT2 expression levels in the tumor tissues of GBM patients is associated with milder peritumoral edema and prolonged survival.

Discussion

Previous studies from our group revealed that APLN is vital for tumor angiogenesis in GBM and that the APLN/APLNR signaling pathway plays a critical role in the resistance to anti-angiogenic treatment^{74, 76}. To further explore the function of APLN in tumoral vascular permeability, we used APLN-KO and APLN-WT mice and GL261 tumor cells to establish APLN-KO GL261 GBM and APLN-WT GL261 GBM mouse models. APLN expression is not detectable in the murine GL261 glioma cell-line⁷⁶. Thus, the APLN-KO GL261 GBM mouse model constitutes an APLN-deficient microenvironment. Compared to the APLN-WT GBM mouse model, the loss of APLN expression in the mouse GL261 glioma model increased tumor vascular permeability. This finding from our experimental glioma model prompted us to investigate a correlative role of APLN with vasogenic edema in GBM patients using bioinformatics methods.

APLN expression levels in TCGA pan-cancer datasets were examined. The highest expression level of APLN was found in the TCGA-GBM dataset (Figure 19). Next, functional enrichment analysis on APLN-associated genes in GBM patients showed that these genes were associated with blood vessel development, vessel branching morphology, as well as blood–brain barrier permeability. Therefore, we wondered if APLN expression level in GBM patients could be directly associated with vascular permeability. Vascular permeability in GBM patients can lead to peritumoral edema, which is detectable by MRI⁶⁴. Comparison of the APLN expression level with the extent of peritumoral edema in GBM did not reveal a significant association

Discussion

between APLN expression with edema level in GBM. Next, the expressions of APLN and ANGPT2 were assessed to explore the potential relationship between pro-angiogenic genes encoding APLN and ANGPT2, and edema of GBM. APLN and ANGPT2 are highly expressed by endothelial tip cells and play an important role in angiogenesis^{122, 123}. In addition, we observed that the gene encoding ANGPT2 was the most significant APLN-associated gene in the TCGA-GBM dataset. Based on the APLN and ANGPT2 expression levels, GBM patients were reclassified into high APLN/high ANGPT2 and low APLN/low ANGPT2 expression levels groups. There was still no significant difference in peritumoral edema of GBM patients in these two groups. Interestingly, GBM patients with high APLN/low ANGPT2 expression levels had milder peritumoral edema compared to the GBM patients with low APLN/high ANGPT2 expression levels. There was also no correlation of ANGPT2 expression level along with peritumoral edema in GBM patients.

A functional enrichment analysis of APLN-associated genes in GBM patients revealed the involvement of these genes in the entire process of blood vessel development in GBM, from sprouting angiogenesis through vascular branching and tumor vessel maturation. A prior study from our group also implicated vascular APLN expression as being critical for the formation of a mature tumor vasculature that supports GBM growth⁷⁶. In addition, an *in vivo* mouse colon adenocarcinoma model, Kidoya et al. also found that the APLN/APLNR signaling pathway induces tumor vessel maturation¹⁴⁹. These findings might suggest that APLN-associated genes in

Discussion

GBM have a central role in controlling the entire process of vascular development from sprouting angiogenesis to vessel maturation.

Functional enrichment analysis of ANGPT2-associated genes in GBM showed that these genes were mainly associated with response to hypoxia, endothelial cell migration, and the HIF2 pathway. Response to hypoxia stimulates angiogenesis¹²⁴. Endothelial cell migration and the HIF2 pathway are also involved in the initial stage of angiogenesis^{125, 126}. The collective findings suggest that ANGPT2-associated genes in GBM are correlated with the initial stage of tumor angiogenesis development. Thus, high APLN/low ANGPT2 expression levels might be indicative of tumors of GBM patients that have more mature and structurally sound blood vessels. In contrast, low APLN/high ANGPT2 expression levels might indicate GBM with a more immature and leakier vascular network. This could explain why GBM patients with high APLN/low ANGPT2 expression levels have milder peritumoral edema, while patients with low APLN/high ANGPT2 expression levels have more prominent peritumoral edema.

Kaplan–Meier survival analysis illustrated those patients with high APLN/low ANGPT2 expression levels in GBM tissue manifested with longer overall survival compared to the patients with low APLN/high ANGPT2 expression levels. Peritumoral edema may cause severe neurological symptoms in GBM patients⁵⁹. Severe peritumoral edema predicts a poor clinical outcome in GBM patients^{129,130, 131}.

Due to the limitations of the public database, we could not validate the vascular permeability at the neuroimaging level in the CGGA database. After re-grouping the

Discussion

patients from the TCGA and CGGA databases, only a limited number of patients were included. These results would have been more reliable with an increased amount of data. Nevertheless, the results of the above analysis are encouraging and warrant further investigation. In the future, we will perform more comprehensive animal experiments and collect more clinical data to validate these findings.

6. Summary

Angiogenesis plays an essential role in GBM development. Thus, in this thesis, I investigated some of the main cellular components and signaling molecules in GBM angiogenesis. These cellular components included pericytes and TAMEP cells (tumor-associated cells with a myeloid-like expression profile), while angiogenic signals comprise the factors Apelin (APLN) and Angiopoetin-2 (ANGPT2).

In the first part of this thesis, I studied the different roles of pericytes in the early and advanced stages of tumor growth. Pericytes are required for angiogenesis and play a critical role in regulating vascular integrity in GBM. Hence, I hypothesized that pericytes may support the expansion of GBM. Consistently tumor volume was reduced after depleting pericytes at early or at advanced stages of GBM growth. When pericytes were depleted in early stage GBM, the tumor vascular network and vascular integrity were significantly and persistently disrupted. Also, the transcytosis ability of ECs was significantly upregulated. These results suggest that pericytes play a critical role in GBM growth and are required at very early tumor stages for the establishment of a pathological vascular network.

Interestingly, when pericytes were depleted at advanced stages of GBM expansion, vascular permeability was not increased as compared to pericyte-containing GBM-controls. This result suggests that in the advanced stage of GBM, pericytes likely do not play an important role in maintaining vascular permeability. Thus, pericytes may be a therapeutic target for GBM treatment at an early stage in GBM growth, and further

Summary

studies will be required to elucidate the function of pericytes in advanced stages of GBM.

In the second part of this thesis, I investigated the role of a previously unknown short-lived avascular cell population during glioma genesis called TAMEP. TAMEP are tumor-associated cells with a myeloid-like expression profile in the tumor microenvironment and characterized by the co-expression of SOX2 and PU.1. This study indicated that in TAMEP-depleted GBM, the tumor volume significantly decreased, and tumor vascular permeability increased as compared to TAMEP containing controls. Moreover, the production of collagen IV was inhibited in the TAMEP-defective GBM. Thus, we concluded that TAMEP could modulate pericytes and the synthesis of collagen IV to regulate vascular permeability and tumor development. In return, TAMEP cell numbers was not affected by a blockade in tumor angiogenesis. Moreover, the appearance of TAMEP turned out to be specific to tumor tissue. Thus, I believe that TAMEP could serve as a novel target for GBM treatment in the future.

In the third part of this thesis, I studied the biological roles of APLN and ANGPT2 in GBM by radiogenomic analysis. I found that for both, their associated genes were involved in the angiogenic process of GBM. However, the broad database analysis indicated that APLN-coregulated genes participate in maintaining vascular integrity, while ANGPT2-coregulated genes are involved in the migration of endothelial cells from mature vessels. Therefore, I hypothesized that high APLN and

Summary

low ANGPT2 expression levels would be preponderant in GBM with a relatively mature vascular network. In contrast, low APLN and high ANGPT2 expression levels may indicate GBM with a relatively immature vascular network. Consistently, patients with high APLN and low ANGPT2 expression levels showed milder edema in MRI protocols. Moreover, survival analysis in TCGA and CGGA GBM datasets showed that patients with high APLN and low ANGPT2 expression levels had a more favorable prognosis than patients with low APLN and high ANGPT2 expression levels. Thus, I conclude that the combination of high APLN and low ANGPT2 expression could be encouraging promising marker for the degree of vascular permeability, tumoral edema, and the outcome of GBM, which will be instrumental in guiding therapeutic decisions for GBM.

Zusammenfassung

Angiogenese spielt eine wichtige Rolle bei der Entstehung eines Glioblastoms (GBM). In meiner Doktorarbeit konzentrierte ich mich daher einerseits auf essentielle zelluläre Komponenten und andererseits auf wichtige Signalmoleküle in der Tumor-Angiogenese. Die zellulären Komponenten beinhalten sowohl Perizyten wie auch die neuartigen TAMEP-Zellen (tumor-associated cells, with a myeloid-like expression profile). Der Fokus bezüglich angiogenetischer Signalwege lag auf den beiden Faktoren Apelin (APLN) und Angiopoetin 2 (ANGPT2).

Der erste Teil meiner Doktorarbeit stellt die verschiedenen Rollen von Perizyten in

Summary

frühen und fortgeschrittenen Stadien des Tumorwachstums dar. Perizyten spielen eine wichtige Rolle für die Regulierung der vaskulären Integrität. Darauf basierend habe ich die Hypothese aufgestellt, dass Perizyten an der Größenzunahme von GBM beteiligt sind. Durch die Ablation von Perizyten sowohl in einem frühen wie auch in einem fortgeschrittenen Stadium des GBM-Wachstums konnte eine Reduktion des Tumorumfangs erreicht werden. Erfolgte dies in einem frühen Stadium wurde die vaskuläre Struktur und Integrität signifikant und andauernd gestört. Zudem zeigte sich eine signifikant erhöhte Transzytoseaktivität der Endothelzellen. Diese Ergebnisse legen nahe, dass die Perizyten im frühen Stadium bei der Ausbildung der pathologischen Gefäßstrukturen, und beim Wachstum des GBM im allgemeinen, eine kritische Rollen spielen. Wenn Perizyten dagegen in einem fortgeschrittenen Stadium des GBM-Wachstums depletiert wurden, zeigte sich kein Anstieg der Permeabilität im Vergleich zur Kontrollgruppe. Dieses Ergebnis lässt darauf schließen, dass Perizyten nicht zur Aufrechterhaltung der vaskulären Permeabilität entscheidend sind. Perizyten könnten daher in Zukunft einen neuartigen Angriffspunkt für therapeutische Behandlungskonzepte von GBM in einem frühen Stadium des GBMs darstellen. Um die Rolle der Perizyten im fortgeschrittenen Stadium des GBM-Wachstums zu klären sind weiterführende Experimente erforderlich.

Im zweiten Teil meiner Doktorarbeit konzentrierte ich mich auf die neuartigen kurzlebigen avaskulären Zellen im GBM, genannt TAMEP. TAMEP sind Tumor-assoziierte Zellen mit einem myeloischen-Expressionsmuster. Sie sind beispielsweise

Summary

charakterisiert durch die Koexpression von SOX2 und PU.1. Meine Arbeit zeigt, dass TAMEP-depletiertes GBM, im Vergleich zur TAMEP enthaltenden Kontrollgruppe, ein signifikant gemindertem Tumorzellen und eine erhöhte vaskuläre Permeabilität aufweist. Im TAMEP-defizienten GBM war zudem die Expression von Collagen IV gestört. Daraus lässt sich schlussfolgern, dass TAMEP durch Modulation der Perizyten und Inhibierung der Collagen-IV Synthese die vaskuläre Permeabilität reguliert und daraus resultierend die Tumorentwicklung. Umgekehrt wurde die TAMEP Zellzahl nicht durch die Blockade der Angiogenese beeinflusst. Des Weiteren waren TAMEP spezifisch nur im Tumorgewebe aufzufinden. Aus diesem Grund glauben ich, dass TAMEP als neues Ziel in der GBM-Behandlung dienen könnten.

Der dritte Teil meiner Arbeit beschäftigt sich mit der biologischen Rolle von APLN und ANGPT2 im GBM unter Betrachtung radiogenomischer Aspekte. Dabei zeigte sich mittels breiter Datenbankanalyse, dass beide Gene mit der Expression von an der Tumor Angiogenese beteiligten Gengruppen korrelierten. Während die Gruppe der APLN-koregulierten Gene die vaskuläre Integrität aufrecht erhält, reguliert die ANGPT2 koregulierten Gengruppe die Migration von Endothelzellen ausgehend von reifen Gefäßen. Darauf basierend stellten wir die Hypothese auf, dass hohe APLN- und niedrige ANGPT2-Expressionslevel im GBM mit relativ reifen Tumorgefäßen korreliert. Im Gegensatz dazu zeigen GBM mit hohen APLN- und niedrigen ANGPT2-Expressionslevel ein relativ unreifes Gefäßsystem. GBM-Patienten mit hohen APLN- und niedrigen ANGPT2-Expressionslevel zeigten ein moderates vasogenes Ödem

Summary

mittels MRT-Protokoll. Eine Eine Analyse des Überlebenskurve in der TCGA- und CGGA-GBM Datenbank wies darauf hin, dass Patienten mit einem hohen APLN- und niedrigen ANGPT2-Expressionslevel eine bessere Prognose haben als Patienten mit einem niedrigen APLN- und hohen ANGPT2-Expressionslevel. Daraus lässt sich schließen, dass sich die Kombination von hohen APLN- und niedrigen ANGPT2-Expressionslevel ls ein vielversprechender Marker für das Maß an vaskulärer Permeabilität, Tumorödem und die Prognose von GBM in Zukunft herausstellen und somit eine Entscheidungshilfe bei der Therapie von GBM darstellen könnte.

References

7. References

1. Wu F, Zhao Z, Chai RC, Liu YQ, Li GZ, Jiang HY, *et al.* Prognostic power of a lipid metabolism gene panel for diffuse gliomas. *Journal of cellular and molecular medicine* 2019, **23**(11): 7741-7748.
2. Xu P, Yang J, Liu J, Yang X, Liao J, Yuan F, *et al.* PI3K β inhibitor AZD6482 exerts antiproliferative activity and induces apoptosis in human glioblastoma cells. *Oncology reports* 2019, **41**(1): 125-132.
3. Smoll N, Schaller K, Gautschi O. Long-term survival of patients with glioblastoma multiforme (GBM). *Journal of clinical neuroscience : official journal of the Neurosurgical Society of Australasia* 2013, **20**(5): 670-675.
4. Claus E, Walsh K, Wiencke J, Molinaro A, Wiemels J, Schildkraut J, *et al.* Survival and low-grade glioma: the emergence of genetic information. *Neurosurgical focus* 2015, **38**(1): E6.
5. Malzkorn B, Reifenberger G. Practical implications of integrated glioma classification according to the World Health Organization classification of tumors of the central nervous system 2016. *Current opinion in oncology* 2016, **28**(6): 494-501.
6. Ostrom Q, Gittleman H, Farah P, Ondracek A, Chen Y, Wolinsky Y, *et al.* CBTRUS statistical report: Primary brain and central nervous system tumors diagnosed in the United States in 2006-2010. *Neuro-oncology* 2013: ii1-56.
7. De Boeck A, Ahn B, D'Mello C, Lun X, Menon S, Alshehri M, *et al.* Glioma-derived IL-33 orchestrates an inflammatory brain tumor microenvironment that accelerates glioma progression. *Nature communications* 2020, **11**(1): 4997.
8. Folkman J. Tumor angiogenesis: therapeutic implications. *The New England journal of medicine* 1971, **285**(21): 1182-1186.
9. Ferrara N, Kerbel R. Angiogenesis as a therapeutic target. *Nature* 2005, **438**(7070): 967-974.
10. Jain R, di Tomaso E, Duda D, Loeffler J, Sorensen A, Batchelor T. Angiogenesis in brain tumours. *Nature reviews Neuroscience* 2007, **8**(8): 610-622.
11. Ameratunga M, Pavlakis N, Wheeler H, Grant R, Simes J, Khasraw M. Anti-angiogenic therapy for high-grade glioma. *The Cochrane database of systematic reviews* 2018, **11**: CD008218.
12. Ahluwalia M, Gladson C. Progress on antiangiogenic therapy for patients with malignant glioma. *Journal of oncology* 2010, **2010**: 689018.

References

13. Cohen M, Shen Y, Keegan P, Pazdur R. FDA drug approval summary: bevacizumab (Avastin) as treatment of recurrent glioblastoma multiforme. *The oncologist* 2009, **14**(11): 1131-1138.
14. Treppe L, Edmond S, Harford-Wright E, Galan-Moya E, Schmitt A, Azzi S, *et al.* Extracellular vesicle-transported Semaphorin3A promotes vascular permeability in glioblastoma. *Oncogene* 2016, **35**(20): 2615-2623.
15. Das S, Marsden P. Angiogenesis in glioblastoma. *The New England journal of medicine* 2013, **369**(16): 1561-1563.
16. Winkler E, Sagare A, Zlokovic B. The pericyte: a forgotten cell type with important implications for Alzheimer's disease? *Brain pathology (Zurich, Switzerland)* 2014, **24**(4): 371-386.
17. Uemura M, Maki T, Ihara M, Lee V, Trojanowski J. Brain Microvascular Pericytes in Vascular Cognitive Impairment and Dementia. *Frontiers in aging neuroscience* 2020, **12**: 80.
18. Eilken H, Diéguez-Hurtado R, Schmidt I, Nakayama M, Jeong H, Arf H, *et al.* Pericytes regulate VEGF-induced endothelial sprouting through VEGFR1. *Nature communications* 2017, **8**(1): 1574.
19. Dore-Duffy P, Cleary K. Morphology and properties of pericytes. *Methods in molecular biology (Clifton, NJ)* 2011, **686**: 49-68.
20. Bell R, Winkler E, Sagare A, Singh I, LaRue B, Deane R, *et al.* Pericytes control key neurovascular functions and neuronal phenotype in the adult brain and during brain aging. *Neuron* 2010, **68**(3): 409-427.
21. Armulik A, Genové G, Betsholtz C. Pericytes: developmental, physiological, and pathological perspectives, problems, and promises. *Developmental cell* 2011, **21**(2): 193-215.
22. Birbrair A, Zhang T, Wang Z, Messi M, Olson J, Mintz A, *et al.* Type-2 pericytes participate in normal and tumoral angiogenesis. *American journal of physiology Cell physiology* 2014, **307**(1): C25-38.
23. Talasila K, Røslund G, Hagland H, Eskilsson E, Flønes I, Fritah S, *et al.* The angiogenic switch leads to a metabolic shift in human glioblastoma. *Neuro-oncology* 2017, **19**(3): 383-393.
24. Armulik A, Abramsson A, Betsholtz C. Endothelial/pericyte interactions. *Circulation research* 2005, **97**(6): 512-523.
25. Ribeiro A, Okamoto O. Combined effects of pericytes in the tumor microenvironment. *Stem cells international* 2015, **2015**: 868475.

References

26. Xian X, Håkansson J, Ståhlberg A, Lindblom P, Betsholtz C, Gerhardt H, *et al.* Pericytes limit tumor cell metastasis. *The Journal of clinical investigation* 2006, **116**(3): 642-651.
27. Sattiraju A, Mintz A. Pericytes in Glioblastomas: Multifaceted Role Within Tumor Microenvironments and Potential for Therapeutic Interventions. *Advances in experimental medicine and biology* 2019, **1147**: 65-91.
28. Cooke V, LeBleu V, Keskin D, Khan Z, O'Connell J, Teng Y, *et al.* Pericyte depletion results in hypoxia-associated epithelial-to-mesenchymal transition and metastasis mediated by met signaling pathway. *Cancer cell* 2012, **21**(1): 66-81.
29. Valdor R, García-Bernal D, Bueno C, Ródenas M, Moraleda J, Macian F, *et al.* Glioblastoma progression is assisted by induction of immunosuppressive function of pericytes through interaction with tumor cells. *Oncotarget* 2017, **8**(40): 68614-68626.
30. Thangaraj A, Sil S, Tripathi A, Chivero E, Periyasamy P, Buch S. Targeting endoplasmic reticulum stress and autophagy as therapeutic approaches for neurological diseases. *International review of cell and molecular biology* 2020, **350**: 285-325.
31. Cuervo H, Pereira B, Nadeem T, Lin M, Lee F, Kitajewski J, *et al.* PDGFR β -P2A-CreER mice: a genetic tool to target pericytes in angiogenesis. *Angiogenesis* 2017, **20**(4): 655-662.
32. Kretzschmar K, Watt F. Lineage tracing. *Cell* 2012, **148**: 33-45.
33. Quail D, Joyce J. The Microenvironmental Landscape of Brain Tumors. *Cancer cell* 2017, **31**(3): 326-341.
34. Broekman M, Maas S, Abels E, Mempel T, Krichevsky A, Breakefield X. Multidimensional communication in the microenvirons of glioblastoma. *Nature reviews Neurology* 2018, **14**(8): 482-495.
35. Tomaszewski W, Sanchez-Perez L, Gajewski T, Sampson J. Brain Tumor Microenvironment and Host State: Implications for Immunotherapy. *Clinical cancer research : an official journal of the American Association for Cancer Research* 2019, **25**(14): 4202-4210.
36. Darmanis S, Sloan S, Croote D, Mignardi M, Chernikova S, Samghababi P, *et al.* Single-Cell RNA-Seq Analysis of Infiltrating Neoplastic Cells at the Migrating Front of Human Glioblastoma. *Cell reports* 2017, **21**(5): 1399-1410.
37. Roesch S, Rapp C, Dettling S, Herold-Mende C. When Immune Cells Turn Bad-Tumor-Associated Microglia/Macrophages in Glioma. *International journal of molecular sciences* 2018, **19**(2).

References

38. Zhu W, Carney K, Pigott V, Falgoust L, Clark P, Kuo J, *et al.* Glioma-mediated microglial activation promotes glioma proliferation and migration: roles of Na⁺/H⁺ exchanger isoform 1. *Carcinogenesis* 2016, **37**(9): 839-851.
39. Kettenmann H, Kirchhoff F, Verkhratsky A. Microglia: new roles for the synaptic stripper. *Neuron* 2013, **77**(1): 10-18.
40. De S, Van Deren D, Peden E, Hockin M, Boulet A, Titen S, *et al.* Two distinct ontogenies confer heterogeneity to mouse brain microglia. *Development (Cambridge, England)* 2018, **145**(13).
41. Chen Z, Feng X, Herting C, Garcia V, Nie K, Pong W, *et al.* Cellular and Molecular Identity of Tumor-Associated Macrophages in Glioblastoma. *Cancer research* 2017, **77**(9): 2266-2278.
42. Locarno C, Simonelli M, Carena C, Capucetti A, Stanzani E, Lorenzi E, *et al.* Role of myeloid cells in the immunosuppressive microenvironment in gliomas. *Immunobiology* 2020, **225**(1): 151853.
43. Chia K, Mazzolini J, Mione M, Sieger D. Tumor initiating cells induce Cxcr4-mediated infiltration of pro-tumoral macrophages into the brain. *eLife* 2018, **7**.
44. Stock K, Kumar J, Synowitz M, Petrosino S, Imperatore R, Smith E, *et al.* Neural precursor cells induce cell death of high-grade astrocytomas through stimulation of TRPV1. *Nature medicine* 2012, **18**(8): 1232-1238.
45. Behnan J, Isakson P, Joel M, Cilio C, Langmoen I, Vik-Mo E, *et al.* Recruited brain tumor-derived mesenchymal stem cells contribute to brain tumor progression. *Stem cells (Dayton, Ohio)* 2014, **32**(5): 1110-1123.
46. Hossain A, Gumin J, Gao F, Figueroa J, Shinojima N, Takezaki T, *et al.* Mesenchymal Stem Cells Isolated From Human Gliomas Increase Proliferation and Maintain Stemness of Glioma Stem Cells Through the IL-6/gp130/STAT3 Pathway. *Stem cells (Dayton, Ohio)* 2015, **33**(8): 2400-2415.
47. Hide T, Komohara Y, Miyasato Y, Nakamura H, Makino K, Takeya M, *et al.* Oligodendrocyte Progenitor Cells and Macrophages/Microglia Produce Glioma Stem Cell Niches at the Tumor Border. *EBioMedicine* 2018, **30**: 94-104.
48. Kim Y, Jeon S, Sin G, Shim J, Kim B, Shin H, *et al.* Existence of glioma stroma mesenchymal stemlike cells in Korean glioma specimens. *Child's nervous system : ChNS : official journal of the International Society for Pediatric Neurosurgery* 2013, **29**(4): 549-563.
49. Hira V, Breznik B, Vittori M, Loncq de Jong A, Mlakar J, Oostra R, *et al.* Similarities Between Stem Cell Niches in Glioblastoma and Bone Marrow: Rays of Hope for Novel Treatment

References

- Strategies. *The journal of histochemistry and cytochemistry : official journal of the Histochemistry Society* 2020, **68**(1): 33-57.
50. Hide T, Komohara Y. Oligodendrocyte Progenitor Cells in the Tumor Microenvironment. *Advances in experimental medicine and biology* 2020, **1234**: 107-122.
51. Huang Y, Hoffman C, Rajappa P, Kim J, Hu W, Huse J, *et al.* Oligodendrocyte progenitor cells promote neovascularization in glioma by disrupting the blood-brain barrier. *Cancer research* 2014, **74**(4): 1011-1021.
52. Kälin R, Cai L, Li Y, Zhao D, Zhang H, Cheng J, *et al.* TAMEP are brain tumor parenchymal cells controlling neoplastic angiogenesis and progression. *Cell systems* 2021.
53. Fang X, Zhou W, Wu Q, Huang Z, Shi Y, Yang K, *et al.* Deubiquitinase USP13 maintains glioblastoma stem cells by antagonizing FBXL14-mediated Myc ubiquitination. *The Journal of experimental medicine* 2017, **214**(1): 245-267.
54. Benz C, Martins V, Radtke F, Bleul C. The stream of precursors that colonizes the thymus proceeds selectively through the early T lineage precursor stage of T cell development. *The Journal of experimental medicine* 2008, **205**(5): 1187-1199.
55. Prinz M, Priller J, Sisodia S, Ransohoff R. Heterogeneity of CNS myeloid cells and their roles in neurodegeneration. *Nature neuroscience* 2011, **14**(10): 1227-1235.
56. Tosic N, Petrovic I, Grujicic N, Davidovic S, Virijevec M, Vukovic N, *et al.* Prognostic significance of SOX2, SOX3, SOX11, SOX14 and SOX18 gene expression in adult de novo acute myeloid leukemia. *Leukemia research* 2018, **67**: 32-38.
57. Lukas R, Wainwright D, Ladomersky E, Sachdev S, Sonabend A, Stupp R. Newly Diagnosed Glioblastoma: A Review on Clinical Management. *Oncology (Williston Park, NY)* 2019, **33**(3): 91-100.
58. Hanif F, Muzaffar K, Perveen K, Malhi S, Simjee S. Glioblastoma Multiforme: A Review of its Epidemiology and Pathogenesis through Clinical Presentation and Treatment. *Asian Pacific journal of cancer prevention : APJCP* 2017, **18**(1): 3-9.
59. Wirsching H, Galanis E, Weller M. Glioblastoma. *Handbook of clinical neurology* 2016, **134**: 381-397.
60. Shukla G, Alexander G, Bakas S, Nikam R, Talekar K, Palmer J, *et al.* Advanced magnetic resonance imaging in glioblastoma: a review. *Chinese clinical oncology* 2017, **6**(4): 40.
61. An J, Kang S, Huh E, Kim Y, Lee D, Jo H, *et al.* Penta-fluorophenol: a Smiles rearrangement-

References

- inspired cysteine-selective fluorescent probe for imaging of human glioblastoma. *Chemical science* 2020, **11**(22): 5658-5668.
62. Johnston C, Krafft A, Russe M, Rog-Zielinska E. A new look at the heart-novel imaging techniques. *Herzschrittmachertherapie & Elektrophysiologie* 2018, **29**(1): 14-23.
63. Hawkins-Daarud A, Rockne R, Anderson A, Swanson K. Modeling Tumor-Associated Edema in Gliomas during Anti-Angiogenic Therapy and Its Impact on Imageable Tumor. *Frontiers in oncology* 2013, **3**: 66.
64. Wu C, Lin G, Lin Z, Zhang J, Liu S, Zhou C. Peritumoral edema shown by MRI predicts poor clinical outcome in glioblastoma. *World journal of surgical oncology* 2015, **13**: 97.
65. Verhaak R, Hoadley K, Purdom E, Wang V, Qi Y, Wilkerson M, *et al.* Integrated genomic analysis identifies clinically relevant subtypes of glioblastoma characterized by abnormalities in PDGFRA, IDH1, EGFR, and NF1. *Cancer cell* 2010, **17**(1): 98-110.
66. Wang Y, Jiang T. Understanding high grade glioma: molecular mechanism, therapy and comprehensive management. *Cancer letters* 2013, **331**(2): 139-146.
67. Dhermain F, Hau P, Lanfermann H, Jacobs A, van den Bent M. Advanced MRI and PET imaging for assessment of treatment response in patients with gliomas. *The Lancet Neurology* 2010, **9**(9): 906-920.
68. Grossmann P, Gutman D, Dunn W, Holder C, Aerts H. Imaging-genomics reveals driving pathways of MRI derived volumetric tumor phenotype features in Glioblastoma. *BMC cancer* 2016, **16**: 611.
69. Tatemoto K, Hosoya M, Habata Y, Fujii R, Kakegawa T, Zou M, *et al.* Isolation and characterization of a novel endogenous peptide ligand for the human APJ receptor. *Biochemical and biophysical research communications* 1998, **251**(2): 471-476.
70. Lv S, Chen W, Wang Y. The Apelin/APJ System in Psychosis and Neuropathy. *Frontiers in pharmacology* 2020, **11**: 320.
71. Tempel D, de Boer M, van Deel E, Haasdijk R, Duncker D, Cheng C, *et al.* Apelin enhances cardiac neovascularization after myocardial infarction by recruiting apInr+ circulating cells. *Circulation research* 2012, **111**(5): 585-598.
72. Wu L, Chen L, Li L. Apelin/APJ system: A novel promising therapy target for pathological angiogenesis. *Clinica chimica acta; international journal of clinical chemistry* 2017, **466**: 78-84.
73. Uribealago I, Hoffmann D, Zhang Y, Kavirayani A, Lazovic J, Berta J, *et al.* Apelin inhibition

References

- prevents resistance and metastasis associated with anti-angiogenic therapy. *EMBO molecular medicine* 2019, **11**(8): e9266.
74. Mastrella G, Hou M, Li M, Stoecklein V, Zdouc N, Volmar M, *et al.* Targeting APLN/APLNR Improves Antiangiogenic Efficiency and Blunts Proinvasive Side Effects of VEGFA/VEGFR2 Blockade in Glioblastoma. *Cancer research* 2019, **79**(9): 2298-2313.
75. Harford-Wright E, Andre-Gregoire G, Jacobs K, Treps L, Le Gonidec S, Leclair H, *et al.* Pharmacological targeting of apelin impairs glioblastoma growth. *Brain : a journal of neurology* 2017, **140**(11): 2939-2954.
76. Frisch A, Kälin S, Monk R, Radke J, Heppner F, Kälin R. Apelin Controls Angiogenesis-Dependent Glioblastoma Growth. *International journal of molecular sciences* 2020, **21**(11).
77. Kälin R, Kretz M, Meyer A, Kispert A, Heppner F, Brändli A. Paracrine and autocrine mechanisms of apelin signaling govern embryonic and tumor angiogenesis. *Developmental biology* 2007, **305**(2): 599-614.
78. Zadeh G, Koushan K, Baoping Q, Shannon P, Guha A. Role of angiopoietin-2 in regulating growth and vascularity of astrocytomas. *Journal of oncology* 2010, **2010**: 659231.
79. Kiss EA, Saharinen P. Anti-angiogenic Targets: Angiopoietin and Angiopoietin-Receptors. 2018.
80. Pousa I, Maté J, Salcedo-Mora X, Abreu M, Moreno-Otero R, Gisbert J. Role of vascular endothelial growth factor and angiopoietin systems in serum of Crohn's disease patients. *Inflammatory bowel diseases* 2008, **14**(1): 61-67.
81. Kim I, Kim H, So J, Kim J, Kwak H, Koh G. Angiopoietin-1 regulates endothelial cell survival through the phosphatidylinositol 3'-Kinase/Akt signal transduction pathway. *Circulation research* 2000, **86**(1): 24-29.
82. Agrawal A, Matthay M, Kangelaris K, Stein J, Chu J, Imp B, *et al.* Plasma angiopoietin-2 predicts the onset of acute lung injury in critically ill patients. *American journal of respiratory and critical care medicine* 2013, **187**(7): 736-742.
83. Sie M, Wagemakers M, Molema G, Mooij J, de Bont E, den Dunnen W. The angiopoietin 1/angiopoietin 2 balance as a prognostic marker in primary glioblastoma multiforme. *Journal of neurosurgery* 2009, **110**(1): 147-155.
84. Stratmann A, Risau W, Plate K. Cell type-specific expression of angiopoietin-1 and angiopoietin-2 suggests a role in glioblastoma angiogenesis. *The American journal of pathology* 1998, **153**(5): 1459-1466.

References

85. Scholz A, Harter P, Cremer S, Yalcin B, Gurnik S, Yamaji M, *et al.* Endothelial cell-derived angiopoietin-2 is a therapeutic target in treatment-naive and bevacizumab-resistant glioblastoma. *EMBO molecular medicine* 2016, **8**(1): 39-57.
86. Holopainen T, Saharinen P, D'Amico G, Lampinen A, Eklund L, Sormunen R, *et al.* Effects of angiopoietin-2-blocking antibody on endothelial cell-cell junctions and lung metastasis. *Journal of the National Cancer Institute* 2012, **104**(6): 461-475.
87. Chae S, Kamoun W, Farrar C, Kirkpatrick N, Niemeyer E, de Graaf A, *et al.* Angiopoietin-2 interferes with anti-VEGFR2-induced vessel normalization and survival benefit in mice bearing gliomas. *Clinical cancer research : an official journal of the American Association for Cancer Research* 2010, **16**(14): 3618-3627.
88. Indra A, Warot X, Brocard J, Bornert J, Xiao J, Chambon P, *et al.* Temporally-controlled site-specific mutagenesis in the basal layer of the epidermis: comparison of the recombinase activity of the tamoxifen-inducible Cre-ER(T) and Cre-ER(T2) recombinases. *Nucleic acids research* 1999, **27**(22): 4324-4327.
89. Giachino C, Taylor V. Lineage analysis of quiescent regenerative stem cells in the adult brain by genetic labelling reveals spatially restricted neurogenic niches in the olfactory bulb. *The European journal of neuroscience* 2009, **30**(1): 9-24.
90. Battiste J, Helms A, Kim E, Savage T, Lagace D, Mandyam C, *et al.* Ascl1 defines sequentially generated lineage-restricted neuronal and oligodendrocyte precursor cells in the spinal cord. *Development (Cambridge, England)* 2007, **134**(2): 285-293.
91. Zudaire E, Gambardella L, Kurcz C, Vermeren S. A computational tool for quantitative analysis of vascular networks. *PloS one* 2011, **6**(11): e27385.
92. Pavlisa G, Rados M, Pavlisa G, Pavic L, Potocki K, Mayer D. The differences of water diffusion between brain tissue infiltrated by tumor and peritumoral vasogenic edema. *Clinical imaging* 2009, **33**(2): 96-101.
93. Zinn P, Mahajan B, Majadan B, Sathyan P, Singh S, Majumder S, *et al.* Radiogenomic mapping of edema/cellular invasion MRI-phenotypes in glioblastoma multiforme. *PloS one* 2011, **6**(10): e25451.
94. Kim B, Kim M, Kim S, Chang C, Kim O. Peritumoral brain edema in meningiomas : correlation of radiologic and pathologic features. *Journal of Korean Neurosurgical Society* 2011, **49**(1): 26-30.
95. Li T, Fu J, Zeng Z, Cohen D, Li J, Chen Q, *et al.* TIMER2.0 for analysis of tumor-infiltrating immune cells. *Nucleic acids research* 2020, **48**: W509-W514.

References

96. Vasaikar S, Straub P, Wang J, Zhang B. LinkedOmics: analyzing multi-omics data within and across 32 cancer types. *Nucleic acids research* 2018, **46**: D956-D963.
97. Zhou Y, Zhou B, Pache L, Chang M, Khodabakhshi A, Tanaseichuk O, *et al.* Metascape provides a biologist-oriented resource for the analysis of systems-level datasets. *Nature communications* 2019, **10**(1): 1523.
98. Caspani E, Crossley P, Redondo-Garcia C, Martinez S. Glioblastoma: a pathogenic crosstalk between tumor cells and pericytes. *PloS one* 2014, **9**(7): e101402.
99. Huizer K, Zhu C, Chirifi I, Krist B, Zоргman D, van der Weiden M, *et al.* Periostin Is Expressed by Pericytes and Is Crucial for Angiogenesis in Glioma. *Journal of neuropathology and experimental neurology* 2020, **79**(8): 863-872.
100. Murakami M, Simons M. Regulation of vascular integrity. *Journal of molecular medicine (Berlin, Germany)* 2009, **87**(6): 571-582.
101. Radu M, Chernoff J. An in vivo assay to test blood vessel permeability. *Journal of visualized experiments : JoVE* 2013(73): e50062.
102. Olsson Y, Svensjö E, Arfors K, Hultström D. Fluorescein labelled dextrans as tracers for vascular permeability studies in the nervous system. *Acta neuropathologica* 1975, **33**(1): 45-50.
103. Hoffmann A, Bredno J, Wendland M, Derugin N, Ohara P, Wintermark M. High and Low Molecular Weight Fluorescein Isothiocyanate (FITC)-Dextrans to Assess Blood-Brain Barrier Disruption: Technical Considerations. *Translational stroke research* 2011, **2**(1): 106-111.
104. Thomsen M, Routhe L, Moos T. The vascular basement membrane in the healthy and pathological brain. *Journal of cerebral blood flow and metabolism : official journal of the International Society of Cerebral Blood Flow and Metabolism* 2017, **37**(10): 3300-3317.
105. Xu L, Nirwane A, Yao Y. Basement membrane and blood-brain barrier. *Stroke and vascular neurology* 2019, **4**(2): 78-82.
106. Mak K, Mei R. Basement Membrane Type IV Collagen and Laminin: An Overview of Their Biology and Value as Fibrosis Biomarkers of Liver Disease. *Anatomical record (Hoboken, NJ : 2007)* 2017, **300**(8): 1371-1390.
107. Chen B, Friedman B, Cheng Q, Tsai P, Schim E, Kleinfeld D, *et al.* Severe blood-brain barrier disruption and surrounding tissue injury. *Stroke* 2009, **40**(12): e666-674.
108. Natarajan R, Northrop N, Yamamoto B. Fluorescein Isothiocyanate (FITC)-Dextran

References

- Extravasation as a Measure of Blood-Brain Barrier Permeability. *Current protocols in neuroscience* 2017, **79**: 9.58.51-59.58.15.
109. Miao L, Huang L. Exploring the tumor microenvironment with nanoparticles. *Cancer treatment and research* 2015, **166**: 193-226.
110. Ma J, Shen Z, Yu Y, Shi S. Neural lineage tracing in the mammalian brain. *Current opinion in neurobiology* 2018, **50**: 7-16.
111. Cedervall J, Dimberg A, Olsson A. Tumor-Induced Local and Systemic Impact on Blood Vessel Function. *Mediators of inflammation* 2015, **2015**: 418290.
112. Devraj K, Guérit S, Macas J, Reiss Y. An In Vivo Blood-brain Barrier Permeability Assay in Mice Using Fluorescently Labeled Tracers. *Journal of visualized experiments : JoVE* 2018(132).
113. Yamazaki Y, Kanekiyo T. Blood-Brain Barrier Dysfunction and the Pathogenesis of Alzheimer's Disease. *International journal of molecular sciences* 2017, **18**(9).
114. Jung Y, Mansfield P, Akagi M, Takeda A, Liu W, Bucana C, *et al.* Effects of combination anti-vascular endothelial growth factor receptor and anti-epidermal growth factor receptor therapies on the growth of gastric cancer in a nude mouse model. *European journal of cancer (Oxford, England : 1990)* 2002, **38**(8): 1133-1140.
115. Verhoeff J, Stalpers L, Van Noorden C, Troost D, Ramkema M, van Bree C, *et al.* Angiogenesis inhibitor DC101 delays growth of intracerebral glioblastoma but induces morbidity when combined with irradiation. *Cancer letters* 2009, **285**(1): 39-45.
116. Comprehensive genomic characterization defines human glioblastoma genes and core pathways. *Nature* 2008, **455**(7216): 1061-1068.
117. Goedhart J, Luijsterburg M. VolcanoNoseR is a web app for creating, exploring, labeling and sharing volcano plots. *Scientific reports* 2020, **10**(1): 20560.
118. Rathore S, Akbari H, Doshi J, Shukla G, Rozycki M, Bilello M, *et al.* Radiomic signature of infiltration in peritumoral edema predicts subsequent recurrence in glioblastoma: implications for personalized radiotherapy planning. *Journal of medical imaging (Bellingham, Wash)* 2018, **5**(2): 021219.
119. Martinez R, Schackert G, Yaya-Tur R, Rojas-Marcos I, Herman J, Esteller M. Frequent hypermethylation of the DNA repair gene MGMT in long-term survivors of glioblastoma multiforme. *Journal of neuro-oncology* 2007, **83**(1): 91-93.
120. Bujko M, Kober P, Matyja E, Nauman P, Dyttus-Cebulok K, Czeremszyńska B, *et al.* Prognostic

References

- value of IDH1 mutations identified with PCR-RFLP assay in glioblastoma patients. *Molecular diagnosis & therapy* 2010, **14**(3): 163-169.
121. Molenaar R, Verbaan D, Lamba S, Zanon C, Jeuken J, Boots-Sprenger S, *et al.* The combination of IDH1 mutations and MGMT methylation status predicts survival in glioblastoma better than either IDH1 or MGMT alone. *Neuro-oncology* 2014, **16**(9): 1263-1273.
122. Mühleder S, Fernández-Chacón M, Garcia-Gonzalez I, Benedito R. Endothelial sprouting, proliferation, or senescence: tipping the balance from physiology to pathology. *Cellular and molecular life sciences : CMLS* 2020.
123. del Toro R, Prahst C, Mathivet T, Siegfried G, Kaminker J, Larrivee B, *et al.* Identification and functional analysis of endothelial tip cell-enriched genes. *Blood* 2010, **116**(19): 4025-4033.
124. Reijnen C, van Weelden W, Arts M, Peters J, Rijken P, van de Vijver K, *et al.* Poor outcome in hypoxic endometrial carcinoma is related to vascular density. *British journal of cancer* 2019, **120**(11): 1037-1044.
125. Lamalice L, Le Boeuf F, Huot J. Endothelial cell migration during angiogenesis. *Circulation research* 2007, **100**(6): 782-794.
126. Stewart A, Houston B, Farquharson C. Elevated expression of hypoxia inducible factor-2alpha in terminally differentiating growth plate chondrocytes. *Journal of cellular physiology* 2006, **206**(2): 435-440.
127. Ruhrberg C, Gerhardt H, Golding M, Watson R, Ioannidou S, Fujisawa H, *et al.* Spatially restricted patterning cues provided by heparin-binding VEGF-A control blood vessel branching morphogenesis. *Genes & development* 2002, **16**(20): 2684-2698.
128. Barakat A, Mittal A, Ricketts D, Rogers B. Understanding survival analysis: actuarial life tables and the Kaplan-Meier plot. *British journal of hospital medicine (London, England : 2005)* 2019, **80**(11): 642-646.
129. Wu C, Lin G, Lin Z, Zhang J, Chen L, Liu S, *et al.* Peritumoral edema on magnetic resonance imaging predicts a poor clinical outcome in malignant glioma. *Oncology letters* 2015, **10**(5): 2769-2776.
130. Wan Y, Rahmat R, Price S. Deep learning for glioblastoma segmentation using preoperative magnetic resonance imaging identifies volumetric features associated with survival. *Acta neurochirurgica* 2020, **162**(12): 3067-3080.
131. Bernabéu-Sanz Á, Fuentes-Baile M, Alenda C. Main genetic differences in high-grade gliomas may present different MR imaging and MR spectroscopy correlates. *European radiology* 2021,

References

- 31(2):** 749-763.
132. Svensson A, Özen I, Genové G, Paul G, Bengzon J. Endogenous brain pericytes are widely activated and contribute to mouse glioma microvasculature. *PLoS one* 2015, **10(4)**: e0123553.
133. Fakhoury M. Drug delivery approaches for the treatment of glioblastoma multiforme. *Artificial cells, nanomedicine, and biotechnology* 2016, **44(6)**: 1365-1373.
134. Morofuji Y, Nakagawa S. Drug Development for Central Nervous System Diseases Using In vitro Blood-brain Barrier Models and Drug Repositioning. *Current pharmaceutical design* 2020, **26(13)**: 1466-1485.
135. Jain R. Molecular regulation of vessel maturation. *Nature medicine* 2003, **9(6)**: 685-693.
136. Betsholtz C. Insight into the physiological functions of PDGF through genetic studies in mice. *Cytokine & growth factor reviews* 2004, **15(4)**: 215-228.
137. Dieterich L, Mellberg S, Langenkamp E, Zhang L, Zieba A, Salomäki H, *et al.* Transcriptional profiling of human glioblastoma vessels indicates a key role of VEGF-A and TGF β 2 in vascular abnormalization. *The Journal of pathology* 2012, **228(3)**: 378-390.
138. Folkman J. Role of angiogenesis in tumor growth and metastasis. *Seminars in oncology* 2002, **29**: 15-18.
139. Sun H, Guo D, Su Y, Yu D, Wang Q, Wang T, *et al.* Hyperplasia of pericytes is one of the main characteristics of microvascular architecture in malignant glioma. *PLoS one* 2014, **9(12)**: e114246.
140. Jamieson J, Linville R, Ding Y, Gerecht S, Searson P. Role of iPSC-derived pericytes on barrier function of iPSC-derived brain microvascular endothelial cells in 2D and 3D. *Fluids and barriers of the CNS* 2019, **16(1)**: 15.
141. Shepro D, Morel N. Pericyte physiology. *FASEB journal : official publication of the Federation of American Societies for Experimental Biology* 1993, **7(11)**: 1031-1038.
142. König J, Weiss G, Rossi D, Wankhammer K, Reinisch A, Kinzer M, *et al.* Placental mesenchymal stromal cells derived from blood vessels or avascular tissues: what is the better choice to support endothelial cell function? *Stem cells and development* 2015, **24(1)**: 115-131.
143. Ellis L, Reardon D. Cancer: The nuances of therapy. *Nature* 2009, **458(7236)**: 290-292.
144. Zhou Z, Pausch F, Schlötzer-Schrehardt U, Brachvogel B, Pöschl E. Induction of initial steps of angiogenic differentiation and maturation of endothelial cells by pericytes in vitro and the role

References

- of collagen IV. *Histochemistry and cell biology* 2016, **145**(5): 511-525.
145. Kose N, Asashima T, Muta M, Iizasa H, Sai Y, Terasaki T, *et al.* Altered expression of basement membrane-related molecules in rat brain pericyte, endothelial, and astrocyte cell lines after transforming growth factor-beta1 treatment. *Drug metabolism and pharmacokinetics* 2007, **22**(4): 255-266.
146. Armulik A, Genové G, Mäe M, Nisancioglu M, Wallgard E, Niaudet C, *et al.* Pericytes regulate the blood-brain barrier. *Nature* 2010, **468**(7323): 557-561.
147. Hirunpattarasilp C, Attwell D, Freitas F. The role of pericytes in brain disorders: from the periphery to the brain. *Journal of neurochemistry* 2019, **150**(6): 648-665.
148. Dalkara T, Gursoy-Ozdemir Y, Yemisci M. Brain microvascular pericytes in health and disease. *Acta neuropathologica* 2011, **122**(1): 1-9.
149. Kidoya H, Kunii N, Naito H, Muramatsu F, Okamoto Y, Nakayama T, *et al.* The apelin/APJ system induces maturation of the tumor vasculature and improves the efficiency of immune therapy. *Oncogene* 2012, **31**(27): 3254-3264.

Acknowledgement

8. Acknowledgement

Firstly, I would like to express my deep gratitude for the enthusiasm, inspiration, and wisdom of Prof. Dr. Rainer Glass and co-supervisor Dr. Roland Kälin. Their guidance helped me in this research and revision of this thesis. I was extraordinarily fortunate to have had wonderful advisors and mentors for my M.D study.

Apart from my supervisors, I will not forget to express my sincere gratitude to the rest of the group: Ms. Stefanie Lange, Dr. Min Li, Dr. Linzhi Cai, Dr. Sabrina V Kirchleitner, Mr. Dongxu Zhao, Ms. Jiying Cheng, Ms. Lisa Niederauer, Ms. Nina Zdouc, Mr. Enio Barci, Mr. Sven Richter, Ms. Lena Schumacher, and Mr. Robin Wechter, Mr. Fabian Binter for giving their support and insightful discussions. I would also like to acknowledge Prof. Dr. Michael Synowitz, Dr. Charlotte Flüh and Ms. Friederike Michels from Kiel University for supporting this thesis. They all have played a role in developing my data interpretation and writing the manuscript. Constant support from my colleagues and I will keep in my heart forever. I also thank the support from China Scholarship Council (CSC).

Last but not least, I would like to express my gratitude to my family, friends, and relatives. I would especially like to thank my girlfriend, Dr. Xinyuan Wang, thank you for your great support in my life and study. They gave me enough moral support, encouragement, and motivation to accomplish my doctoral degree.

9. Affidavit



Affidavit

Zhang, Huabin

Surname, first name

I hereby declare, that the submitted thesis entitled:

A study on the control of vascular permeability in GBM.

The role of pericytes, myeloid-like cells (TAMEP) and the angiogenic factors APLN and ANGPT2.

is my own work. I have only used the sources indicated and have not made unauthorized use of services of a third party. Where the work of others has been quoted or reproduced, the source is always given.

I further declare that the submitted thesis or parts of thesis have not been presented as part of an examination degree to any other university.

Guangzhou, 25.11.2021

Place, date

Huabin Zhang

Signature doctoral candidate